BIOMIMETIC SYNTHESIS, MAGNETIC PROPERTIES AND APPLICATIONS OF MAGNETITE NANOPARTICLES

by

Cem Levent Altan

Submitted to Graduate School of Natural and Applied Sciences

in Partial Fulfillment of the Requirements

for the Degree of Doctor of Philosophy in

Chemical Engineering

Yeditepe University

2015

BIOMIMETIC SYNTHESIS, MAGNETIC PROPERTIES AND APPLICATIONS OF MAGNETITE NANOPARTICLES

APPROVED BY:

Assoc. Prof. Seyda Bucak ....

Assoc. Prof. Nico A.J.M. Sommerdijk ....

Prof. Nurcan Bac ....

Prof. Gijsbertus de With ....

Assoc. Prof. Amitav Sanyal ....

Assoc. Prof. Funda Yağcı Acar ....

Assist. Prof. Erde Can ....

DATE OF APPROVAL: ... / ... / ...

ACKNOWLEDGEMENTS

ABSTRACT

BIOMIMETIC SYNTHESIS, MAGNETIC PROPERTIES AND APPLICATIONS OF MAGNETITE NANOPARTICLES

Iron oxides are one of major classes of inorganic compounds widespread in nature and important for many disciplines. As a member, magnetite is one of the most studied naturally occurring mineral owing to its excellent magnetic and biocompatible properties. Magnetite nanoparticles are also suitable for several applications where their effective use depends on corresponding size, shape thus magnetic properties and stability of the particles. Although it is a challenge to take control over magnetite morphology without use of high temperatures and complicated synthesis pathways, the synthesis of magnetite nanoparticles through partial oxidation of ferrous hydroxide precursor at biomimetic conditions, i.e. at room temperature and in water, demonstrated the possibility of growth regulation as a result of interaction with a soluble poly(amino acid). As the stability of magnetite nanoparticles in aqueous medium is essential for several applications such as drug delivery, heat transfer and magnetic hyperthermia, the nanoparticles in the superparamagnetic and ferrimagnetic domains synthesized through co-precipitation and partial oxidation were functionalized with poly(ethylene imine)-graft-poly(oligo(ethylene glycol methyl ether) and poly(acrylic acid) respectively. The stability achieved in aqueous medium by using these polymers made the polymer-magnetite complexes suitable for various applications. As it is known from the literature, these nonmagnetic coatings may form a magnetically disordered layer on the nanoparticles which reduces the total amount of the magnetic phase. For this purpose, reduction of magnetic phase was studied for similar amine and carboxylic acid functionalized magnetite nanoparticles. Results indeed showed a reduction in the magnetic phase for both coatings which highlight again the necessity of considering this reduction for optimizing the magnetic properties of magnetite nanoparticles. Finally, the effect of superparamagnetic magnetite nanoparticles on the thermal conductivity of water was investigated. The contradictory results showed deteriorations in the thermal conductivity of water upon addition of magnetite nanoparticles which was independent of the synthesis method, the type of surfactant used and the interfacial thermal resistance.

ÖZET

MAGNETİT NANOPARÇACIKLARININ BİYOMİMETİK SENTEZİ, MANYETİK ÖZELLİKLERİ VE UYGULAMALARI

Demir oksitler doğada yaygın olan ve bir çok farklı disiplin için önemi büyük olan inorganik bileşiklerdir. Bu bileşiklerin bir üyesi olan magnetit, mükemmel manyetik özellikleri ve biyouyumluluğu sayesinde üzerinde en çok çalışılmış, doğal yollarla oluşan bir mineraldir. Magnetit nanoparçacıkların farklı uygulamalarda, etkin kullanımları stabilitelerine, boyutlarına ve şekillerine göre değişkenlik göstermektedir. Her ne kadar, yüksek sıcaklık ve/veya komplike sentez yöntemleri kullanımı olmadan magnetit morfolojisini kontrol etmek zor olsa da, magnetit nanoparçacıklarının demir (II) hidroksit prekursörünün kısmi oksidasyonunun doğal koşullarda (oda sıcaklığı ve su içerisinde) sentezi esnasında çözülebilir bir poli(amino asit) ile etkileşim sayesinde manyetik nanoparçacıklarının oluşumlarının düzenlenebilme olasılığı gösterilmiştir. Magnetit nanoparçacıkların sulu ortamdaki stabiliteleri ilaç taşınımı, ısı transferi ve manyetik hipertermi gibi uygulamalarda esas olduğu için, kısmi oksidasyon ve birlikte çöktürme yöntemleri ile sentezlenen ferrimanyetik ve süperparamanyetik magnetit nanoparçacıklar sırasıyla poli(akrilik asit) ve poli(etilen imin)-graft-poli(oligo(etilen glikol metil eter) ile işlevselleştirilmiştir. Bu polimerleri kullanarak elde edilen sulu ortam stabilitesi, magnetit-polimer komplekslerinin farklı uygulamalarda kullanımını elverişli hale getirmiştir. Literatürden elde edilen bilgilere göre, bu tarz yüzey kaplamaları manyetik olarak düzensiz bir katman oluşturup toplam manyetik faz miktarını azaltabilmektedirler. Bu sebepten ötürü, manyetik fazda gerçekleşen azalma miktarı amin ve karboksil grubu ile işlevselleştirilmiş magnetit nanoparçacıkları için incelenmiştir. Sonuçlar gerçekten de toplam manyetik fazda bir azalma olduğunu göstermiş ve magnetit nanoparçacıklarının manyetik özelliklerinin optimize edilmesi için bu düşüşün dikkate alınması gerekliliğinin altını çizmiştir. Son olarak, süperparamagnetik magnetit nanoparçacıklarının eklenmesi sonucu suyun termal iletkenliğinin değişimi incelenmiştir. Literatüre göre çelişkili olan sonuçlar, suyun termal iletkenliğinin magnetit nanoparçacıklarının eklenmesi sonucu azaldığını ve bu azalmanın sentez yöntemi, sürfaktan çeşidi ve arayüzey termal rezistansı ile ilgili olmadığını göstermiştir.

TABLE OF CONTENTS

LIST OF FIGURES

LIST OF TABLES

LIST OF SYMBOLS / ABBREVIATIONS

A	Absorbance
a_0	Thickness of the nonmagnetic layer
ATRP	Atom transfer radical polymerization
c	Molar concentration
CCD	Charged coupled device
C_M	Mass concentration calculated from the Tiron test
cryo-ET	Cryo-Electron tomography
C_T	Mass concentration from the magnetization curves
d	Thickness of cuvette
DF	Dilution factor
D_i	Diameter of particles
DLS	Dynamic light scattering
DNA	Deoxyribonucleic acid
dNBpy	4,4'-dinonyl-2,2'-bipyridine
DP	Degree of polymerization
ED	Electron diffraction
EMT	Effective medium theory
G	Interfacial conductance
H	Applied magnetic field
h	Equivalent thickness
φ	Volumetric concentration of magnetic phase

k	Boltzmann constant
k	Thermal conductivity
k_{eff}	Effective thermal conductivity
k_f	Fluid thermal conductivity
K_{sp}	Solubility product constant
LDED	Low dose electron diffraction
M	Molar mass
M_b	Saturation magnetization of bulk magnetite
M_n	Number average molecular weight
MPI	Magnetic particle imaging
MRI	Magnetic resonance imaging
M_S	Saturation magnetization
M_{S1}	Saturation magnetization of the core
M_{S2}	Saturation magnetization of the shell
n	Number of moles
n_i	Number of particles
PAA	poly(acrylic acid)
pAsp	α,β-poly(aspartic acid)
PEI	poly(ethylene imine)
PEO	poly(ethylene oxide)
POEGMA	poly(oligo(ethylene glycol methyl ether)
PPO	poly(propylene oxide)
PVP	poly(vinylpyrrolidone)
r_p	Radius of nanoparticle

SAED	Selected area electron diffraction
SAR	Specific absorption rate
STEM	Scanning transmission electron microscopy
T	Temperature
TEM	Transmission electron microscopy
TGA	Thermogravimetric analysis
THF	Tetrahydrofuran
V_{Final}	Final volume of the sample for the Tiron test
V_i	Total volume of the particle + nonmagnetic layer
v_i	Effective volume of the magnetic core
V_{sample}	Magnetic fluid volume
VSM	Vibrating sample magnetometer
XPS	X-ray photo electron spectroscopy
XRD	X-ray diffraction
γ	Ratio of nanoparticle radius to equivalent thickness
ε	Specific wavelength
ρ_p	Mass density of magnetite
σ	Supersaturation
ω	Weight fraction

1. INTRODUCTION

Iron oxides are encountered frequently in our daily life and exist in different forms in nature. These compounds derived from iron and oxygen differ and for some types compare according to their crystal structure, morphology and magnetic properties. There are versatile synthetic methods for the production of iron oxides among which magnetite is possibly the most important type. The essential reasons behind the use of magnetite in various applications are its biocompatibility and superior magnetic properties as it is the most magnetic naturally occurring mineral known. Fields of application are versatile as the magnetic properties of magnetite particles vary according to the synthesis method used. Although magnetite was the subject of countless studies for decades, the synthesis pathways at ambient conditions mimicking the perfection of nature still remain a challenge. As the range of its applications in various fields continue to expand, it is no doubt that magnetite will get growing attention in the coming future.

The objective of the research presented in this thesis is to study extensively the formation, properties and applications of magnetite which is the most magnetic naturally occurring mineral. For this purpose, initially the control over magnetite formation via different synthetic routes was investigated. As the effective use of magnetite in desired applications depends on the stability and the magnetic properties of the particles, various polymers and surfactants were introduced to the most common synthetic methods to enhance the colloidal stability in aqueous medium. Furthermore the effect of these surface agents on the magnetic properties of the particles was studied. Finally, the possible applications of magnetite nanoparticles in heat transfer systems were analyzed by investigating the impact of the presence of magnetite nanoparticles on the thermal conductivity of different base fluids.

Chapter 2 gives a general summary of the iron oxides and in particular magnetite. Literature survey on the synthesis methods and various applications that require tailored magnetic properties are also presented in this chapter.

Chapter 3 presents study that focuses on the control over magnetite formation via co-precipitation and partial oxidation methods at ambient conditions in the presence of

poly(amino acids) which mimic the mineralization process in nature specifically that of magnetotactic bacteria. The effect of these additives on the size, shape, organization and magnetic properties of magnetite are discussed in this chapter.

In chapter 4 and 5, the studies on the colloidal stability of both superparamagnetic and ferromagnetic magnetite nanoparticles are demonstrated. For this purpose magnetite is synthesized by co-precipitaton and partial oxidation methods in the presence of biocompatible polymers and their effect on morphology and stability are examined.

Chapter 6 presents the reduction of magnetic properties due to the change in the thickness of the magnetically disordered layer at the outmost shell of magnetite nanoparticles upon application of surface agents that are mainly used to stabilize magnetite. Reduction of this magnetic phase was investigated for commercial (amine and carboxyl funtionalized) and synthesized (oleic acid coated) magnetite nanoparticles of 7nm – 12nm by using vibrating sample magnetometry and the tiron chelation test.

Finally, chapter 7 describes the effect of superparamagnetic magnetite nanoparticles on the thermal conductivity of polar base fluids. Magnetite nanoparticles were prepared by different synthetic routes in the presence of hydrophilic additives and the changes in thermal conductivity of water and ethylene glycol which are common heat transfer fluids were studied as a function of temperature and particle concentration.

2. IRON OXIDES AND MAGNETITE

2.1. IRON OXIDES

Iron oxides are compounds encountered in many different parts of nature and have an essential role in various geological and biological systems thus receive multidisciplinary attention, as shown in Figure 2.1. There are 16 known iron oxides classified in two different groups according to their ion content (Table 2.1). Oxides are composed of only iron ($Fe^{2+,3+}$) and oxygen (O^{2-}) ions while oxy-hydroxides contain additional hydroxide (OH^-) ions. Those oxides and oxy-hydroxides differ in composition of the stated ions and/or their crystal structure.
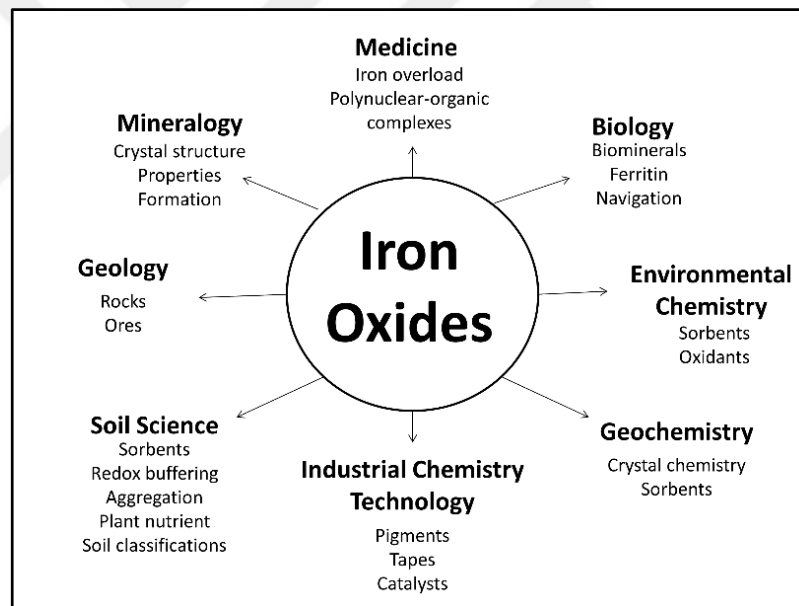
Figure 2.1. Multi-disciplines of the iron oxides [1].

Geologically these iron oxides may form and also transform to another type according to the pathways and conditions given in Figure 2.2. Goethite can be readily found in rocks and is one of the most stable iron oxides at ambient conditions. As a consequence, it is believed to be either the first type that is formed or the one that formed as a result of many transformations [1]. Goethite powder is yellow and is also used as a pigment. Lepidocrocite,

having an orange color, can also be found in rocks as well as in soils and rusts. It is formed mainly as a result of Fe^{2+} oxidation. Akageneite is a rare iron oxide which is encountered in chloride- or fluoride-rich environments. On the other hand, ferrihydrite is a common iron oxy-hydroxide, which can be found as nanocrystals in nature, and is an essential precursor for more stable iron oxides. Ferrous hydroxide ($Fe(OH)_2$) is an important iron oxide, however, it is not found in nature as a mineral. It is easily oxidized to form another intermediate, green rust (containing chloride or sulphate ions) and its further oxidation leads to the formation of magnetite. Hematite is also one of the oldest iron oxide minerals known. It has a red color and is common in rocks and soils. Along with goethite, it is quite stable and believed to be an end product of many transformations. Magnetite is a ferrimagnetic iron oxide that contains both Fe^{2+} and Fe^{3+} ions. It has a black color and gives magnetic properties to the rocks which can be used to determine the age or structural history of formation by using the remaining magnetization as a result of earth's geomagnetic field. This remaining magnetization is called remanence and is a property of ferromagnetic materials (also of ferrimagnetic as in magnetite) where the magnetic domains are partially aligned if magnetized by an external magnetic field and remain magnetized when the field is removed. Magnetite can easily be oxidized in the presence of oxygen and transforms to maghemite, which is also a ferrimagnetic mineral, however with reduced magnetic properties.

Table 2.1. Classification of the iron oxides.

Iron oxides		Iron (oxy)-hydroxides	
Hematite	α-Fe_2O_3	Goethite	α-FeOOH
Magnetite	Fe_3O_4	Lepidocrocite	γ-FeOOH
Maghemite	γ-Fe_2O_3	Akagenite	β-FeOOH
Wüstite	FeO	Feroxyhyte	$\delta^{'}$-FeOOH
	β-Fe_2O_3	Ferrihydrite	$Fe_5HO_8.4H_2O$
	ε-Fe_2O_3	Bernalite	$Fe(OH)_3$
		Ferrous Hydroxide	$Fe(OH)_2$
		Green Rusts	$Fe^{III}_xFe^{II}_y(OH)_{3x+2y-z}A_z$
			δ-FeOOH
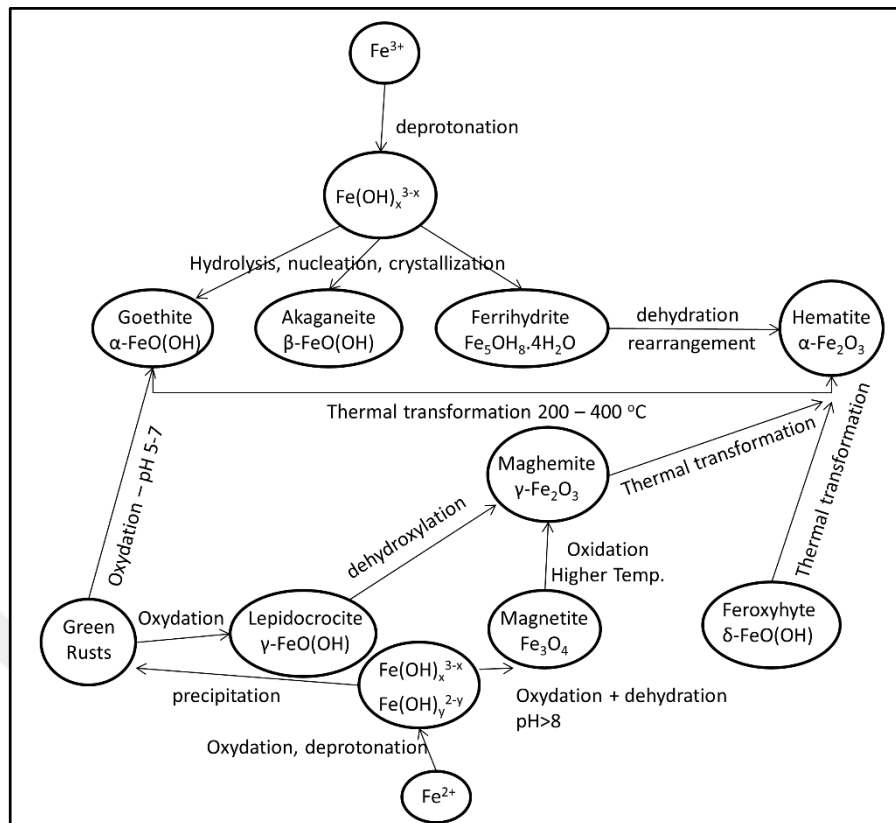
Figure 2.2. Formation pathways of the iron oxides and (oxy)-hydroxides [1].

On the other hand, iron oxides can be prepared synthetically via different procedures which affect the final properties of the material, such as particle size, morphology, crystallinity, size distribution, etc. Generally hematite, akageneite, goethite and ferrihydrite may be produced by hydrolysis of ferric salts. For this method it is important to control the hydrolysis rate, pH, temperature and ferric salt concentration in order to obtain single phase iron oxide [2, 3]. As mentioned before, ferrihydrite can also be used as a precursor for more stable iron oxides, such as goethite, hematite or their corresponding mixtures [1, 4, 5]. As goethite and hematite form via different pathways, formation conditions for one through a ferrihydrite precursor prevent the formation of the other. For instance, aggregation of ferrihydrite near its isoelectric point favors hematite formation, while increasing or decreasing the solution pH promotes goethite formation [6]. Oxidative hydrolysis of ferrous salts is a widely used method to produce goethite, lepidocrocite, magnetite, ferrihydrite and feroxyhyte. The transformation of ferrous ions via hydrolysis and oxidation to ferric compounds is accomplished through green rust of ferrous hydroxide intermediates. This is a

complicated method as it may produce different iron oxides or their mixtures. Like the hydrolysis of ferric salts, it is important to precisely control the reaction conditions to obtain a pure product. For some species, e.g. magnetite, it is essential to prevent oxidation by using an inert atmosphere. Generally, at low pH, lepidocrocite or goethite can form, while increasing the pH in the presence of a mild oxidant favors the formation of magnetite [7-9]. The presence of oxygen generally leads to the formation of goethite [10] while rapid oxidation as a result of a strong oxidant such as H_2O_2 yields feroxyhyte [11, 12]. The ratio of ferrous ion, base and oxidant concentrations can also result in a mixture of different iron oxides [13]. In addition physical phase transformations may take place under specific conditions for which the final product retains the crystal structure of the initial material as in the case of cubic maghemite particles formed through the oxidation of magnetite. Finally hydrothermal or thermal decomposition methods can be used to produce almost monodisperse iron oxide particles [14, 15]. This method involves continuous liberation of iron ions (especially Fe^{III}) at high temperature and pH and by the help of an oxidizing or a reducing agent the final phase is formed. The advantage of this pathway is controlling the supply of the reactant via decomposition of iron salt throughout the formation.

The synthesis pathways for iron oxides generally yield particles with diameters from a few nanometers to several micrometers with various morphologies. As mentioned before, it is also quite possible to have a mixture of various iron oxides as a result of specific conditions used for the synthesis of the particles, thus it is important to carefully characterize the product. The characterization of these particles is generally accomplished by transmission electron microscopy (TEM) for crystal size and morphology, X-ray diffraction (XRD) or electron diffraction (ED) for phase identification. Infrared absorption, Mössbauer and Raman spectroscopy can also be used for additional and supporting information. Furthermore, the color of the product may be indicative, as each iron oxide has a characteristic color which can be quantified by using theoretical colors of iron oxide given in the Munsell color system [1, 16]. It should be noted that XRD or Mössbauer spectroscopy are more reliable techniques as iron oxides often exist as mixtures and use of color as an indicator may not be conclusive. For phase identification of iron oxides generally XRD is preferred. By using the Bragg equation, the positions of the reflections obtained for a sample lead to the calculation of distances between the atomic layers (*d*-spacing) that can identify

the iron oxide phase(s) present, although it is important to account for lattice strain as is often neglected. For some iron oxides which have similar crystal structures (e.g. magnetite – maghemite) Raman and Mössbauer spectroscopy can be used as a complementary method to identify the structure [17].

2.2. MAGNETITE

Magnetite nanoparticles became one of the most used magnetic nanomaterials in heat transfer [18-20], water purification [21-23], biosensing [24, 25] and cell separation [26, 27] as well as in the biomedical field including drug delivery [28-30], magnetic hyperthermia [31, 32] and magnetic resonance imaging (MRI) [33, 34] due to its unique magnetic and biocompatible properties (Table 2.2). Magnetite contains both divalent ferrous and trivalent ferric ions and it is a member of the spinel group. In Nature it is most commonly encountered as octahedral crystals expressing their [111] faces (Figure 2.3). However, synthetic magnetite may have round, cubic or octahedral morphologies. Among all minerals it is the first one for which X-ray diffraction was applied.[35] Magnetite is ferrimagnetic at room temperature where the preferred magnetization is along [111] direction. Coercivity and remanence of magnetite are highly affected by morphology, size and size distribution of the particles [36, 37]. The arrangement of the different valence iron ions in two specific sites causes an electron transfer through a path generating a magnetic field. If the grain size of magnetite particles is less than about ~20 nm, individual particles have single randomly aligned magnetic domains leading to superparamagnetic behavior [38]. The effective usage of magnetite in specific applications is dependent on their size, shape and stability which are determined by the synthesis method. Magnetite nanoparticles also have a large surface-to-volume ratio and therefore easily aggregate in order to decrease the surface energy. Over-oxidation of magnetite, e.g. to maghemite due to the presence of oxygen during the synthesis or storage, affects the magnetization of the particles. As a consequence it is important to apply suitable surface agents such as polymers or biomolecules to prevent aggregation (i.e. increase colloidal stability) and oxidation of the magnetic core. There are versatile synthesis methods for preparing magnetite nanoparticles with different size, morphology and magnetic properties.

Table 2.2. Applications of magnetite nanoparticles. (Methods; 1: coprecipitation, 2: thermal decomposition, 3: hydrothermal synthesis, 4: physical transformation).

Method	Size (nm)	Application	Notes	Ref.
1,2	6 – 10	Heat transfer	28% increase in thermal conductivity of water upon addition of 2.5 wt. % particles. Changes in thermal conductivity depend on particle concentration, synthesis method and base fluid.	[18]
1	15	Heat transfer	Thermal conductivity of ethylene glycol increases with volume fraction and this enhancement is temperature independent.	[19]
1	60	Heat transfer	Laminar flow heat transfer coefficient of magnetic nanofluid increased up to 300% in the presence of an external magnetic field. This enhancement depends on Reynolds number as well as magnetic field strength.	[20]
3	9	Water purification	Magnetite-reduced graphene oxide composites were used. Over 91% and 94% removal of dye pollutants, rhodamine B and malachite green were achieved respectively.	[21]
4	12.5	Water purification	Effect of particles size on arsenic removal was studied and results showed that when particle size decreases from 300 nm to 12.5 nm, adsorption capacity increases 300 times.	[22]

Table 2.2. Applications of magnetite nanoparticles. (Methods; 1: coprecipitation, 2: thermal decomposition, 3: hydrothermal synthesis, 4: physical transformation – Continued).

Method	Size (nm)	Application	Notes	Ref.
1	10	Water purification	Magnetite-reduced graphene oxide composites were used. Composites show nearly complete removal of arsenic from water.	[23]
1	7	Biosensor	Aging of synthesized magnetite nanoparticles for 19 months did not influence the morphology and magnetic properties of the particles which were proposed to be used as microbeads for biosensor applications.	[24]
1	8	Cell separation	Particles were synthesized in the presence of a surfactant, polyethylene oxide/polypropylene oxide. 95% of *E. coli* was removed from the feed by countercurrent magnetophoresis after one pass. Separation efficiency increases with decreasing flow rate and increasing magnetic particle concentration.	[26]
1	10	Cell separation	Particles were coated with anionic, cationic and nonionic surfactants. Chitosan coated particles gave the highest recovery of *E. coli* (over 90%).	[27]
3	70	Drug delivery	Mesoporous magnetite nanoparticles have higher doxorubicin loading capacity than normal particles. 90% of the incorporated drug was released after 12 hours.	[29]

Table 2.2. Applications of magnetite nanoparticles. (Methods; 1: coprecipitation, 2: thermal decomposition, 3: hydrothermal synthesis, 4: physical transformation – Continued).

Method	Size (nm)	Application	Notes	Ref.
1	10-25	Drug delivery	Oleic acid coated magnetite nanoparticles were loaded with anti-cancer drugs doxorubicin and paclitaxel. Drug incorporation efficiency was 75% and 95% for doxorubicin and paclitaxel respectively. Complete release of the drug obtained after 2-3 weeks.	[28]
1	20	Drug delivery	Temperature responsive magnetite/PEO-PPO-PEO block copolymer nanoparticles were used. Uptake and release of ibuprofen was controlled by changing the temperature. Monosialotetrahexosylganglioside loaded magnetite was shown to be effective for spinal cord damage treatment.	[30]
1	10	Hyperthermia	Magnetic nanoparticles coated with cationic liposomes were used. The surface of 15 mm tumors in mice was maintained at 45 $^{\circ}$C by alternating magnetic field for 30 minutes and 2 rounds per day. Complete tumor regression was achieved after 1 to 6 rounds.	[39]
1	6	MRI	Measurements showed notably decreased T_1 and T_2 relaxation times. MRI signal intensity was 62% of the original after 5 days which offer prolonged monitor without further dosing	[33]

Briefly, co-precipitation [40], partial oxidation [8], high temperature thermal decomposition [14, 41, 42], microemulsion [43, 44] and hydrothermal synthesis [45, 46] are the most used methods for the production of magnetite nanoparticles [47-50]. The summary and specific properties of the abovementioned synthetic methods are presented in Table 2.3.

Figure 2.3. Natural octahedral magnetite from Cerro Huanaquino/Bolivia [51].

Among these pathways, co-precipitation (or chemical precipitation) is a facile and simple technique which uses the stoichiometric mixing of ferrous and ferric ions (2/1) in an inert environment followed by the addition of base to precipitate superparamagnetic magnetite particles (Figure 2.4b) leading to the following reaction [40]:

$$Fe^{+2} + 2Fe^{+3} + 8OH^- \rightarrow Fe_3O_4 + 4H_2O$$

The essential advantages of this method are that it can be carried out at room temperature and is easily scaled-up. It is also possible to reproduce the product if the reaction conditions (e.g. pH, temperature, type of the iron salt) are kept constant. However, it is difficult to control the size, shape and size distribution of the particles. Furthermore the saturation magnetization of the synthesized superparamagnetic particles is considerably less than that of bulk magnetite.

Several authors investigated magnetite formation using the co-precipitation method by altering the reaction conditions. Lin et al. synthesized magnetite nanoparticles having mean

size of 18 nm and broad size distribution using a chemical precipitation method without surfactant [52]. Frimpong et al. showed that applying a citric acid coating on magnetite nanoparticles in a two-step coprecipitation reaction leads to considerably different physical and magnetic properties compared to a one-step reaction in which more stable hydrophilic particles are obtained [53]. Kumar et al. successfully coated 14 nm superparamagnetic magnetite nanoparticles with poly(glutamic acid) sodium salt [54]. Martinez-Mera et al. prepared 4 nm to 43 nm of magnetite nanoparticles with coprecipitation method without surfactant at room temperature by varying the duration of the reaction [55]. Iwasaki et al. prepared size-controlled, highly crystalline magnetite nanoparticles in aqueous medium at room temperature and showed the particle size to be affected by the coexisting anions in the system [56]. Kang et al. reported a modified co-precipitation method where iron salts were added to a base solution in a controlled manner after which monodisperse and spherical magnetite nanoparticles were obtained. Furthermore, it was shown that maghemite particles can be obtained via direct oxidation of magnetite nanoparticles by aeration [57]. Recently, co-precipitation by slow addition of reactants was also demonstrated to produce single domain magnetite nanoparticles [58, 59].

Superparamagnetic magnetite nanoparticles can also be produced by the thermal decomposition method. These reactions are performed at high pressures and temperatures by using relatively expensive systems and solvents. In this method, nanoparticles with a high level of monodispersity can be achieved by the high temperature decomposition of iron precursors such as ferric acetylacetonate. However, without additional treatments, the synthesized particles are only dispersible in organic solvents. Sun and Zeng reported on the well-known procedure for the synthesis of monodisperse oleic acid capped magnetite nanoparticles. It was further shown that these particles can also be used to produce larger particles of desired size by using them as seeds in successive reactions [14]. Zhang and Misra used thermal decomposition method to produce magnetite nanoparticles with an average size of 5 nm [60], while, Wang et al. reported an alternative thermal decomposition method for magnetite particles using oleic acid as a stabilizer at relatively low temperature (140 $^\circ$C) [61].

The use of micoemulsions and hydrothermal synthesis are two other methods for the production of highly crystalline magnetite nanoparticles. Microemulsions are co-dispersions

of two immiscible liquids which are separated and stabilized by a suitable surfactant layer. The micro-droplets that are formed serve as a reactant compartment and also limit the nucleation and growth of the particles, thus allowing control of the final morphology.[62] Although it is possible to tune the reaction conditions in order to prepare magnetite nanoparticles with different properties [43], the yield is relatively low for such a complicated system which makes this method unsuitable for commercial production. On the other hand, hydrothermal synthesis, where particles are formed in a sealed reactor from an aqueous solution at high pressure and temperature, can be used as an alternative for the production of monodisperse magnetite nanoparticles [63, 64].
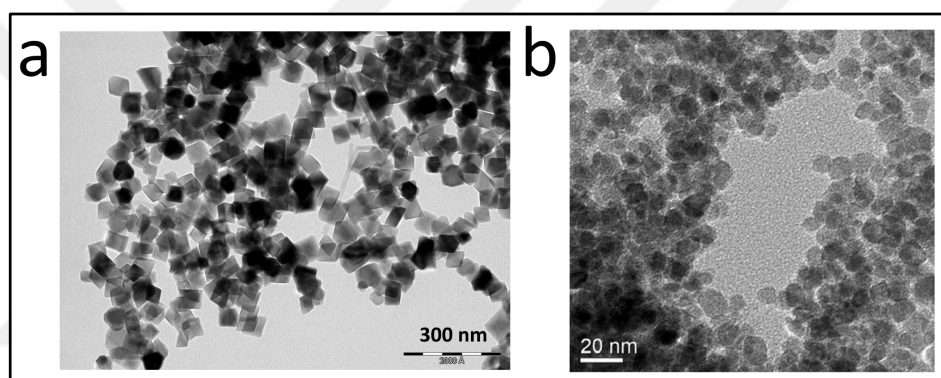
Figure 2.4. TEM images of the product synthesized by a) partial oxidation showing octahedral ferromagnetic nanoparticles [7] b) co-precipitation showing superparamagnetic particles with various morphologies [65].

In addition to the abovementioned synthesis methods which are capable of producing small, superparamagnetic magnetite nanoparticles, it is also possible to use the aqueous partial oxidation method for the synthesis of magnetite nanoparticles in the ferrimagnetic domain. In this method, ferrous ions are partially oxidized to ferric ions at basic conditions by the help of a mild oxidant. The method was first described by Sugimoto and Matijevic who performed the reaction at elevated temperatures; however, it is also possible to obtain monodisperse ferrimagnetic particles at ambient conditions [8, 9, 13]. The pioneering work of Sugimoto and Matijevic was then used and analyzed by many other groups [66]. Morales et al. used an ethanol/water mixture as solvent for the precipitation of ferrous sulphate in alkaline medium where it was partially oxidized to form magnetite nanoparticles. They

reported that the particles synthesized were stable at neutral conditions due to the presence of sulphate anions on the surface of the particles [67]. Vereda et al. followed the same approach and described specific iron/base/oxidant ratios for the synthesis of highly monodisperse ferromagnetic magnetite nanoparticles (Figure 2.4a) [68]. Although the majority of the published reports carried out the partial oxidation method at elevated temperatures, Nishio et al. reported a protocol for a size-controlled synthesis at various temperatures below 37 ºC. Their results also indicated that an increase in the reaction temperature from 4 to 37 ºC leads to a decrease in the average size of the particles from roughly 100 nm to 30 nm [9]. As this method can produce mixtures of various iron oxides, it is important to tightly control the reaction conditions in order to obtain pure magnetite (e.g. slower oxidation, higher pH) [1].

Table 2.3. Characteristics of the synthesis methods for magnetite [48].

Method	Temp.	Duration	Solvent	Size distribution	Control	Yield
Co-precipitation	20-90	Hours	Water	Relatively narrow	Poor	High
Partial oxidation	20-90	Hours	Water	Relatively narrow	Good	High
Thermal decomposition	>100	Hours-Days	Organic	Very narrow	Very good	High
Microemulsion	20-50	Hours	Organic	Relatively narrow	Good	Low
Hydrothermal synthesis	>200	Hours	Water Ethanol	Very narrow	Very good	Medium

In nature magnetotactic bacteria produce species-specific magnetite nanoparticles with uniform size and morphology at ambient conditions which suggest that a controlled biomineralization process takes place [69, 70]. Magnetite particles produced in

magnetotactic bacteria have average sizes of 35 to 120 nm[70] and are in the single domain size range of magnetite [71].
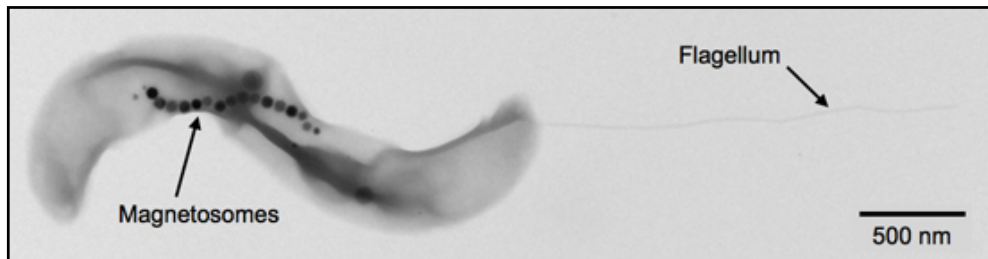
Figure 2.5. TEM image of a single magnetotactic bacteria [72].

Magnetite produced by magnetotactic bacteria can have different morphologies, including cuboctahedra, hexahedra and octahedra according to the bacteria species [73]. Magnetite particles produced in magnetotactic bacteria are enveloped by a lipid bilayer membrane vesicle called magnetosomes, which contain several membrane proteins (Figure 2.5) [70]. Magnetosomes are organized in a chain on a protein strand that follows the primary axis of the bacteria, which results in a magnetic dipole allowing the bacteria to orient itself in the geomagnetic field of earth [74-76]. Several magnetosome proteins have a hydrophobic N terminal and hydrophilic C terminal containing carboxylic and hydroxyl side chains that are known to bind iron ions [77]. Mms6, which is one of those proteins, was found to have an active role for the magnetite formation in some magnetotactic bacteria [77]. Later work by Prozorov et al. also support the hypothesis that the Mms6 serves for the formation of uniform and isomorphic magnetite nanocrystals [78]. Magnetite formed by the co-precipitation method in the presence of Mms6 produced uniform crystals with average sizes of 25 nm while the absence of this protein yields irregular shapes and a broad size distribution [77]. Amemiya et al. used partial oxidation of ferrous hydroxide with the addition of Mms6 to produce 20 nm cubic magnetite crystals, whilst in the absence, the particles were octahedral with an average size of 32 nm. In addition, the particles formed in the presence of Mms6 showed a narrower size range [79]. Iron binding analysis suggested that the C-terminal region of Mms6 is the iron binding site while the N-terminal was suggested to be the binding site for the magnetosome [77]. By using the functionality of the opposite ends of the peptide, for surface anchoring and mineral binding, respectively, Staniland et al. achieved a pattern

of uniform magnetite nanoparticles grown on a patterned self-assembled monolayer [80]. Further studies of Arakaki et al. concentrated on using short synthetic peptides mimicking the C-terminal and N-terminal of Mms6 protein in the partial oxidation method for producing magnetite nanoparticles. Magnetite synthesis using the peptide named M6A which contains the C-terminal acidic region of Mms6 resulted in the formation of uniform-sized cubo-octahedral crystals with narrow size distribution [81].

2.3. CONCLUSION

Iron oxides are encountered frequently in our daily life and exist in different forms in nature. These compounds, derived from iron and oxygen, differ in their crystal structure, morphology and magnetic properties. There are versatile synthetic methods for the production of iron oxides among which magnetite is possibly the most important one. The essential reasons behind the use of magnetite in various applications are its biocompatibility and superior magnetic properties as it is the most magnetic naturally occurring mineral known. Fields of application are versatile as the magnetic properties of magnetite particles vary according to the synthesis method used. Although magnetite was the subject of countless studies for decades, the synthesis pathways at ambient conditions mimicking the perfection of nature still remain a challenge. As the range of its applications in various fields continues to expand, it is no doubt that magnetite will get growing attention in the coming future.

2.4. AIM AND OUTLINE OF THE THESIS

The objective of the research presented in this thesis is to study extensively the formation, properties and applications of magnetite which is the most magnetic naturally occurring mineral. For this purpose, initially the control over magnetite formation via different synthetic routes was investigated. As the effective use of magnetite in desired applications depends on the stability and the magnetic properties of the particles, various polymers and surfactants were introduced to the most common synthetic methods to enhance the colloidal stability in aqueous medium. Furthermore the effect of these surface agents on the magnetic properties of the particles was studied. Finally, the possible applications of magnetite

nanoparticles in heat transfer systems were analyzed by investigating the impact of the presence of magnetite nanoparticles on the thermal conductivity of different base fluids.

Chapter 2 gives a general summary of the iron oxides and in particular magnetite. Literature survey on the synthesis methods and various applications that require tailored magnetic properties are also presented in this chapter.

Chapter 3 presents a study that focuses on the control of magnetite formation via co-precipitation and partial oxidation methods at ambient conditions in the presence of poly(amino acids), which mimics the mineralization process in Nature, specifically that of magnetotactic bacteria. The effect of these additives on the size, shape, organization and magnetic properties of magnetite are discussed in this chapter.

In chapters 4 and 5, the studies on the colloidal stability of both superparamagnetic and ferromagnetic magnetite nanoparticles are presented. For this purpose magnetite is synthesized by co-precipitaton and partial oxidation methods in the presence of biocompatible polymers and their effect on morphology and stability are examined.

Chapter 6 presents the reduction of magnetic properties due to the change in the thickness of the magnetically disordered layer at the outmost shell of magnetite nanoparticles upon application of surface agents that are mainly used to stabilize magnetite. Reduction of this magnetic phase was investigated for commercial (amine and carboxyl funtionalized) and synthesized (oleic acid coated) magnetite nanoparticles of 7 nm – 12 nm by using vibrating sample magnetometry and the tiron chelation test.

Finally, chapter 7 describes the effect of superparamagnetic magnetite nanoparticles on the thermal conductivity of polar base fluids. Magnetite nanoparticles were prepared by different synthetic routes in the presence of hydrophilic additives and the changes in thermal conductivity of water and ethylene glycol, which are common heat transfer fluids, were studied as a function of temperature and particle concentration.

3. BIOINSPIRED SYNTHESIS OF MAGNETITE NANOPARTICLES

3.1. INTRODUCTION

Nature produces materials with excellent chemical and physical properties and offers inspiration to understand ideal systems to understand and implement the corresponding formation pathways of these materials to synthetic pathways for producing novel materials with enhanced properties. For instance, many biominerals have superior mechanical [82, 83], optical [84, 85], and magnetic [86, 87] properties and most are composed of nano-scale substructures in mutual interaction with organic compounds [88-90]. Magnetite (Fe_3O_4) is a wide-spread magnetic iron oxide encountered in biological and geological systems and also used in many technological and biomedical applications [49], e.g. in drug delivery [28, 91], separation techniques [26] and as contrast agent in magnetic resonance imaging [92], due to its biocompatible and excellent magnetic properties. As magnetic properties are highly affected by the crystal size and morphology, it is crucial to control the formation of magnetite nanoparticles. In Nature this is achieved by organisms - such as magnetotactic bacteria, producing size-controlled magnetically aligned single crystals of magnetite within magnetosome membranes [93, 94], i.e. vesicles containing several proteins [77]. This controlled synthesis of magnetite is believed to be accomplished via precursor phases, which is a common pathway for other biominerals [95, 96]. Mms 6, which is one of the proteins in the magnetosome membrane vesicles was found to have an active role for the controlled magnetite formation in magnetosomes [79]. Further studies showed that hydrophilic acidic C-terminal region of Mms6 is responsible for the formation of uniform sized cubo-octahedral crystals with narrow size distribution [81].

Synthetically, the co-precipitation of Fe^{2+} and Fe^{3+} is the most applied route for the synthesis of magnetite [97]. This method uses the exact stoichiometric ratio needed for magnetite formation which is 1:2 for $[Fe^{2+}]$ and $[Fe^{3+}]$. As the amounts of the iron ions are well controlled, it is convenient to obtain magnetite particles preventing oxidation within the system by using an inert atmosphere (if not maghemite, Fe_2O_3, is obtained) [98]. This route generally produces superparamagnetic particles (<20 nm) with various morphologies. However, although the method is fully reproducible, the control over particle morphology,

mean size, size distribution and hence the magnetic properties is challenging without additional treatments due to fast reaction kinetics [99, 100]. It was previously shown that the corresponding fast reaction kinetics may be controlled through additives [77, 99, 101-103], the slow addition of reagents [59, 104] or using a more viscous reaction medium [101]. Additionally, the use of ferrihydrite precursor in the synthesis was shown to be an alternative pathway to improve control during magnetite formation [104]. Magnetite can also be synthesized through the gradual oxidation of Fe^{2+} to Fe^{3+} in the presence of an oxidant at high pH [66, 68, 105-109]. This oxidation step combined with the nucleation and growth of the particles requires longer reaction times than the more frequently used co-precipitation method. This gives better opportunities for surface active polymers to interact with the iron oxide surface and take a role in the nucleation and growth during formation. It is possible to obtain particles in the ferrimagnetic domain by using the partial oxidation method for which mostly elevated temperatures have been preferred [66, 68, 108]. This method is also capable of producing other iron oxides, such as goethite, feroxyhyte and ferrihydrite if the reaction conditions, e.g. pH and rate of oxidation, are not optimized for a particular product [98]. If the pH is around 7, goethite is formed, while at higher pH values magnetite formation is favored. Under these conditions, if the oxidation is too rapid due to aeration or presence of a strong oxidant then feroxyhyte is formed [98].

Several authors used the partial oxidation method for the synthesis of magnetite nanoparticles both in the presence and absence of additives using high temperatures or ambient conditions. Nishio et al. controlled the size of magnetite nanoparticles prepared by partial oxidation at pH 12.3 by varying the reaction temperature from 4 ºC to 37 ºC. It was shown that oxidation of ferrous hydroxide by the weak oxidant sodium nitrate yielded pure magnetite in this temperature range. It was further shown that by increasing the reaction temperature, the average size of the particles decreased from 100 nm to 30 nm (Figure 3.1) [107]. Amemiya et al. synthesized magnetite nanoparticles in the presence of Mms6 -an acidic protein that was shown to be active in the formation of bacterial magnetite in magnetotactic bacteria- and reported that the produced crystals had a uniform size, a narrow size distribution as well as a uniform morphology [79]. Furthermore, M6A, the acidic region of Mms6 that is leading the control over magnetite formation was used to control the morphology of the particles synthesized through in this method [81].
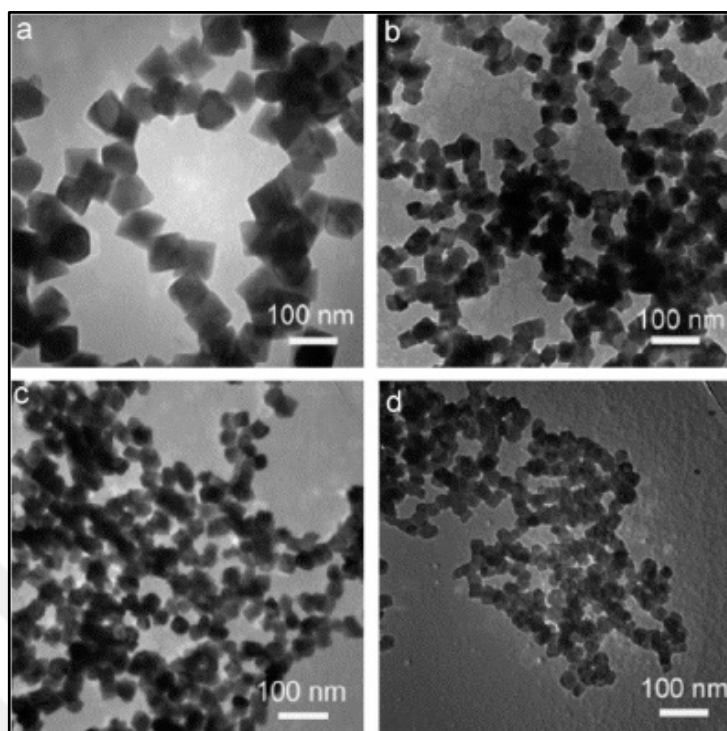
Figure 3.1. TEM micrographs of bare magnetite nanoparticles synthesized by partial oxidation of ferrous hydroxide at a) 4 ºC, b) 15 ºC, c) 25 ºC, d) 37 ºC [107].

Vereda et al. adopted the method described by Sugimoto and Matijevic [108] in which a ferrous hydroxide intermediate is oxidized by potassium nitrate at 90 ºC and obtained 50 nm octahedral magnetite nanoparticles without other iron oxide phases [68]. Osaka et al. further investigated the effect of different ferrous ion sources in the formation of magnetite particles by partial oxidation and their results showed that chloride and sulfate species yielded almost identical particles with sizes of 35 nm [110].

The present study aims to achieve biomimetic control over the size and shape of magnetite crystals but also over their organization in solution. For this, α,β-poly(aspartic acid) (pAsp) will be used as an additive for the synthesis of magnetite via partial oxidation of a ferrous hydroxide precursor to control the corresponding reaction kinetics. Results demonstrate that due to the fast reaction kinetics co-precipitation method is only capable of producing superparamagnetic magnetite nanoparticles that are not significantly affected by the presence of pAsp. On the other hand, the partial oxidation of the ferrous hydroxide precursor at room temperature yields larger ferrimagnetic nanoparticles in aqueous media. It is shown

that lower solution supersaturation allows control over nucleation, growth and colloidal stability of the particles using a negatively charged polymer.

3.2. EXPERIMENTAL

3.2.1. Materials

For the synthesis of iron oxide nanoparticles, analytical grade ferric chloride ($FeCl_3$) and ferrous sulfate heptahydrate ($FeSO_4.7H_2O$) were obtained from Riedel-de Haen. Ferrous chloride tetrahydrate ($FeCl_2.4H_2O$), sodium hydroxide (NaOH) and Sodium nitrate ($NaNO_3$) were purchased from Merck. α,β poly(Aspartic Acid) sodium salt (pAsp, M_w 7.7 kg/mol, DP 56) was obtained from Sigma Aldrich (Figure 3.2). All chemicals were used as received.
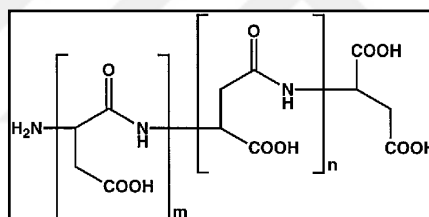
Figure 3.2. Structure of α,β poly(aspartic acid).

3.2.2. Characterization

3.2.2.1. Transmission electron microscopy (TEM)

For dry TEM, 200 mesh Cu grids with carbon films (Agar Scientific) were used. Sample preparation involved dropping 3 µL aqueous dispersion onto a TEM grid, filtering and drying by air. For cryoTEM, 200 mesh Cu grids with Quantifoil R 2/2 holey carbon films (Quantifoil Micro Tools GmbH) were used. Sample preparation was performed using an automated vitrification robot (FEI Vitrobot Mark III) by plunging in liquid ethane [111]. All TEM grids were surface plasma treated for 40 seconds using a Cressington 208 carbon coater prior to use. TEM samples were studied using a FEI Tecnai 20 (type Sphera) operated at 200

kV, equipped with a LaB$_6$ filament and a 1k x 1k Gatan CCD camera, or on the TU/e cryoTITAN (FEI, www.cryotem.nl) operated at 300 kV, equipped with a field emission gun (FEG), a post-column Gatan Energy Filter (GIF) and a post-GIF 2k x 2k Gatan CCD camera. Gatan DigitalMicrograph (including DiffTools) and ImageJ softwares were used for TEM image and SAED pattern analysis.

3.2.2.2. *Crystal size and shape measurements*

Crystal size distributions were determined by manually measuring both the long and short axis of 100-200 individual crystals per sample in calibrated TEM images in MATLAB. The average of the long and short axis per crystal was taken as the crystal size. The measured particles were categorized according to their morphology and classified as "octahedral" when the crystal facets could be clearly discriminated, or "rounded" when not.

3.2.2.3. *Cryo-electron tomography*

The 3-dimensional (3D) reconstructions were obtained from tilt series recorded on the TU/e CryoTitan. The alignment and 3-dimensional (3D) reconstruction of the raw data sets was performed with the software IMOD [112]. The segmentation and visualization of the 3D volumes was performed with the software Amira 4.1 (Mercury Computer Systems) and Avizo (Visualization Science Group).

3.2.2.4. *X-ray diffraction (XRD)*

XRD measurements were performed on a Rigaku Geigerflex powder diffractometer using copper radiation at 40 kV and 30 mA and a graphite monochromator to eliminate Cu K$_\beta$ radiation. Samples were prepared on cover glasses from dried ground powder. The XRD patterns were acquired by step scans with step sizes of 0.01°- 0.02° and an appropriate dwell time.

3.2.2.5. *Vibrating sample magnetometry (VSM)*

VSM measurements were performed on a TM-VSM101483N7-MRO magnetometer (Tamakawa Co., Ltd., Sendai, Japan). Samples were prepared by dispersing ~ 3 mg dried sample in a mixture of 1 mL 40% SDS-PAGE solution, 10 µL TEMED (N,N,N',N'-tetramethylethylenediamine, crosslinker) and 10 µL 10% APS buffer (activator), which

gellifies in a few minutes to fix the sample. The magnetic hysteresis loops were acquired at room temperature from +1 T to −1 T. The results were corrected for the diamagnetic background of the sample container/holder and normalized with respect to the sample mass.

3.2.2.6. Raman spectroscopy

Raman spectroscopy was performed on a Jobin-Yvon Labram spectrometer equipped with HeNe laser (excitation wavelength 632.81 nm), a holographic grating (600 grooves/mm), an ultra-long working distance objective (Olympus, magnification 100 x, numerical aperture 0.8) and a CCD camera.

3.2.2.7. Zeta Potential measurements

Surface charge analysis was performed on a Malvern Zetasizer Nano SZ instrument. Magnetite particles were dispersed in water via ultrasonication. Disposable DTS1060 zeta cells were used for zeta potential measurements consisting of 12 zeta runs at 20 °C.

3.2.3. Synthesis of superparamagnetic magnetite nanoparticles by co-precipitation

Ferrous (Fe^{2+}) and ferric (Fe^{3+}) salts (molar ratio 0.5, total Fe concentration 32.5 mM) were dissolved in 80 mL ultrapure water, which was de-aerated for 30 min using a N_2 flow to remove dissolved oxygen, by mixing for 15 min using a mechanical stirrer at a constant stirring rate of 50 rpm. Addition of 10 mL, 1.285 M NaOH solution to the aqueous iron mixture caused immediate precipitation of magnetite as indicated by a rapid color change from yellow (Figure 3.3a) to black (Figure 3.3b). The resulting mixture was aged for 30 min while stirring. For the synthesis in the presence of pAsp, the polymer was dissolved in water to which the iron chloride salts were added (amino acid/Fe ratio = 1/5). All reactions were performed at 20 °C in a jacketed vessel and the temperature was controlled by an external thermostat bath. Finally nanoparticles were collected from the suspension for further analyses and dried in a vacuum oven for overnight at 60 °C.
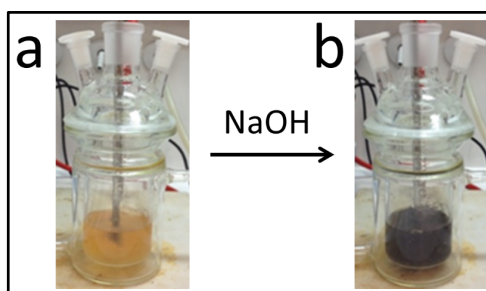
Figure 3.3. Color change of the reaction mixture during magnetite synthesis by co-precipitation from a) orange to b) black after addition of NaOH.

3.2.4. Synthesis of ferrimagnetic magnetite nanoparticles by partial oxidation

The synthesis of magnetite nanoparticles by partial oxidation was adopted from previous studies with minor modifications [106, 107]. First, 10 mL 0.1 M ferrous chloride solution was added to 190 mL 21 mM NaOH solution. Both solutions were de-aerated for 1 hour. Then, 0.3 g NaNO$_3$ was added for the partial oxidation of ferrous hydroxide. The resulting mixture was aged for 24 hrs while stirring at 50 rpm. Throughout the synthesis, a gradual color change from whitish green to dark green and finally to black was observed, indicating the formation of intermediates and magnetite, respectively (Figure 3.4). For the synthesis in the presence of pAsp, the polymer was dissolved in the NaOH solution before the ferrous chloride solution was added (amino acid/Fe ratio = 1/5). All reactions were performed at 20 °C. Nanoparticles were collected from the suspension for further analyses and dried in a vacuum oven for overnight at 60 °C.
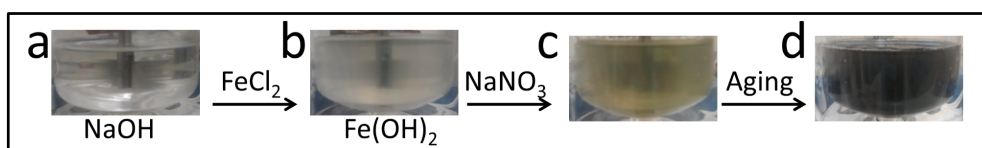
Figure 3.4. Color change of the reaction mixture during magnetite synthesis by partial oxidation from a) clear to b) whitish green after the addition of ferrous salt indicating formation of Fe(OH)$_2$ precursor and to c) dark green showing the intermediate formation and finally to d) black.

3.3. RESULTS AND DISCUSSION

Magnetite nanoparticles were first synthesized via a fast co-precipitation method where sodium hydroxide solution is added rapidly to a mixture of ferrous and ferric salts in de-aerated water (final pH 12.5) to instantaneously precipitate magnetite nanoparticles. Superparamagnetic magnetite synthesized by this method is known to consist of crystalline random oriented nanoparticles with various morphologies, having an average size in between 6-10 nm with a broad size distribution [99].
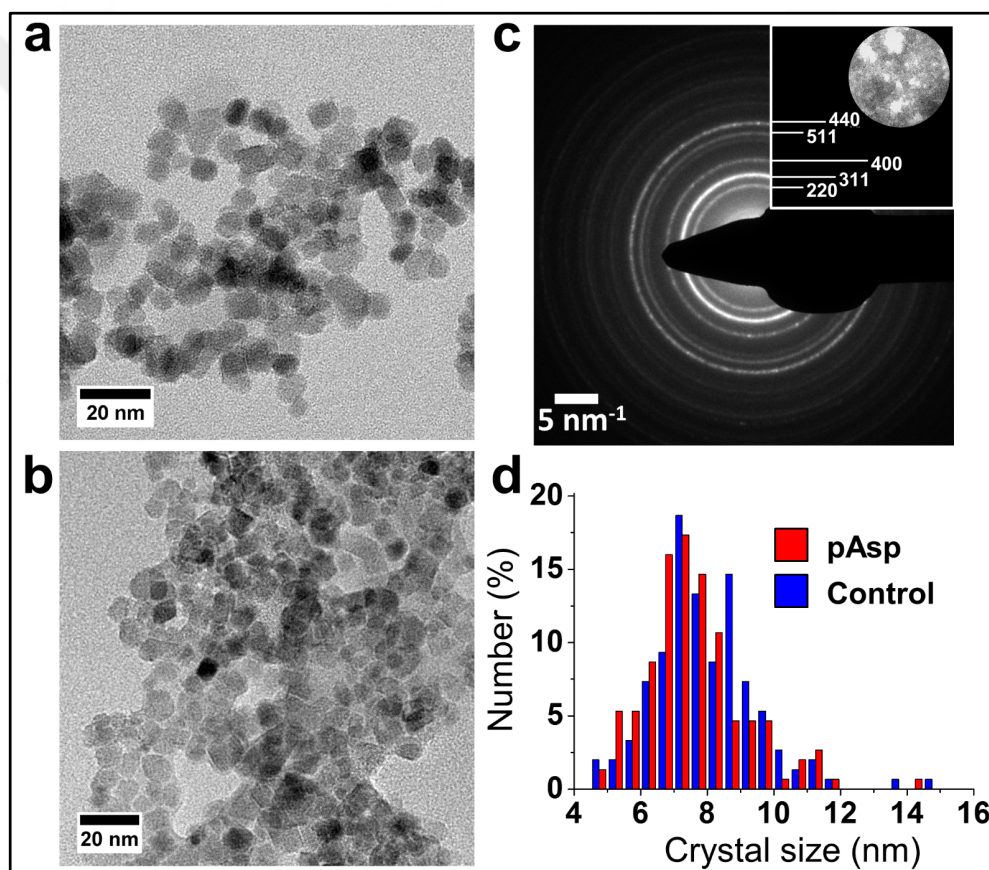
Figure 3.5. Magnetite synthesis by co-precipitation. a) TEM image of control particles, b) TEM image of particles synthesized in the presence of pAsp, c) Typical SAED pattern of particles via co-precipitation showing diffraction rings indexed as magnetite crystal planes, d) Crystal size distributions without (Conrol) and with pAsp as an additive.

Initially, the presence of a magnetite phase was confirmed by selected area electron diffraction as shown in Figure 3.5c, which exhibited characteristic lattice indices of Magnetite/Maghemite phases and white spots/bright diffraction rings indicated the formation of highly crystalline nanoparticles [98]. According to TEM, particles had various morphologies from cubic to spherical when the synthesis was performed either in the presence or absence (control) of pAsp (Figures 3.5a and 3.5b). Size analysis by measuring particle sizes on TEM micrographs showed that the synthesis performed in the presence of pAsp gave particles in the range of 4 nm to 15 nm having an average size of 7.6 nm. Similarly when the synthesis was performed without any additive (control experiment), magnetic nanoparticles had an average size of 8 nm. The sample standard deviations of the populations were found to be as 1.5 nm for both of the experiments conducted with and without pAsp, respectively (Figure 3.5d and Table 3.1).

Table 3.1. Crystal size and shape measurements for products of co-precipitation, without (control) and with poly(aspartic acid) (pAsp) as an additive.

Sample	Number of measured crystals	Crystal size ± standard deviation
Control	150	8.0 ± 1.5 nm
pAsp	150	7.6 ± 1.5 nm

Finally, the magnetic properties of particles synthesized in the presence and absence of pAsp via co-precipitation method was investigated by Vibrating sample magnetometry (VSM). Hysteresis loops for both control and pAsp samples showed no coercivity and remanence, indicating superparamagnetic behavior as expected on the basis of their small particle diameters (<10 nm) (Figure 3.6). As the saturation magnetization values were similar for both cases and no significant influence on neither the morphology nor the size of the magnetite nanoparticles were obtained via addition of pAsp, it was concluded that the additive had no significant influence on the formation of magnetite nanoparticles. This was attributed to the fast reaction kinetics associated with the rapid increase in pH which induced a high supersaturation and the consequent formation of many nucleation points.

In order to slow down the reaction kinetics, oxidative aging of ferrous hydroxide precursor was applied for the synthesis of magnetite nanoparticles in ferrimagnetic domain. Synthesis was performed using a method previously described by Nishio et al [107]. Briefly, ferrous chloride and sodium hydroxide solutions (pH 12.3) which were previously deaerated for 1 hour, are mixed in a well-sealed jacketed reactor. Upon mixing, the color of the solution immediately turns into a whitish green, indicating the expected formation of ferrous hydroxide precursor, which is then gradually turned to dark green and black after the addition of the oxidant. Reactions were performed at room temperature under continuous nitrogen flow.
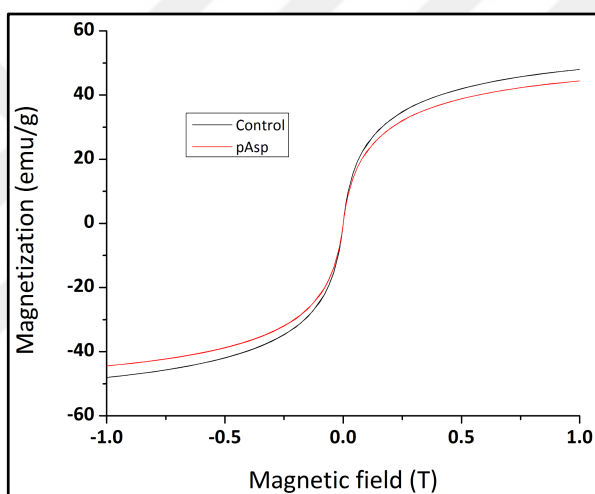
Figure 3.6. Hysteresis loops for particles synthesized in the presence and absence (control) of pAsp.

Initially, time resolved experiments were performed on the control experiment (without additives) in order to have detailed insight in the early stages of magnetite formation by partial oxidation. For this purpose, samples were taken in their native state at different time intervals and collected samples were immediately vitrified in liquid ethane using a FEI Vitrobot [111] which was also deaerated with nitrogen to prevent the uncontrollable oxidizing by air. Later on, samples were analyzed with Cryo-TEM. It was decided to take samples at $t = 0$ which is defined as the time when the ferrous salt solution was added into the sodium hydroxide solution, and one and then two hours after the addition of the oxidant which promotes the gradual oxidation of initially formed ferrous hydroxide precursor.

Low dose electron diffraction (LDED) analysis showed that the addition of ferrous chloride solution to the base solution precipitated the expected platelets of $Fe(OH)_2$ which was validated by matching corresponding *d*-spacing values with the literature (Figure 3.7a) [98]. After the addition of nitrate, the whitish green color of the ferrous hydroxide changed to dark green. While cryo-TEM did not show any changes on the morphology or size of the precursor, additional reflections obtained by low dose electron diffraction indicated a phase transition to other intermediates with different stoichiometries (Figure 3.7b).
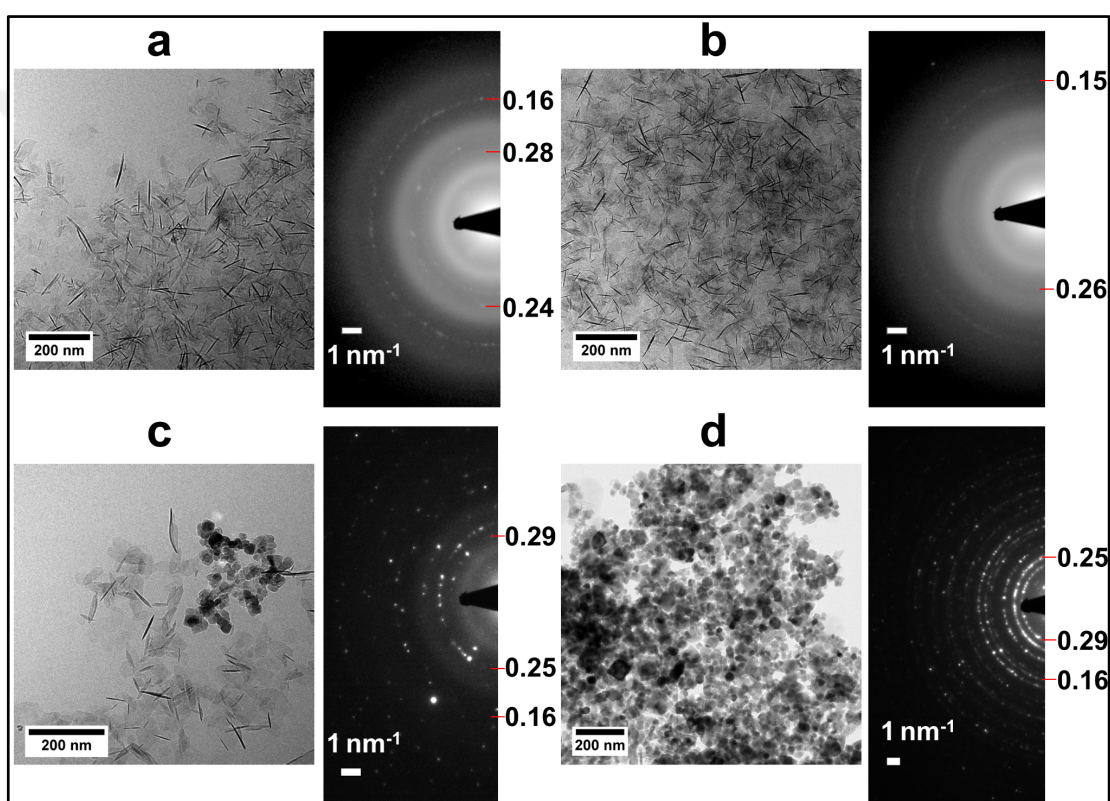
Figure 3.7. Low-dose electron diffraction patterns for the early stages of magnetite formation through partial oxidation of $Fe(OH)_2$ precursor in the absence of pAsp. a) SAED pattern of particles after addition of Fe(II) to the base solution indicating formation of $Fe(OH)_2$ precursor b) SAED pattern of particles 1 hour after the addition of oxidant showing additional reflections c) SAED pattern of particles 2 hours after the addition of oxidant showing phase change of the precursor and formation of magnetite crystals d) SAED pattern of particles after 24 hours showing diffraction rings matching with magnetite. Brightness and contrast are adjusted in all images for better visibility.

As the obtained d-spacing values of these intermediates were close to many other iron oxides, no definite assignment could be made. However, after two hours, the conversion of these intermediates to magnetite was observed (Figure 3.7c) and full transformation was achieved after 24 hours (Figure 3.7d). As the average size and morphology of the precursors formed at the early stages (hexagonal platelets of typically ≈ 70 nm) were completely different to those of the magnetite particles obtained after 2 hours (octahedral, ≈ 30 nm), suggests that the conversion occurs through a dissolution-reprecipitation mechanism rather than through a solid state conversion. It was also suggested that due to the formation and precipitation of the $Fe(OH)_2$ precursor and other possible intermediates as a result of their low solubility at the corresponding pH, high supersaturation levels as in the case of co-precipitation method were avoided. This provides an extended period of growth after nucleation and enhances the possibility of interaction in between the additives and the formed crystal surface.

After showing the possibility of using the partial oxidation of ferrous hydroxide for controlled synthesis of magnetite, experiments were performed both in the presence and absence of pAsp. The formation of magnetite was first demonstrated by XRD and SAED analyses (Figure 3.8b and 3.8c). Along with magnetite, the formation of minor amounts of goethite was also indicated by XRD which was possibly formed due to local low pH regions [98]. Although XRD is sufficient for distinguishing magnetite and/or maghemite from other types of iron oxides, it is not straight forward to classify magnetite and maghemite separately as those have almost the same d-spacing values and diffraction patterns. As a consequence Raman spectroscopy was carried out which was found to be adequate for distinguishing magnetite from maghemite [113]. As illustrated in Figure 3.8e, iron oxide nanoparticles synthesized in the absence of any additives via the partial oxidation method has an intense peak at 671 cm^{-1}, confirming that sample consisted of magnetite only [113].
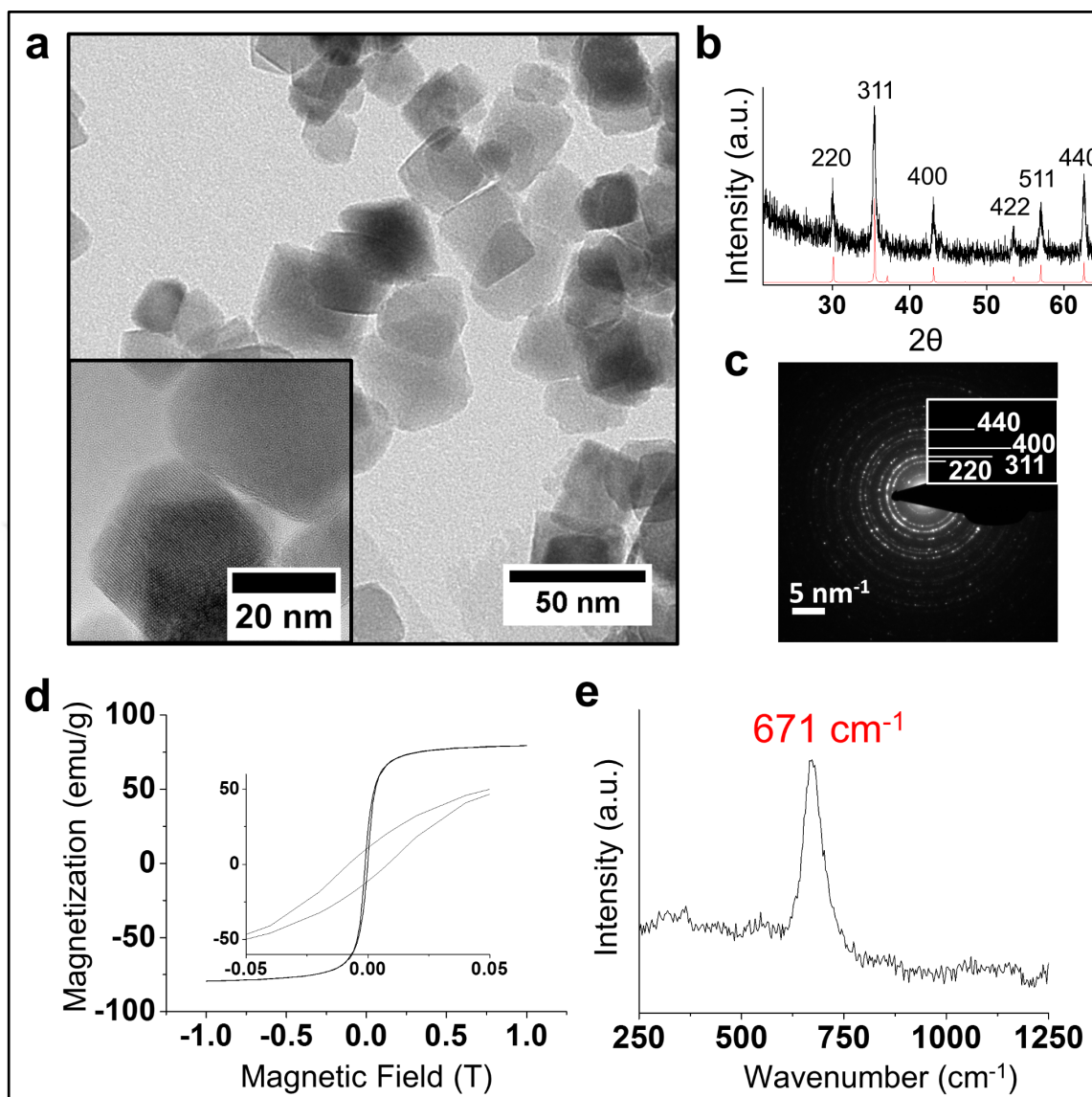
Figure 3.8. Magnetite synthesis through partial oxidation without additives. a) TEM images of the particles Inset: TEM image at higher magnification b) XRD pattern with indexation to magnetite crystal planes c) SAED pattern showing diffraction rings indexed to magnetite d) Hysteresis loop by VSM measurement Inset: Enlargement of magnetic hysteresis showing coercivity and remanence e) Raman spectrum indicating non-oxidized magnetite.
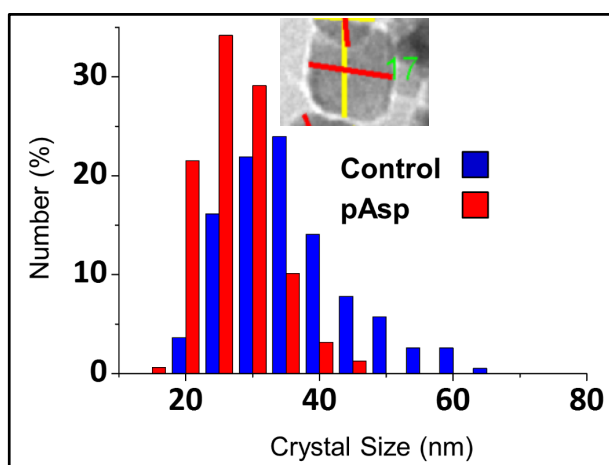
Figure 3.9. Size distribution of the particles synthesized by partial oxidation in the absence (control) and presence of pAsp. Inset : Long and short axis measurement of an individual particle.

Table 3.2. Crystal size and shape measurements for products of partial oxidation, without (control) and with poly(aspartic acid) (pAsp) as an additive.

Sample	Number of measured crystals	Crystal size ± sample standard deviation	Number of octahedral crystals (fraction)	Number of rounded crystals (fraction)
Control	192	34 ± 11 nm	131 (65%)	72 (35%)
pAsp	158	25 ± 6 nm	29 (15%)	165 (85%)

TEM results showed that particles formed in the absence of pAsp had an average size of 34 ± 11 nm (Figures 3.8a and 3.9) of which 65% had octahedral morphology (Figures 3.11b-d, Table 3.2). On the other hand, when the synthesis was performed in the presence of pAsp, the average size of the particles decreased to 25 nm (Figures 3.10a and 3.9). TEM and cryo-TEM analysis revealed that, unlike for the control experiment, the product consisted of 85% rounded particles showing the role of polymer as a growth control agent (Figures 3.11f-h, Table 3.2). The size analysis further showed that the change in the short axis length of the particles is comparable to the change in long axis length when the synthesis was performed

in the presence of pAsp, indicating no elongation on a specific direction due to polymer attachment. This result indicates that pAsp inhibits the particle growth by unspecific surface binding. Further comparison of the relative amounts of rounded vs. facetted shapes for magnetite nanoparticles of the same size range (25 – 35 nm) synthesized in the presence and absence of pAsp showed that the number of rounded morphologies were consistently higher for the particles synthesized under the influence of pAsp which demonstrated that the development of facets is not connected to the larger particles size of the control crystals and underlines the role of polymer as a growth controller (Figures 3.11a-c-e-g). Additionally, the reduced size distribution suggests that pAsp is also able to control the nucleation period as compared to the control experiment. Unlike for the control experiment, which led to the formation of random aggregates, TEM showed that the particles synthesized in the presence of pAsp formed long strings (Figures 3.10b-c), which was attributed to the corresponding alignment of magnetic dipoles and/or the chelation of functional (active) carboxyl groups of pAsp on the magnetite surface during nucleation and growth stages, as proposed previously [114, 115]. Additionally cryo-TEM and cryo-ET were used in order to clarify whether the particles had formed strings on the TEM grid due to drying or whether string formation occurred already in solution. Figures 3.10d and 3.10f clearly show that the particles had already formed chains in solution and are not the result of drying. It should also be noted that the strings of particles were dispersible in water, in contrast to the control particles that precipitated immediately. Furthermore, zeta potential measurements of the sample showed that the net charge of the particle surface was around -30 mV, suggesting that the polymer is present on the surface and prevents the uncontrolled aggregation that occurs for bare particles. Additionally, the obtained reduction in particle size and the observed morphological changes also suggested that pAsp was adsorbed to the nanoparticle surface and inhibits the growth.
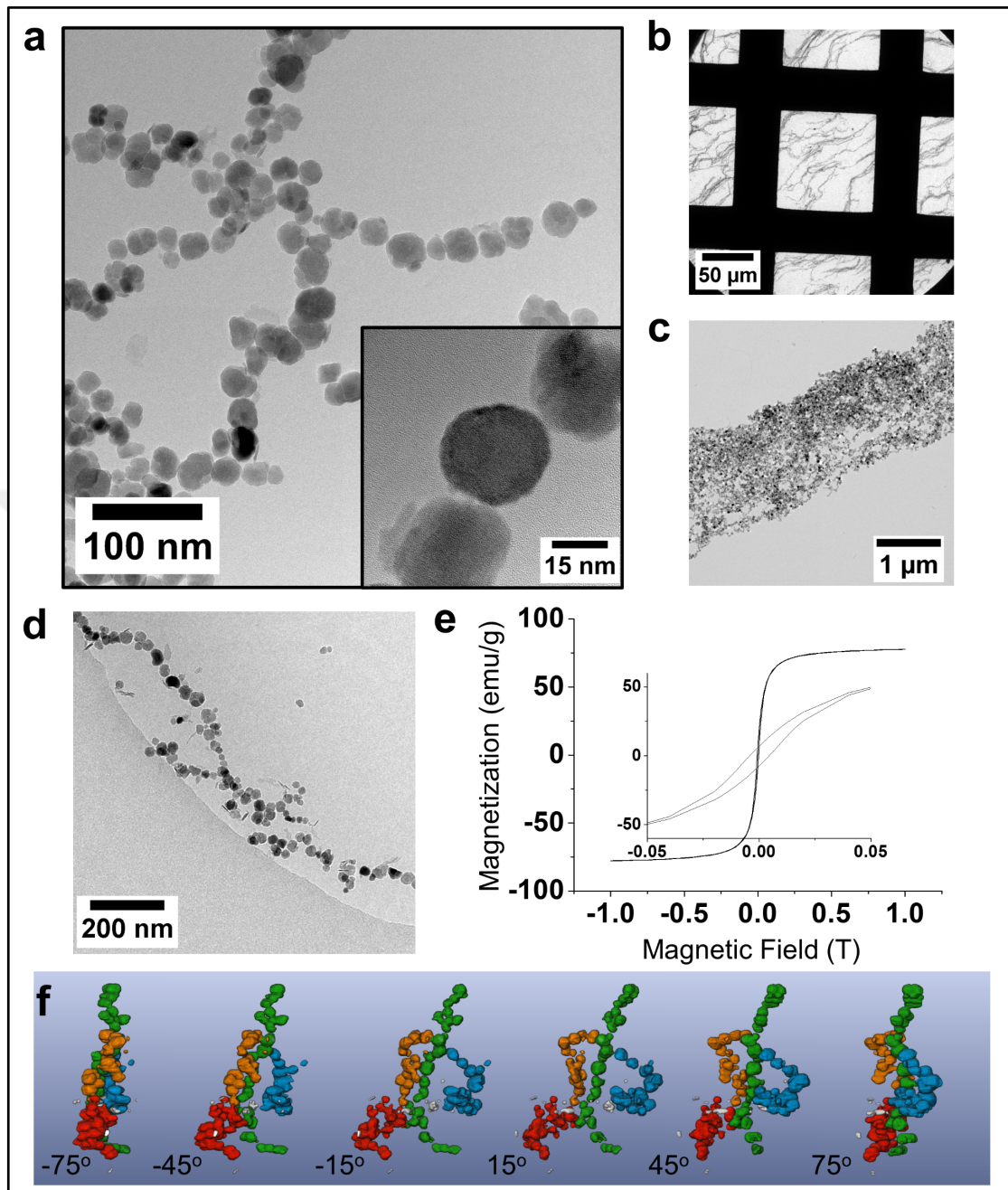
Figure 3.10. Magnetite synthesis through partial oxidation in the presene of pAsp. a) TEM images of the particles Inset: TEM image at higher magnification b,c) Low-magnification dry TEM images of the product showing the nanoparticles assemble into long strings d) Cryo-TEM image of the particles e) Hysteresis loop by VSM measurement Inset: Enlargement of magnetic hysteresis showing coercivity and remanence f) Computer visualization of an assembly of nanoparticles viewed under different tilt angles showing attachment of different strings with different colors.
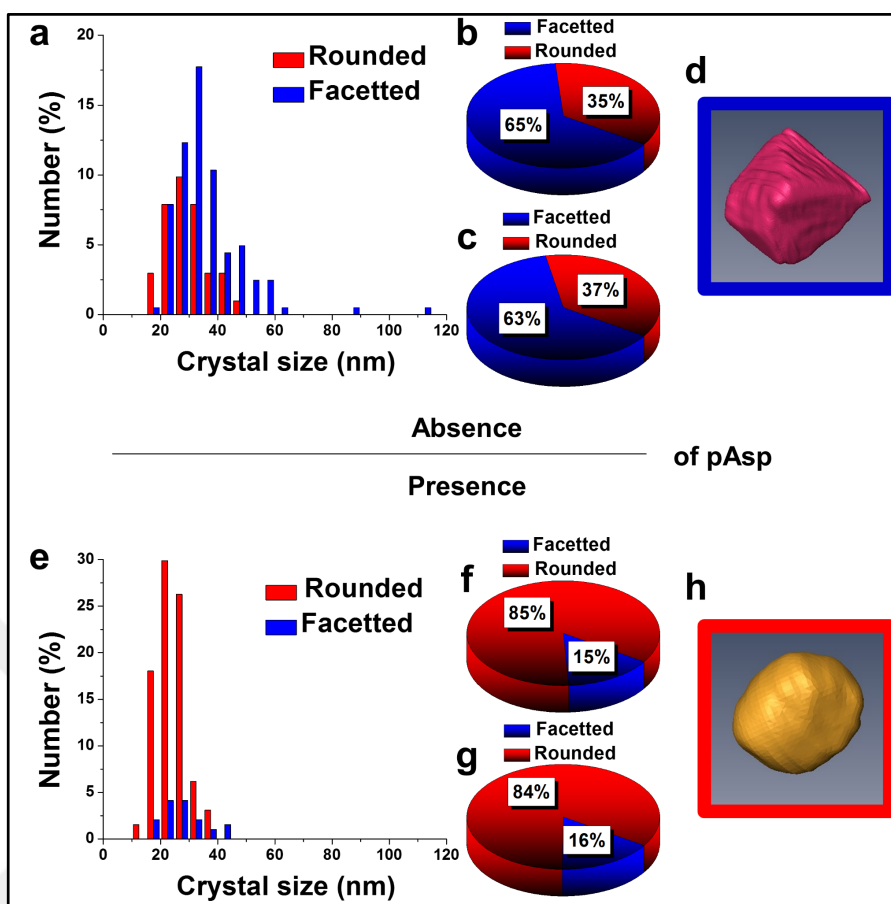
Figure 3.11. Size and morphology distributions for particles synthesized in the absence (a,b,c,d) and presence (e,f,g,h) of pAsp. a,e) Size distribution of particles, b,f) Morphology distributions of particles, c,g) Morphology distributions of particles in the size range of 25 nm – 35 nm, d,h) 3D visualizations of the main morphology obtained by cryo-electron tomography (Cryo-ET).

Magnetite nanoparticles synthesized by partial oxidation in the presence of pAsp were also analyzed by liquid cell STEM for which a sample is introduced in a chamber defined by two Si_3N_4 membranes and which allows visualization of a specimen in aqueous medium via scanning transmission electron microscopy [116]. STEM imaging for particles prepared in the presence of pAsp, given in Figure 3.12, confirmed the existence of strings composed of individual particles dispersed in solution, as was demonstrated by cryo-TEM. The measurement also showed that the individual particles within the solution were fixed in distinct chains and did not attach/detach or exchange between chains. Shorter chains were found to be more mobile while the aggregated chains had no movement at all. Liquid cell

TEM analysis could not be performed on bare control particles as those were not stable in aqueous medium and accumulated on the Si₃N₄ windows of the chamber.

For the investigation of their magnetic properties, hysteresis loops were obtained with a vibrating sample magnetometer (VSM) at room temperature for dry particles and are given in Figures 3.8-d and 3.10-e. Both in the presence and absence of pAsp, the particles have ferrimagnetic properties as is demonstrated by the existence of remanence and coercivity in the magnetization loop.
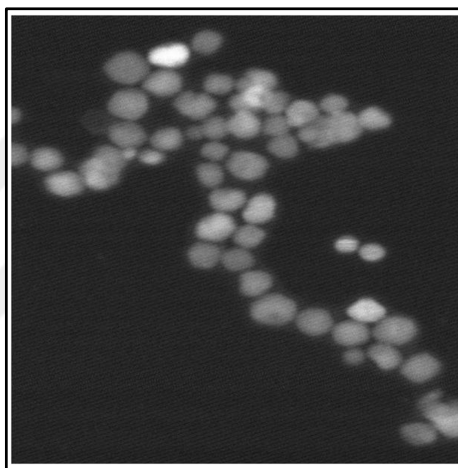
Figure 3.12. Scanning Transmission Electron Microscopy (STEM) image of particles synthesized in the presence of pAsp through partial oxidation.

This observed ferrimagnetism for both the control and the polymer-stabilized particles is solely due to larger average particle size (25 – 35 nm) compared to the ~8 nm particles obtained from the co-precipitation reaction. For bare particles saturation magnetization (M_s) value is around 79.4 emu/g which is slightly lower than the value of 87.8 emu/g stated by Nishio et al. for the same type of particles [107]. The saturation magnetization for the particles synthesized in the presence of pAsp was found to be 77.7 emu/g, which is slightly lower than for the bare particles and attributed to the smaller particle size. In addition, this decrease in saturation magnetization will be partially due to the adsorption of non-magnetic pAsp onto the surface of the particles, as shown previously by Yuan et al. and as is also discussed in chapter 6 [117]. The coercivity of pAsp-coated magnetite particles was found

to be lower than that of bare particles as the average size was smaller. It is further known that the morphology of the magnetic particles also affects the coercivity in the order of spheres<cubes<octahedral [98].

For the comparison of co-precipitation and partial oxidation methods that produce different particles with different magnetic properties (superparamagnetic and ferrimagnetic particles, respectively), it is important to consider the corresponding reaction conditions. In the case of co-precipitation, solution supersaturation (σ) with respect to magnetite is quite high, as shown in Equation 3.1:

$$\sigma = \ln\left(\frac{[Fe]_0}{[Fe]_{eq}}\right) \approx 14 \tag{3.1}$$

where, $[Fe]_0$ is the total initial iron concentration that is equal to 2.9×10^{-2} M and $[Fe]_{eq}$ is the solubility of magnetite (3×10^{-8} M) [118]. This high supersaturation leads to immediate formation of many nucleation sites after the addition of base. As the formation of magnetite nanocrystals consumes all the iron ions in the solution, while the pH remains constant, further growth of the particles is prevented. On the other hand, for partial oxidation, the soluble ferrous ion concentration drops remarkably from initial $[Fe^{2+}] = 5$ mM to $[Fe^{2+}]_{eq} \approx 2.8 \times 10^{-12}$ M, as shown below:

$$K_{sp}(\text{ferrous hydroxide}) = [Fe^{2+}]\,[OH^-]^2 = 10^{-15.15} \approx 7.1 \cdot 10^{-16} \text{ [98]} \tag{3.2}$$

$$[Fe^{2+}]_{eq} = K_{sp} / [OH^-]^2 = 7.1 \cdot 10^{-16} / (1.6 \cdot 10^{-2})^2 \approx 2.8 \cdot 10^{-12} \text{ M} \tag{3.3}$$

Although it is difficult to estimate the solubility of magnetite under these conditions due to the continuous change in $[Fe^{3+}]$, the low solubility of ferrous hydroxide precursor ensures that high supersaturation levels are prevented during conversion of Fe^{2+} to Fe^{3+}, which reduce the number of nucleation events and thus allow continuous growth after nucleation, leading to larger particles.

3.4. CONCLUSION

Magnetite nanoparticles were successfully synthesized by the aqueous partial oxidation of ferrous hydroxide precursor in alkaline medium. The control experiment which was conducted at room temperature produced large aggregates of octahedral, ferrimagnetic magnetite nanoparticles having an average size of roughly 35 nm. When the synthesis was performed in the presence of pAsp, the average size, morphology, organization and stability in aqueous medium was found to be affected due to polymer attachment onto the surface of magnetite crystals. Results showed a decrease of the average particle size from 35 nm to 25 nm, while the morphology of the particles changed from facetted to spherical. It was demonstrated by liquid STEM and cryo-TEM analysis that the particles formed micro-chains composed of many individual magnetite crystals due to interparticle magnetic or electrostatic interactions. No detachment of the nanoparticles was observed in liquid cell TEM experiments. The presence of pAsp also enhanced the colloidal stability of the particles due to negative surface charge which gives the opportunity to use the synthesized particles in different applications. As the same additive had no influence on the final product in the co-precipitation method, the importance of the reaction kinetics on the controlled formation of magnetite nanoparticles is pointed out. It is proposed that the polymer additive does not affect the crystal nucleation or growth throughout the co-precipitation method. This is a result of faster reaction kinetics, which leads to the immediate formation of many nucleation sites and depleting the iron source needed for further growth. In contrast, for partial oxidation which is based on the gradual oxidation of ferrous hydroxide precursor, the slower reaction kinetics allows the pAsp to interact with the developing mineral and to have considerable effect on mineralization process. The decrease in average size, the changes in particle morphology from octahedral to spherical and the narrower size distribution suggest that pAsp is active during both nucleation and growth. The alignment of the particles is most likely due to magnetic dipole interactions while the polymer prevents the aggregation of individual strings composed of several ferrimagnetic magnetite nanoparticles.

Hence, with this bio-inspired approach, it is possible to alter the kinetics of mineralization of magnetite nanoparticles by the addition of simple polymeric additives which allows the control over size, shape and organization thus magnetic properties in aqueous medium and at ambient conditions as are also used by magnetotactic bacteria

4. DISPERSION OF SUPERPARAMAGNETIC MAGNETITE NANOPARTICLES USING THERMORESPONSIVE STABILIZER POLY(ETHYLENE IMINE)-GRAFT-POLY(OLIGO(ETHYLENE GLYCOL METHYL ETHER) METHACRYLATE

4.1. INTRODUCTION

Magnetic iron oxide particles having sizes from a few nanometers to several micrometers are widely used in a number of biomedical applications such as drug delivery [49, 119], magnetic resonance imaging (MRI) [120-122] and separation techniques [26]. For drug delivery systems, magnetic particles with suitable polymer coatings containing drugs are directed to tumor sites by using a controlled external magnetic field. Specific thermoresponsive polymers can trigger drug release due to local temperature changes induced by magnetic nanoparticles via an applied magnetic field. Thus thermoresponsive polymer - magnetic nanoparticle complexes are potential candidates for magnetically directed targeting, magnetically induced drug delivery and hyperthermia [49, 123, 124].

Magnetite (Fe_3O_4), which contains both Fe^{+2} and Fe^{+3} ions is the most used material for magnetic nanoparticles due to its excellent magnetic properties and biocompatibility. Many synthesis methods have been reported for the aqueous synthesis of superparamagnetic magnetite nanoparticles of which chemical co-precipitation is the most frequently used owing to its simplicity. In this method, ferrous and ferric ions are mixed in a stoichiometric ratio of 1 to 2 in the presence of a base at high pH under inert conditions. The latter is to prevent oxidation of particles to maghemite which is also a magnetic iron oxide but has a lower saturation magnetization. Superparamagnetic magnetite nanoparticles are generally stabilized with surfactants or polymers preventing sedimentation and/or aggregation in solution [119]. It has previously been shown that poly(ethylene imine) (PEI) can absorb onto magnetic nanoparticles as primary layer and a secondary layer of poly(ethylene oxide)-co-poly(glutamic acid) can give particles long term stability in physiological salt solution [125]. Poly(ethylene glycol) (PEG) or poly(ethylene oxide) (PEO) has also been used by several groups to obtain stability in aqueous medium [126-128]. PEO possesses the advantage of being non-toxic and biocompatible and is widely used in biomedical applications. PEI has also been investigated as a gene therapy carrier due to the high number of ammonium groups

that are available to electrostatically interact with phosphate groups in DNA [129-131]. Such polymeric ammonium groups are ideal cationic stabilizers for magnetite nanoparticles however PEI is relatively cytotoxic. Copolymers formed from PEI and stimulus responsive polymers have been used for systems which are effective for controlled release [132, 133]. The PEI-*graft*-POEGMA copolymers used for the synthesis of stable superparamagnetic nanoparticles were specifically designed to take advantage of a number of design principles for nanoparticle stabilization and biomedical application. The PEI backbone (of which a significant variety is commercially available) has the function of providing a number of amine groups that can directly interact with the iron oxide surface. A recent research reported an improved nanoparticle stability by using a dendritic stabilizer rather than linear analogues [134]. While dendritic stabilizers are attractive for many applications, the synthesis of such materials is multistep, time consuming and costly. On the other hand, branched or hyperbranched materials offer many of the advantages that dendritic compounds can offer at a fraction of the cost and synthetic effort. For this, a low molecular weight branched PEI backbone was chosen for the synthesis of PEI-*graft*-POEGMA. The POEGMA polymer component is a bottle – brush type polymer with a polymethacrylic backbone containing side chains of oligoethylene oxide. POEGMA has shown significant promise for bioconjugate systems due to its water solubility and thermoresponsive properties [135, 136].

This chapter presents the stabilization of superparamagnetic magnetite nanoparticles via a synthetic PEI-*graft*-POEGMA polymer by taking advantage of the adsorption ability of the PEI backbone with magnetite surface and steric stabilization from the comb - like POEGMA chains [137] which also have thermoresponsive properties.

4.2. EXPERIMENTAL

4.2.1. Materials

Ferric chloride ($FeCl_3$) and ferrous sulfate heptahydrate ($FeSO_4.7H_2O$) were purchased from Riedel-deHaen and sodium hydroxide (NaOH) was purchased from J.T. Baker. All were analytical grade and used without further purification. Oligo(ethylene glycol methyl ether) methacrylate ($M_n \approx 360$, Sigma-Aldrich) , 2-bromo-2-methylpropanoyl bromide (98%,

Sigma-Aldrich), tetrahydrofuran (analytical reagent grade, Fisher Scientific) and ethanol (analytical reagent, Fisher Scientific) were purchased and used without further purification.

4.2.2. Characterization

Particle sizes, distributions and morphologies of the nanoparticles were analyzed by FEI Tecnai G2 Sphera Transmission electron microscope (TEM) operating at 200 kV by drying 30 µL of samples on carbon coated 200 mesh copper grids. Phase identification of synthesized nanoparticles was obtained by Rigaku X-Ray difractometer (XRD) by scanning 2-theta range of 20º to 70º at room temperature with 0.02 theta increments per 10 s. Magnetic properties of both bare and PEI-b-POEGMA coated particles were analyzed by vibrating sample magnetometry (VSM) in a dry state and room temperature. DLS measurements were performed on the PEI-*graft*-POEGMA stabilised nanoparticle dispersions using a Malvern Zetasizer Nano ZS with Dispersion Technology Software (DTS). For all measurements, 10 scans were repeated three times and the average at each temperature were reported.

4.2.3. Synthesis of magnetic nanoparticles

Superparamagnetic magnetite nanoparticles were prepared by facile chemical co-precipitation method with slight modifications. Typically, $FeCl_3$ (0.141 g) and $FeSO_4.7H_2O$ (0.121 g) were dissolved in 40 mL distilled water which was de-aerated by bubbling with nitrogen for 30 minutes to remove any dissolved oxygen before use. The solution was then stirred for 15 minutes for complete mixing under nitrogen atmosphere. A solution of PEI-*graft*-POEGMA (38 mg) in aqueous NaOH (0.257 g in 10 mL) was added to the iron salts solution rapidly and solution changes color from orange to black immediately indicating the formation of magnetite nanoparticles. Amount of PEI-b-POEGMA was adjusted in such a way that iron to amine groups of PEI backbone molar ratio was 100:1. The resulting solution was then stirred for another 30 minutes at room temperature. Particles were collected after centrifugation and final precipitate was then dried in vacuum oven overnight at 60 ºC. Magnetite nanoparticles without stabilizer were prepared with identical procedure but without the addition of PEI-*graft*-POEGMA.
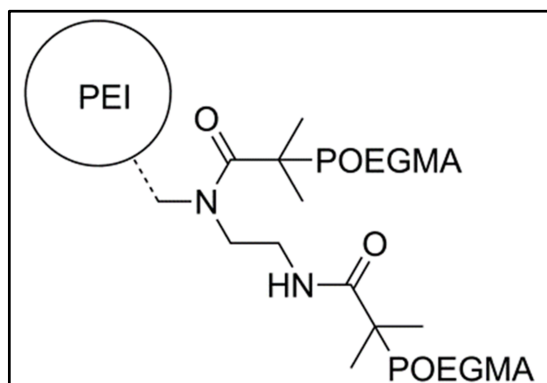
Figure 4.1. Structure of PEI-graft-POEGMA copolymer.

4.2.4. Synthesis of poly(ethylene imine)-*graft*-poly(oligo(ethylene oxide) methyl ether methacrylate) (PEI-*graft*-POEGMA)

OEGMA (M_n = 300, 5 g, 18.1 mmol), CuCl (0.0036 g, 0.362 mmol), 4,4'-dinonyl-2,2'-bipyridine (dNBpy) (0.2959 g, 0.724 mmol) and ethanol (14 ml) were mixed and sealed in a Schlenk tube. The reaction of 2-bromo-2-methylpropanoyl bromide with low molecular weight PEI sample (M_n = 600) produced a PEI macro-initiator (PEI-Br) suitable for the atom transfer radical polymerization (ATRP) of OEGMA and after 45 minutes of degassing with nitrogen, PEI – initiator in ethanol (0.1 g/mL) was injected via gastight syringe. The mixture was left stirring at room temperature under nitrogen for 48 hours. The polymer was isolated by slow addition of THF solution to an excess of hexane. The product finally precipitated as a green viscous liquid and was collected by centrifugation prior to drying overnight under vacuum at 35 °C. The synthesis of PEI-*graft*-POEGMA copolymer was performed by A. Kleine from the Functional Materials Group of the University of Kent. Additional synthesis details and corresponding characterization can be found elsewhere [138].

4.3. RESULTS AND DISCUSSION

4.3.1. Characterization of PEI-*graft*-POEGMA stabilized magnetic nanoparticles

The synthesis of superparamagnetic magnetite nanoparticles by chemical co-precipitation is known to yield crystalline random oriented particles with various morphologies, having an average size between 6 to 10 nm with a fairly broad size distribution [99]. The morphology of the particles prepared in the presence of PEI-*graft*-POEGMA was analyzed by Transmission Electron Microscopy (TEM) while size and size distribution analyses were performed by measuring 150 particles on TEM images (Figure 4.2-a). The presence of the polymer does not seem to affect the size and size distribution significantly. As seen from Figure 4.2-b, the average size of the bare particles was determined to be 7.9 nm while particles coated with PEI-*graft*-POEGMA had an average size of 7.4 nm. The size distributions of both samples were almost the same with sample standard deviations of 1.35 nm and 1.50 nm for PEI-*graft*-POEGMA coated and bare magnetite nanoparticles, respectively. Dynamic light scattering (DLS) analysis of a 1 wt% dispersion of the stabilized particles at 20.1 °C gave a number average particle diameter of 48.3 nm with a standard deviation of 8.58 nm. This particle diameter is considerably larger than that is observed by TEM and indicated that the particles form aggregates in solution, as is well documented [139-143].
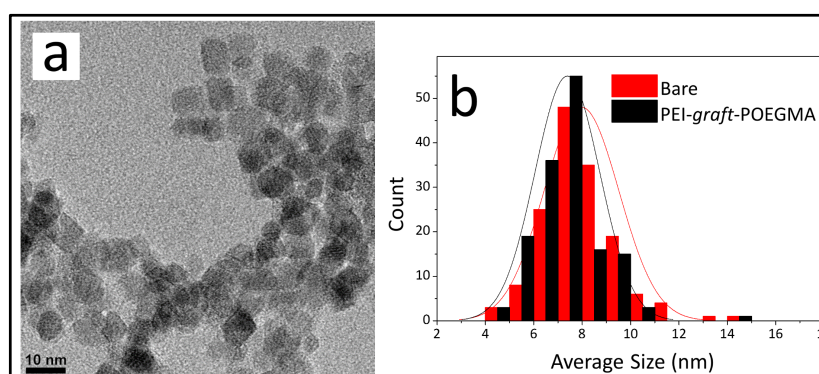
Figure 4.2. TEM micrograph of PEI-graft-POEGMA stabilized superparamagnetic iron oxide nanoparticles (a), Size distributions of bare and PEI-graft-POEGMA stabilized nanoparticles (b).

As can be seen from Figure 4.2, the particles show no specific shape but irregular morphologies which is not different than the particles synthesized in the absence of PEI-*graft*-POEGMA. Higher magnification analysis of the particles via TEM showed cubic, octahedral and spherical morphologies as are often obtained from chemical co-precipitation. X-ray diffraction analysis of the nanoparticles synthesized in the presence of PEI-*graft*-POEGMA, given in Figure 4.3, shows the characteristic reflections of peaks assigned to magnetite and/or maghemite without existence of other iron oxide phases. As was expected for the co-precipitation method, there was no difference in the morphology or diffraction pattern between the particles prepared with and without PEI-*graft*-POEGMA.
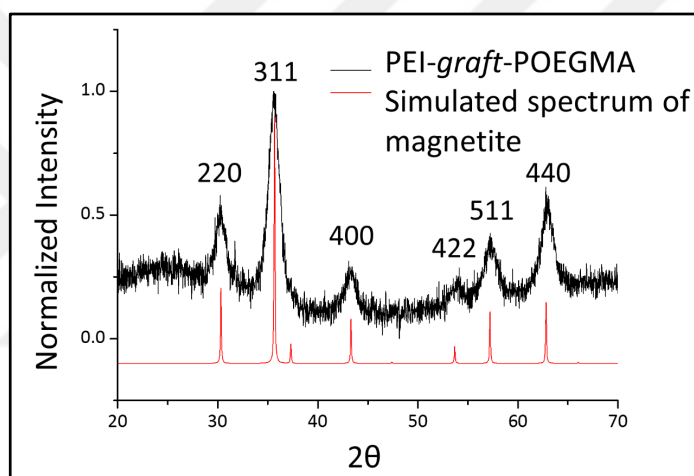
Figure 4.3. X-ray diffraction pattern for PEI-graft-POEGMA stabilized superparamagnetic nanoparticles compared with simulated pattern of magnetite.

The magnetic properties including saturation magnetization, coercivity and remenance of the particles prepared in the presence and absence of PEI-*graft*-POEGMA were analyzed by Vibrating Sample Magnetometry (VSM). Figure 4.4-a shows the corresponding hysteresis loops with no coercivity or remenance indicating that both samples have a superparamagnetic nature. The saturation magnetization of particles coated with PEI-*graft*-POEGMA was found to be 40.7 emu/g while for bare particles it is 48 emu/g which in both cases is less than for bulk magnetite [144]. The lowering of saturation magnetization for the particles prepared in the presence of copolymer can be attributed to the presence of the non – magnetic PEI-*graft*-POEGMA coating as the crystal structure, morphology and average

size of the nanoparticles remain unchanged [145]. The effect of surface coatings on the magnetic properties of magnetite nanoparticles is investigated in the chapter 6 of this thesis [145].
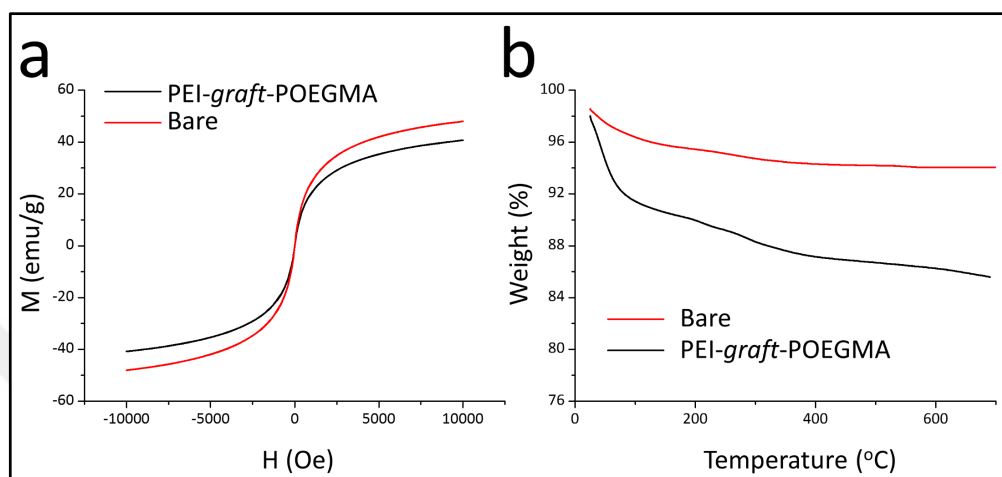
Figure 4.4. Magnetization (a) and TGA (b) curves of bare and PEI-graft-POEGMA stabilized iron oxide nanoparticles.

Thermogravimetric analysis (TGA) given in Figure 4.4-b showed a 6 % weight loss for uncoated superparamagnetic iron oxide nanoparticles due to the release of adsorbed water from the nanoparticle surface. On the other hand PEI-*graft*-POEGMA coated magnetic nanoparticles showed a further loss of 8.5 weight % demonstrating the existence of a degradable organic component (PEI-*graft*-POEGMA) on the iron oxide nanoparticles.

As many applications require stable superparamagnetic iron oxide nanoparticles, it is essential to apply a suitable surfactant or polymer coating during (one-step) or after (two-step) the synthesis. Superparamagnetic magnetite nanoparticles prepared in the presence of PEI-*graft*-POEGMA copolymer were dispersed in distilled water by sonication after drying. Although some settling occurred over time, the dispersed particles largely remained stable over days. It should be noted that bare particles without any surface modifications aggregated and precipitated in a matter of minutes.

4.4. CONCLUSION

In summary, a facile synthetic route is presented for the preparation of thermoresponsive poly(ethylene imine)-*graft*-poly(oligo(ethylene glycol methyl ether) (PEI-*graft*-POEGMA) functionalized superparamagnetic iron oxide nanoparticles. It was our aim to obtain an attachment between the polymer backbone and the magnetite surface via the PEI amine groups and stabilization via ethylene glycol tails in polar solvents. XRD and ED results validated the formation of magnetite and/or maghemite phase and TGA results showed the existence of a polymer coating on the nanoparticle surface. Particles prepared in the presence of the PEI-*graft*-POEGMA copolymer were superparamagnetic while saturation magnetization was found to be less than bulk magnetite but comparable with that of the bare nanoparticles taking the PEI-*graft*-POEGMA layer into account. The function of the synthetic PEI-*graft*-POEGMA was demonstrated as a stabilizer in the preparation of superparamagnetic iron oxide nanoparticles which retained all the characteristics of bare nanoparticles.

5. POLYMER-DIRECTED SYNTHESIS AND STABILIZATION OF FERRIMAGNETIC MAGNETITE NANOPARTICLES IN WATER

5.1. INTRODUCTION

There is a growing interest in the synthesis of magnetite nanoparticles due to their excellent magnetic and biocompatible properties. The effective use of these nanoparticles in a variety of applications such as heat transfer [146, 147], drug delivery [28], magnetic hyperthermia [148] and MRI [149] mainly depends on their magnetic properties and colloidal stability. Therefore efforts are being made towards the synthesis and stabilization of magnetite in both polar and organic solvents with suitable additives that have affinity to the magnetite surface without affecting the magnetic properties. These properties can be tuned by using different synthetic routes with or without additives, as magnetic properties are largely determined by particle size and morphology. Magnetite nanoparticles with sizes below 20 - 30 nm are superparamagnetic at room temperature while larger single domain particles are ferrimagnetic having higher magnetic saturation with persistent coercivity and remanence [150].

There are versatile synthesis methods for the production of magnetite nanoparticles, using thermal decomposition [151-153], microemulsions [43, 154] and hydrothermal synthesis [155, 156]. However, the most used method to synthesize magnetite nanoparticles is co–precipitation due to its simplicity [157]. In this method both Fe^{2+} and Fe^{3+} salts are mixed at a 1:2 stoichiometric ratio in aqueous medium under inert conditions and particles are precipitated after a sharp increase of pH by the addition of a suitable base. While this is a very convenient way to produce superparamagnetic magnetite nanoparticles, it yields particles with a wide size distribution and irregular morphologies all of which prevent uniform magnetic, chemical and physical properties [99, 158]. On top of that, the saturation magnetization of these superparamagnetic nanoparticles is usually considerably less than that of the bulk phase. Alternatively, magnetite nanoparticles can be synthesized via the partial oxidation method in a aqueous medium, where a ferrous salt solution is gradually oxidized by a mild oxidant at basic conditions. One of the advantages of this method is the capability of producing single domain ferrimagnetic nanoparticles in water with a uniform

morphology and size distribution. Oxidative aging of ferrous salt was first described by Baudisch.[105] Sugimoto and Matijevic then studied this method to prepare magnetite nanoparticles of different sizes [108]. Their work later on was used and intensively analyzed by several other groups [66]. Morales et al. synthesized magnetite from 30 nm to 300 nm by precipitation of $Fe(SO_4)$ in alkaline medium in the presence of an oxidant. They reported that using a mixture of ethanol/water as the medium lead to particles which are colloidally stable at pH 7 due to sulphate anions being strongly bound to the surface. Additionally their calorimetric experiments showed that a sample prepared in ethanol/water mixture had a specific absorption rate (SAR) value of 95 W g^{-1} at a particle concentration of 5 mg ml^{-1} which is among the highest values reported [109]. Vereda et al. also used the same synthesis method and reported specific conditions for the preparation of uniform single domain octahedral magnetite nanocrystals [68]. Tada et al. performed the oxidaton of $Fe(OH)_2$ in the presence of H_2O_2 at room temperature and neutral conditions and showed the possibility of immobilizing biomolecules during magnetite synthesis [159]. Partial oxidation of $Fe(OH)_2$ was also used to control the size and morphology of magnetite nanoparticles where the small acidic protein Mms6, isolated from *Magnetospirillum magneticum,* was introduced to the reaction and acted as a nucleation and/or growth modifier [79]. These ferrimagnetic magnetite nanoparticles are interesting for specific applications, such as magnetic hyperthermia [160, 161], magnetic particle imaging (MPI) [162] and other biomedical applications [163]. However, strong magnetic attractions due to the high degree of magnetization and hydrophobic interactions in many cases cause ferrimagnetic particles to aggregate and precipitate easily [164]. Although oxidative aging of ferrous hydroxide has been used to synthesize magnetite nanoparticles at different conditions for many years, studies that concentrate on the colloidal stability of the corresponding particles are limited. As a consequence, a simple route that can produce ferrimagnetic magnetite nanoparticles readily stabilized in water is needed for the development of future potential applications. An appropriate coating with polymers, biomolecules or surfactants can improve stability and protect the surface of magnetite from oxidation which deteriorates the magnetic properties. While these additives enhance stability, they can also tailor the surface functionality for additional attachments in specific applications. Such a core – shell structure of functionalized magnetite nanoparticles benefits both from the basic magnetic properties of the core and the intrinsic properties of the coating agent e.g. biocompatibility or biodegradability. However

a non – magnetic coating around the particles may also alter the magnetic properties of the particles, which should be taken into consideration [145].

The aim of this study is to formulate a one-step synthesis method for stabilized ferrimagnetic magnetite nanoparticles with poly(acrylic acid) using partial oxidation. As poly(acrylic acid) is deprotonated at all pH values > ~6 (pK_a = 4.2), it is expected to bind to the iron cations on the magnetite surface [127], but also extend into the solution providing electrostatic stabilization. Indeed there have been many reports showing the successful applications of poly(acrylic acid) in many biomedical applications [165-168]. Previously poly(acrylic acid) was used in the synthesis of magnetite nanoparticles, either as stabilizer or as growth control agent. Yin et al. used high-temperature hydrolysis for the synthesis of water soluble superparamagnetic magnetite nanoparticles by using poly(acrylic acid) as a capping agent [169]. The same group also showed that it is possible to synthesize uniform colloidal clusters of superparamagnetic magnetite nanoparticles that were again highly dispersible in water due to surrounding poly(acrylic acid) chains [170]. Lin et al. showed that superparamagnetic magnetite particles synthesized via co-precipitation in the presence and absence of poly(acrylic acid) have different mean particle sizes, indicating that poly(acrylic acid) acted as a nucleation and growth control agent. It was also shown that the stability of the particles can be tuned as a result of electrostatic and steric repulsion by changing the pH of the medium [171].

Although synthetic routes for superparamagnetic magnetite nanoparticles stabilized in aqueous medium are well established in the literature. Here we demonstrate the first synthetic route to obtain *ferrimagnetic* particles with narrow size distribution and high saturation magnetization suspended in aqueous medium by a commercial polymer. These colloidally stable magnetic nanoparticles synthesized via partial oxidation with a hydrophilic biocompatible polymer at neutral pH lend themselves for potential biomedical applications.

5.2. EXPERIMENTAL

5.2.1. Materials

Potassium hydroxide and potassium nitrate were purchased from J.T. Baker and Sigma Aldrich respectively. Ferrous sulfate heptahydrate ($FeSO_4.7H_2O$) was purchased from Riedel-de Haen and poly(acrylic acid) (M_w: 250 kDa and 450 kDa) were purchased from Aldrich. All chemicals were used without further purification.

5.2.2. Characterization

Transmission electron microscopy (TEM) images and selected area diffraction patterns (SAED) for the samples were obtained with a FEI Tecnai G2 Sphera operating at 200 kV with LaB_6 filament and a bottom-mounted 1024 x 1024 Gatan 794^{TM} CCD camera. For analysis, 30 µL of samples were dried on carbon coated 200 mesh copper grids. Phase identification of the particles synthesized in the presence of poly(acrylic acid) was obtained by Rigaku X-Ray difractometer (XRD) by scanning 2-theta range of 10° to 70° at room temperature with 0.02 theta increments per 10 s. Magnetic properties of both bare and poly(acrylic acid) coated particles were analyzed and hysteresis loops were obtained by Vibrating Sample Magnetometry (VSM) in a dry state and at room temperature. Dynamic light scattering (DLS) measurements were performed on a Malvern Zetasizer Nano ZS by dispersing functionalized particles in ultrapure water using ultrasonic agitation.

5.2.3. Synthesis of ferrimagnetic magnetite nanoparticles

The synthesis of ferrimagnetic magnetite nanoparticles was adopted from a previous study of Vereda et al. [68] which is a slight modification of Sugimoto and Matijevic's method [108]. Briefly, 12.5 mL KNO_3 solution (2 M) and 6.25 mL KOH solution (2.78 M) were added to 100 mL of water and transferred to a 500 mL round bottom flask. Then the solution was degassed for 60 minutes. Simultaneously, a ferrous salt solution (0.5 M) was prepared by dissolving 0.868 g $FeSO_4.7H_2O$ in 6.25 mL of degassed water. The iron solution was then

added to the main flask containing the base and the oxidant. The mixture was bubbled with nitrogen for another minute. The flask was immediately sealed airtight with a rubber stopper and put in an oil bath that was preheated and maintained at 90 ^{o}C. After 4 hours the reaction mixture was cooled down and particles were isolated with a handheld magnet. The collected particles were washed with ultrapure water and recollected with a handheld magnet several times. Finally, the particles were dried in a vacuum oven at 60 ^{o}C for overnight. Polymeric additives and surfactants were introduced into the synthesis by dissolving them in the KOH & KNO_3 solution and concentrations were adjusted either 1:1 or 1:5 according to the ratio of the iron ions present to functional groups of the additives respectively. The rest of the synthesis procedure was identical.

5.3. RESULTS AND DISCUSSION

Magnetite nanoparticles were prepared by oxidation of iron(II) ions in the presence of an oxidant at high pH. The method is based on the gradual oxidation of ferrous ions to ferric ions in order to form magnetite nanoparticles. This step combined with the nucleation and growth of the particles requires significantly longer reaction times (hours) than the frequently used fast chemical precipitation method (seconds) and thus provides a better opportunity for surface active polymers to interact with the iron oxide surface.

The size and morphology of the particles synthesized by partial oxidation were analyzed by transmission electron microscopy (TEM). TEM analysis showed that the synthesis performed in the absence of any additives yields octahedral particles with a uniform morphology and narrow size distribution. As shown in Figure 5.1, the average particle size was found to be 54.6 nm with a sample standard deviation of 10 nm by measuring the length of the two diagonals of the corresponding octahedron (Figure 5.2). This result exactly matches the previous findings of Vereda et al [68].
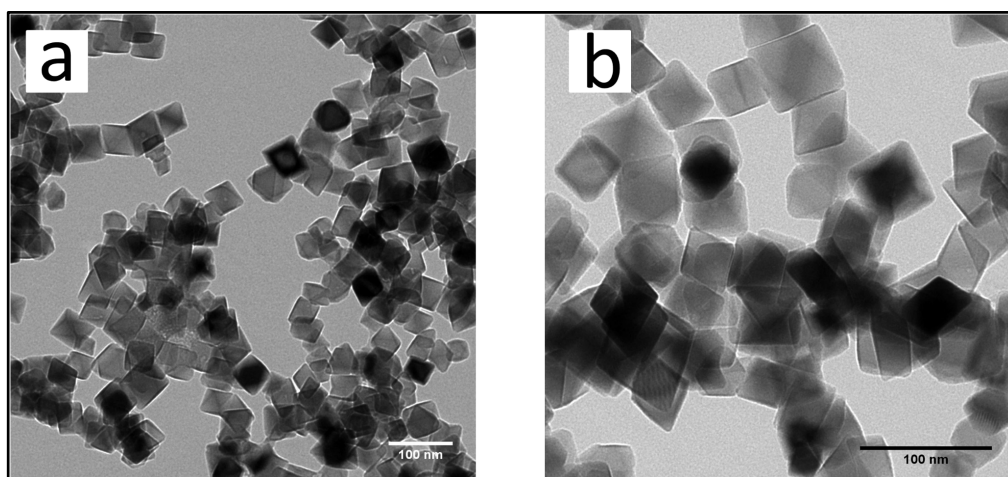
Figure 5.1. TEM micrographs of bare magnetite nanoparticles synthesized by partial oxidation of ferrous hydroxide.

Phase identification of the samples prepared in the absence of additives was performed by X-ray and electron diffraction analyses. Results showed that bare particles were highly crystalline and all the *d*-spacings and corresponding peak positions matched well with those of magnetite. It has been reported that unless the reaction conditions are accurately controlled, this method is capable of producing various iron oxides [172]. Nevertheless XRD and SAED analysis showed that the product was phase pure and no other iron oxide phases were present.
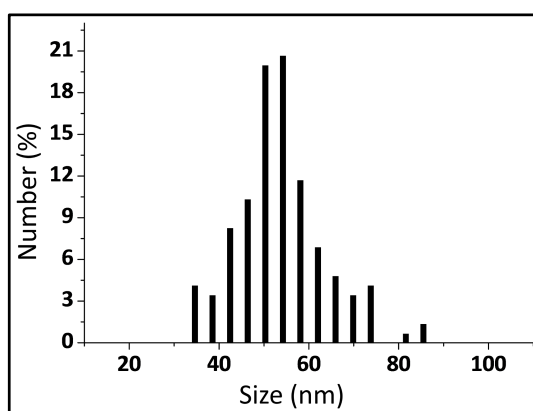
Figure 5.2. Size distributions of magnetite nanoparticles synthesized without additives (55±10 nm).

The synthesis of the magnetite nanoparticles was first performed in the presence of trisodium citrate, poly(ethyleneimine) (25 kDa), poly(ethylene oxide) (100 kDa), poly(ethylene oxide) (600 kDa) and poly(acrylic acid) (8 kDa) as these additives were previously shown to enhance the stability of magnetite nanoparticles when other synthetic routes were employed [170, 171, 173-180]. According to the TEM analysis the average particle sizes were in the range of 50 – 80 nm (Figure 5.3). Moreover, it was clearly seen that the presence of trisodium citrate affected the growth of the particles as the morphology changed from octahedral to rounded particles as compared to the control experiment. Similar effects of citrate were also reported previously in several other studies [178-180]. It is evident that trisodium citrate aided the growth of the particles as the average particle size increases compared to bare particles. Additionally when the concentration of trisodium citrate is increased, the average particle size of the sample decreased from 79 nm to 52 nm while in both cases the size distributions of the particles were still wider than the control experiment implying that trisodium citrate affects both the nucleation and growth of the nanoparticles. This decrease in average particle size by the increase in the concentration of citrate groups is in line with the previous study of Jing et al [180].
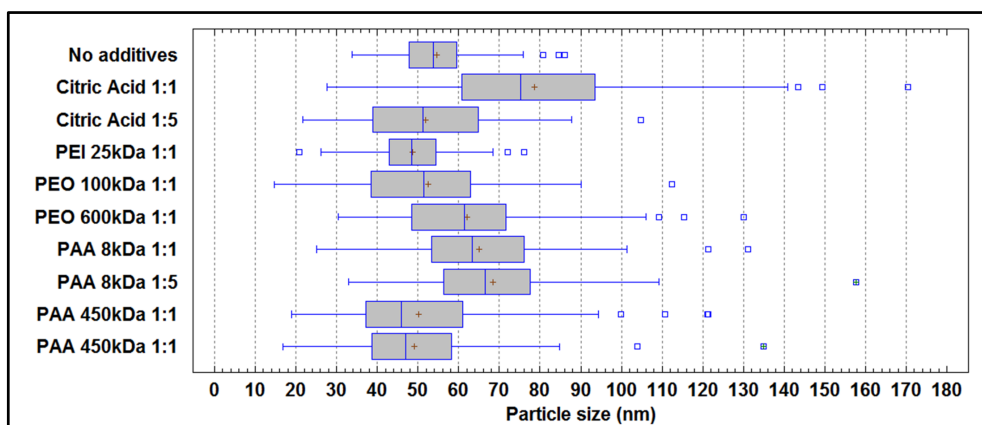
Figure 5.3. Particle size distributions of samples prepared in the presence of different additives with mean markers and outliers. Concentrations were adjusted either 1:1 or 1:5 according to the ratio of the iron ions present to functional groups of the additives respectively.

In contrast to trisodium citrate, the presence of poly(ethylene oxide) (600 kDa) and poly(acrylic acid) (8 kDa) resulted in larger particles with octahedral morphology as shown in Figure 5.3 and Figure 5.4. On the other hand, poly(ethyleneimine) (25 kDa) and poly(ethylene oxide) (100 kDa) were not found to have much influence on the formation of magnetite nanoparticles as the average sizes of the particles were comparable with the control experiment. However, in the case of poly(ethylene oxide), the size distribution was broader than with poly(ethyleneimine) where the particles had almost the same distribution as the bare particles. Hence all additives, apart from poly(ethyleneimine) led to particles having a broader size distribution as compared to the bare particles. Moreover, none of the abovementioned additives did significantly increase the colloidal stability of the synthesized magnetite nanoparticles in either neutral or basic conditions.

Partial oxidation of ferrous hydroxide at high temperature was also performed in the presence of poly(acrylic acid) (450 kDa) at 1:1 ratio of iron ions present to functional groups of the polymer (Fe^{2+}/-COO^-). The corresponding particles were analyzed by TEM (Figure 5.4-f and Figure 5.5) and the average particle size was found to be around 49 nm with a sample standard deviation of 16 nm. The obtained nanoparticles showed a wider size distribution as compared to the control experiment (Figure 5.6) which suggest that the presence of the polymer promoted the nucleation of new particles during the growth process.
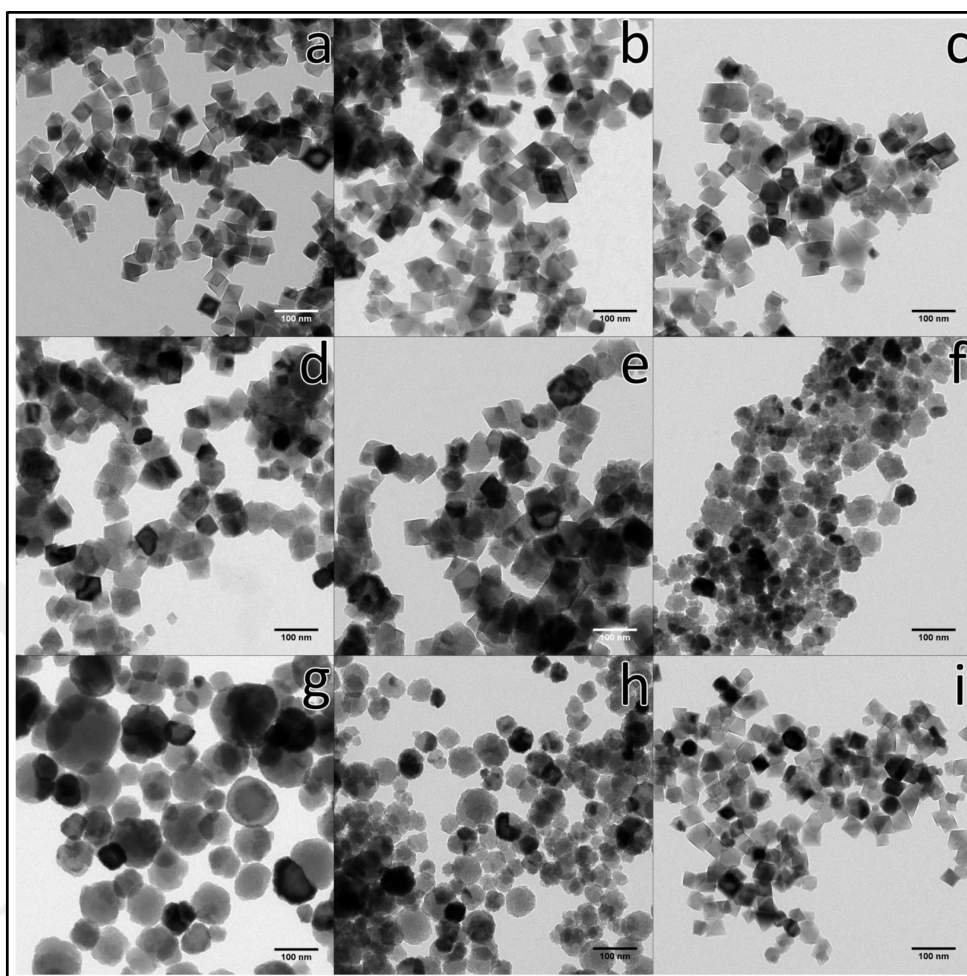
Figure 5.4. TEM micrographs of the particles synthesized in the presence of various additives. a) Bare b) poly(ethylene oxide) (100 kDa) 1:1 c) poly(ethylene oxide) (600 kDa) 1:1 d) poly(acrylic acid) (8 kDa) 1:1 e) poly(acrylic acid) (8 kDa) 1:5 f) poly(acrylic acid) (450 kDa) 1:1 g) trisodium citrate 1:1 h) trisodium citrate 1:5 i) poly(ethyleneimine) (25 kDa) 1:1 – Scale bars are 100 nm.

Comparable to the effect of trisodium citrate, the morphology of the particles was also changed from octahedral to spherical which is most likely due to the interaction of the functional groups on the polymer with magnetite surface during growth. Most strikingly, these particles exhibited a colloidal stability that was not achieved by any other additive or the same polymer of lower molecular weight.
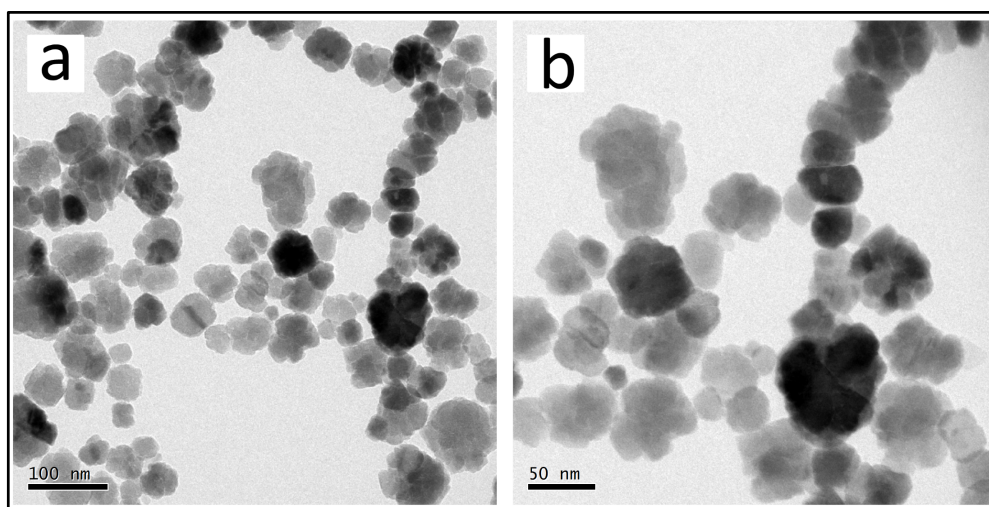
Figure 5.5. TEM micrographs of the particles synthesized in the presence poly(acrylic acid) (450 kDa).

X–ray and Electron diffraction analyses of the particles synthesized in the presence of poly(acrylic acid) (450 kDa) confirm the formation of single phase magnetite without existence of any other iron oxides by comparing the positions and relative intensities of all reflections (Figure 5.7).
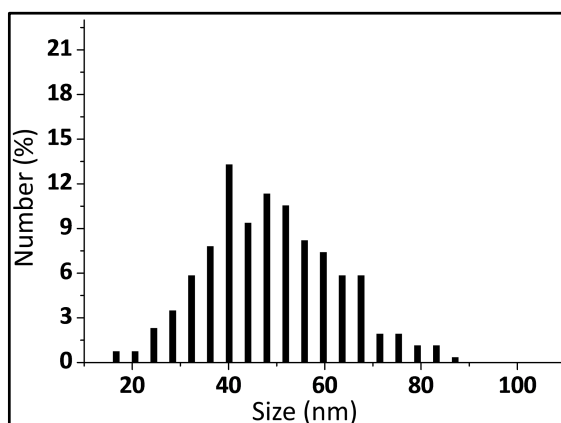
Figure 5.6. Size distributions of magnetite nanoparticles synthesized in the presence of poly(acrylic acid) (450 kDa) (49±16 nm).
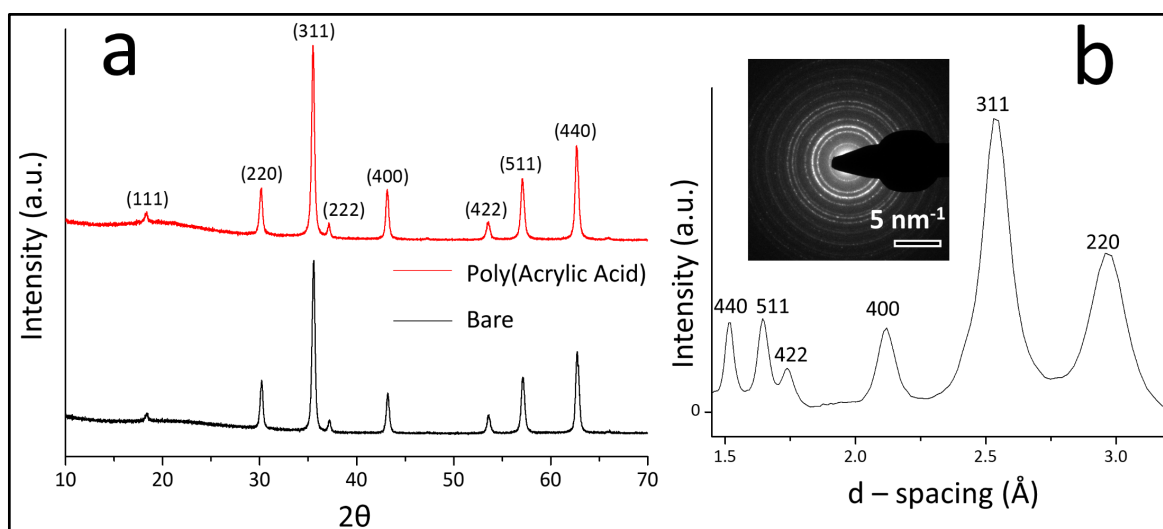
Figure 5.7. a) Dry powder X–ray diffraction patterns of particles prepared in the presence and absence of poly(acrylic acid) (450 kDa) b) Electron diffraction radial average of bare particles synthesized in the absence of any additives. The inset shows the corresponding Selected area diffraction pattern (SAED).

Dynamic light scattering (DLS) analysis showed that the number average hydrodynamic diameter was 72 nm for particles synthesized in the presence of poly(acrylic acid) (450 kDa) which is significantly higher than the diameter of 49 nm that was obtained with TEM analysis for the same particles. This increase in size shown by DLS obtained can be attributed to the presence of the polymer on the surface of the magnetite particles (Figure 5.8).

For magnetic properties, hysteresis loops obtained at room temperature are given in Figure 5.9. Bare particles prepared by oxidation of ferrous hydroxide were found to have saturation magnetization (M_s) value around 69.2 emu/g which is less than 81.6 emu/g stated by Vereda et al. for the same type of particles [68]. Particles synthesized in the presence of poly(acrylic acid) (450 kDa) had a comparable saturation magnetization of 68.7 emu/g. Although both particles showed ferrimagnetic properties due to the existence of remanence and coercivity on the magnetization loop, these ferrimagnetic properties were lower for the poly(acrylic acid) coated particles due to their reduced average size.
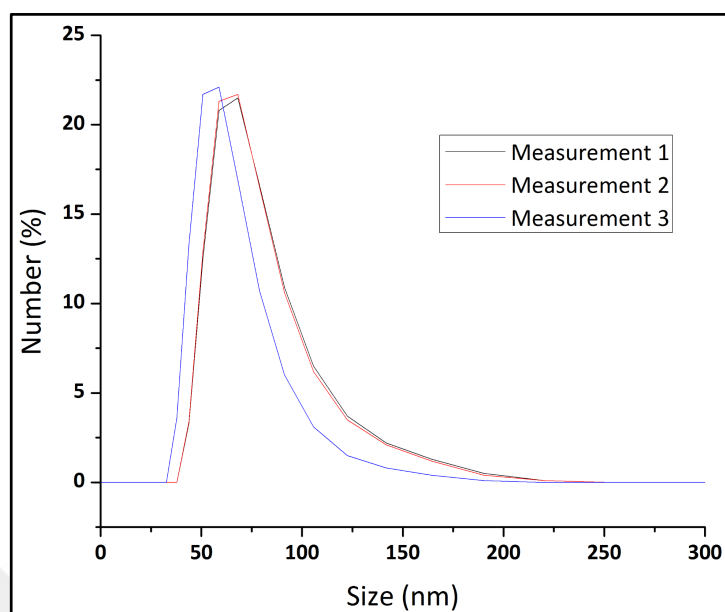
Figure 5.8. Number average distribution given by DLS measurement for particles synthesized in the presence of poly(acrylic acid) (450 kDa).
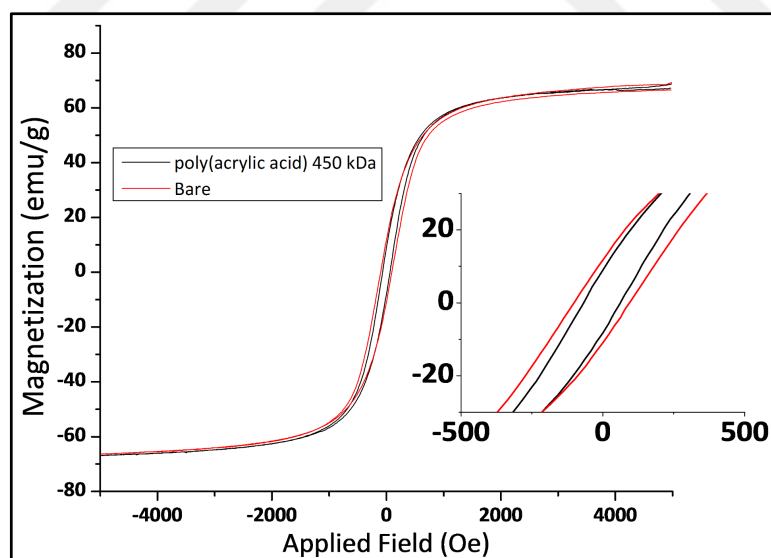
Figure 5.9. VSM measurements of particles synthesized in the presence and absence of poly(acrylic acid) (450 kDa).
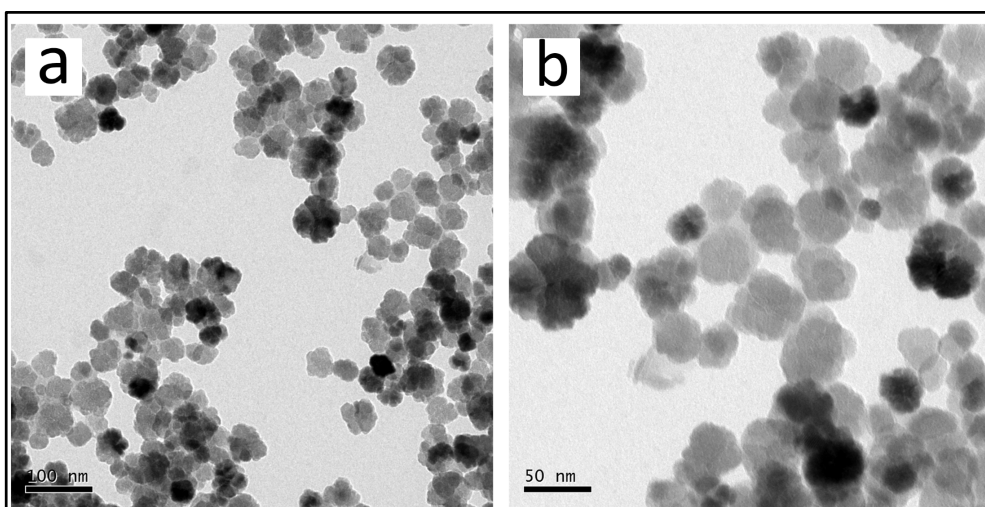
Figure 5.10. TEM micrographs of the particles synthesized in the presence of poly(acrylic acid) (250 kDa).
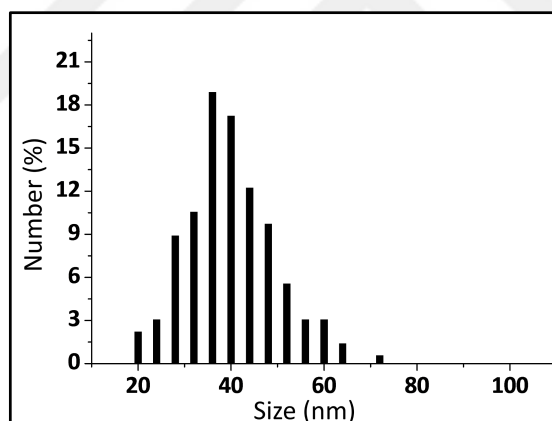
Figure 5.11. Size distributions of magnetite nanoparticles synthesized in the presence of poly(acrylic acid) (250 kDa) (40±10 nm).

The synthesis of magnetite nanoparticles was also performed in the presence of a lower molecular weight poly(acrylic acid) (250 kDa) in order to compare the effect of chain length of the polymer on the stabilization of the particles in water. TEM analysis, given in Figure 5.10, illustrated similar spherical morphology for the particles as in the case of higher molecular weight PAA. The average size of the particles was found to be 40±10 nm, which is smaller than particles prepared both in the absence and presence of PAA having higher

degree of polymerization (Figure 5.11). This result illustrates that the lower molecular weight polymer interacted better with the surface of the particles and prevent their further growth. Furthermore, although a moderate stability in aqueous medium was obtained with poly(acrylic acid) (250 kDa) for those comparably smaller ferrimagnetic particles, precipitation is faster (~2 days) than particles synthesized in the presence of poly(acrylic acid) (450 kDa).

In the literature, several stabilizers are reported that provide colloidally stable magnetic nanoparticles. This shows that several surfactants and polymers potentially interact with the magnetite surface. However, colloidally stable ferrimagnetic magnetite particles at this higher size end of the nanoparticle range have not been produced. As the size of the nanoparticle become larger, the sedimentation force acting on the particle increases. In the case of highly magnetic particles, the magnetization also increases with size and particles have a tendency to form aggregates by magnetically sticking to each other [47]. This results in the loss of colloidal stability and the sedimentation of particles. It appears that a large steric barrier is needed in order to prevent this interaction and resulting sedimentation. The change in morphology from octahedral to spherical shows that citric acid and poly(acrylic acid) (250 kDa) interact with the surface of the magnetic particles. This suggests that sedimentation occurs due to insufficient colloidal stability to overcome the attractive magnetic force between the nanoparticles. For poly(acrylic acid) with a higher molecular weight, the large steric stabilization coupled with the electrostatic repulsion of the carboxyl groups as well as the viscosity increasing effect of the polymer (more than 5 times) [181] provide the required colloidal stability to resist the aggregate formation induced by magnetic forces.

5.4. CONCLUSION

Ferrimagnetic magnetite nanoparticles were synthesized by partial oxidation of ferrous hydroxide, resulting in highly crystalline octahedral particles of 55 nm with a narrow size distribution. Several additives at various concentrations were applied with the aim of stabilizing these ferrimagnetic particles. Only when the synthesis was carried out in the presence of poly(acrylic acid) (450 kDa), dispersible particles were obtained which showed

excellent colloidal stability for several days. The obtained dispersions contained mainly spherical nanoparticles with an average size of 49 nm which were identified as pure magnetite using XRD. Existence of poly(acrylic acid) (450 kDa) on the magnetite surface, which was shown by DLS analysis, increased the colloidal stability of the ferrimagnetic nanoparticles by electrostatic repulsion at neutral conditions. To our knowledge this is the first study that is capable of producing ferrimagnetic magnetite nanoparticles with high saturation magnetization via partial oxidation of ferrous hydroxide which can be stabilized in aqueous medium using a hydrophilic biocompatible polymer at neutral pH.

6. EFFECT OF SURFACE MODIFICATION ON MAGNETIZATION OF IRON OXIDE NANOPARTICLE COLLOIDS

6.1. INTRODUCTION

There is a growing interest in magnetic iron oxide nanoparticles because of their unique physical and chemical properties. In recent years they have been extensively studied especially for specific applications, such as drug delivery [182-184], magnetic resonance imaging (MRI) [185-189] and cancer hyperthermia [190-194]. For all these applications, it is essential to coat magnetic iron oxide nanoparticles with surfactants and polymers to enhance stability and functionality. However, this surface treatment may decrease the effective size and the total amount of magnetic phase due to the formation of a nonmagnetic layer as a result of the interaction between the coating and the nanoparticle surface atoms. The formation of this nonmagnetic layer thus affects the concentration of the magnetic phase and the effective size can alter the efficacy of many biomedical applications. For example, in magnetic nanoparticle-driven cancer hyperthermia and MRI, these two parameters regulate the heat generation rate [195, 196]. In order to optimize the properties of the magnetic nanoparticles for these applications, it is important to understand how surface coatings change the effective size of the magnetic core. However, some studies indicate that the magnetic properties of magnetic particles change after surface modification [197, 198]. Kaiser et al. showed that the saturation magnetization for oleic acid coated magnetite nanoparticles depends on the type of the solvent [197]. Chantrell et al. studied more solvents and particles of different sizes, all stabilized with oleic acid. They showed that the product of saturation magnetization of the bulk phase and volume fraction of nanoparticles is higher than the saturation magnetization of the ferrofluid. This decrease was attributed to the interaction of the stabilizing surfactant with the magnetic core [199]. So far, none of these studies focused on coatings related to biomedical applications.

In this work, commercial magnetite nanoparticles suspended in water and having different biocompatible coatings as well as bare particles are investigated. For comparison, hydrophobic oleic acid coated iron oxide nanoparticles suspended in hexane and heptane were also studied. The particles were characterized by transmission electron microscopy

(TEM) for average size and particle morphologies. X–ray diffraction (XRD) and Raman spectroscopy were performed to identify the type of iron oxide present. X-ray photo-electron spectroscopy (XPS) was used to analyze the coatings of the commercial samples. The saturation magnetization values obtained from vibrating sample magnetometry (VSM) measurements were used to determine the amount of the magnetic phase by normalizing with respect to the saturation value of the bulk phase. The results were then compared with the total iron concentrations determined from the tiron chelation test showing the reduction in the magnetic phase for each type of coating and solvent used. For all samples the thickness of the nonmagnetic layer between the magnetic core and surface coating was calculated by fitting the experimental magnetization to the modified Langevin equation.

6.2. EXPERIMENTAL

6.2.1. Materials

Commercial aqueous nanofluids, FluidMAG-amine, FluidMAG-UC/A and FluidMAG-CMX were purchased from Chemicell. FluidMAG-UC/A contains non-functionalized bare nanoparticles that have a positive surface charge. The aminosilane coated particles in FluidMAG-amine have an amine (-NH$_2$) group while the carboxymethyl-dextran coated nanoparticles in FluidMAG-CMX are terminated with carboxyl groups (-COOH). The mentioned coatings were selected for their wide range of applications, for example as cell targeting agents [200, 201]. Synthesized oleic acid coated iron oxide nanoparticles were also suspended in hydrophobic base fluids, hexane (MAG/OA-HEX) and heptane (MAG/OA-HEP). These nanoparticles were synthesized by a thermal decomposition method which was adopted from a previous report of Sun et al [202]. Oleic acid used is a hydrophobic surfactant that binds to the surface via carboxyl groups leaving the hydrophobic tail free which facilitates suspension in nonpolar solvents [203].

6.2.2. Characterization

The size and morphology of the particles were investigated with a JEOL 2011 transmission electron microscope (TEM) operating at 200 kV. For TEM analysis, commercial samples

were diluted with water and the oleic acid coated synthesized particles were dispersed either in heptane or hexane. For each sample a droplet is placed on a carbon coated copper grid. Crystal structure and phase identification of both commercial and synthesized particles were obtained by X-ray diffraction (XRD) (X'pert PRO) by placing a droplet of the corresponding sample on a silicon based sample holder and drying at 70 $^{\circ}$C. Raman spectroscopy was performed to complement XRD results. A confocal raman microscopy (WITec 300R), equipped with a 532 nm green light laser and CCD camera, was used to characterize the samples with 1 s integration time and 30 accumulations. The laser power was in the range of 0.04 – 0.2 mW and calibrated with a Newport Optical Power/Energy meter before each use. For sample preparations, a drop of nanofluid was placed on a microscope cover slide and dried at 40 $^{\circ}$C in the dark for 24 h. X-ray photoelectron spectroscopy (XPS) was used to validate the surface coatings on commercial samples. XPS was carried out on a PHI VersaProbe 5000 having monochromatic 100 μm beam of Al Kα radiation as X-ray source. Finally, the magnetic properties of the samples were obtained by a vibrating sample magnetometer (VSM – Lake Shore Inc.) at room temperature in a field strength range of ±1500 kA/m.

6.2.3. Synthesis of magnetite nanoparticles

Magnetite nanoparticles were synthesized by thermal decomposition as reported previously [202]. In a typical synthesis, Iron (III) acetylacetonate (0.706 g) and 1,2 tetradecanediol (2.3 g) were mixed with 20 mL dibenzyl ether in the presence of 1.9 mL oleic acid and 1.69 mL oleylamine in a round bottom flask. Under nitrogen atmosphere and constant magnetic stirring, the sample was heated up to 100 $^{\circ}$C with a heating rate of 2.5 $^{\circ}$C/min. The temperature was maintained at 100 $^{\circ}$C for 15 min and then gradually increased up to 200 $^{\circ}$C with the same heating rate, where it stayed for 2 hours. Finally, the temperature was increased to 300 $^{\circ}$C and kept at this temperature for 1 hour after which the solution was cooled down to room temperature. To collect the particles, methanol was added to the mixture and upon centrifugation at 7500 RPM for 15 minutes, a black precipitate was obtained which was dried in a vacuum oven overnight.

6.2.4. The Tiron chelation test

The Tiron chelation test was used to determine the total iron concentrations of the samples which then could be converted to the total concentration of magnetite phase in solution. Tiron (4,5-dihydroxy-1,3-benzenedisulfonic acid disodium salt) chelates with iron (II) and iron (III) ions at a ratio of three Tiron molecules to each iron ion. This complex exhibits a strong absorbance at 480 nm for samples with a pH greater than 9 [204]. In a typical experiment, 0.4 mL concentrated hydrochloric acid solution was added to a 0.1 mL of magnetic fluid (V_{sample}) in order to liberate ferrous and ferric ions. The addition of acid also removes the existing surface coating around the particles. The obtained solution was heated with a heating gun for 15 s and cooled down to room temperature. Then 0.6 mL Tiron solution (0.083 g/mL) was added to the mixture and the pH was increased to above 9 by adding 3 mL of sodium hydroxide solution (4 M). The immediate color change from yellow to red indicates the chelation of iron ions with Tiron molecules. The resulting mixture was diluted with water up to 25 mL (V_{final}), followed by a second dilution with a dilution factor (*DF*) of 12. The absorbance of the final solution was then measured with a spectrophotometer. The absorbance (*A*) of the liquid sample is related to the molar extinction coefficient at a specific wavelength, ε (L/mol.cm), the molar concentration, *c* (mol/L) and the thickness of the cuvette, *d* (cm) via the Beer-Lambert Law. The molar extinction coefficient for the complex, ε, was previously reported as 39.986 L/cm.mol [205]. The number of moles of ferric ions in the sample can be determined by the following equation:

$$n_{Fe^{+3}} = \left(\frac{A}{\varepsilon.d}\right) \cdot \left(\frac{DF.V_{final}}{M_{Fe^{3+}}}\right) \tag{6.1}$$

The stoichiometric coefficient for Fe_3O_4 and Fe^{3+} is 1:3 from the reaction between ferric oxide and hydrochloric acid. The concentration of iron oxide is calculated by multiplying the amount of Fe^{3+} (mol) with molecular weight of magnetite, followed by division with sample volume (V_{sample}):

$$c_{\text{magnetite}} = \left(\frac{A}{\varepsilon.d}\right) \cdot \left(\frac{DF.V_{\text{final}}}{M_{Fe^{3+}}}\right) \cdot \left(\frac{1}{3}\right) \cdot \left(\frac{M_{\text{magnetite}}}{V_{\text{sample}}}\right) \tag{6.2}$$

6.3. RESULTS AND DISCUSSION

The average size and size distributions of both commercial and synthesized magnetite nanoparticles were analyzed by measuring more than 100 particles for each sample on corresponding transmission electron microscopy (TEM) images. TEM micrographs, average particle diameter, size distributions and corresponding sample standard deviations of FluidMAG-UC/A, FluidMAG-Amine, FluidMAG-CMX and oleic acid coated iron oxide nanoparticles are shown in Figure 6.1.
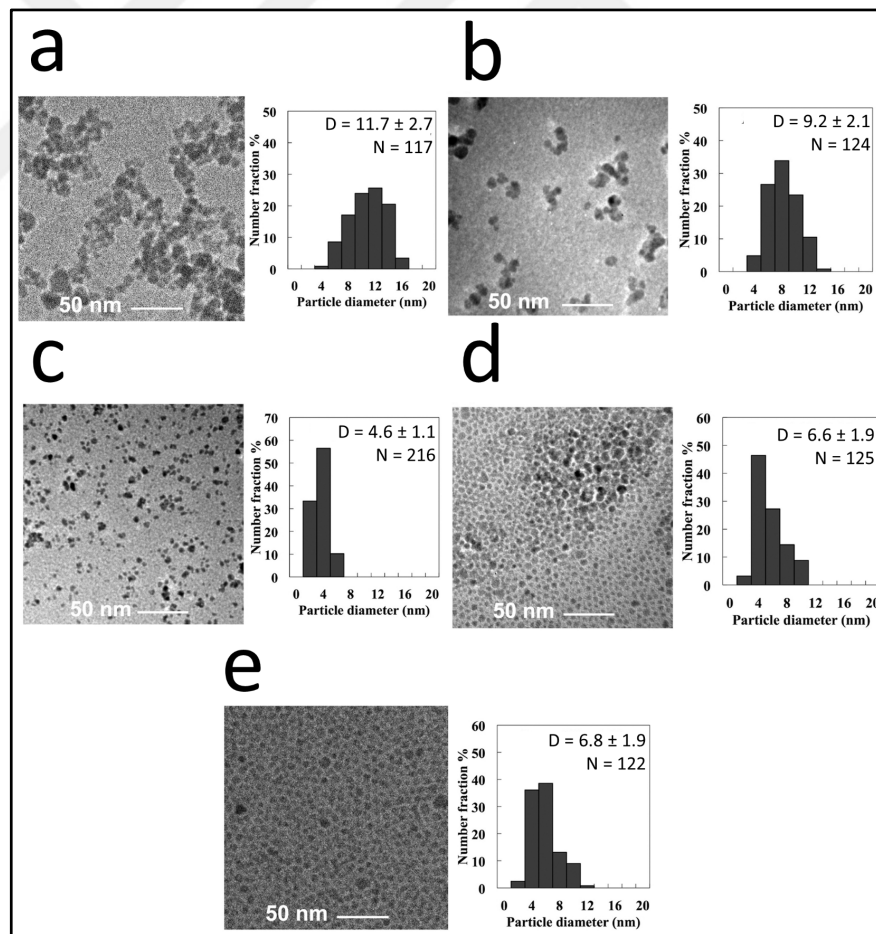
Figure 6.1. TEM images and corresponding particle size histograms of FluidMAG-UC/A (a), FluidMAG-Amine (b), FluidMAG-CMX(c), MAG/OA-HEP (d), MAG-OA-HEX (e).

The average particle size for bare particles (FluidMAG-UC/A) was measured as 11.7 nm with a sample standard deviation of 2.69 nm (Figure 6.1-a). On the other hand, the average size of aminosilane (FluidMAG-Amine) and carboxymethyl-dextran (FluidMAG-CMX) coated particles were measured as 9.24 nm and 4.58 nm, respectively, while the synthesized particles prepared by thermal decomposition method which are dispersed in heptane and hexane had average sizes of 6.64 nm and 6.82 nm, respectively (Figure 6.1-b,c,d,e). Crystal structure and phase identification of the samples were obtained by X-ray diffraction. As shown in Figure 6.2, XRD spectra of all samples match with the simulated diffraction data of magnetite.
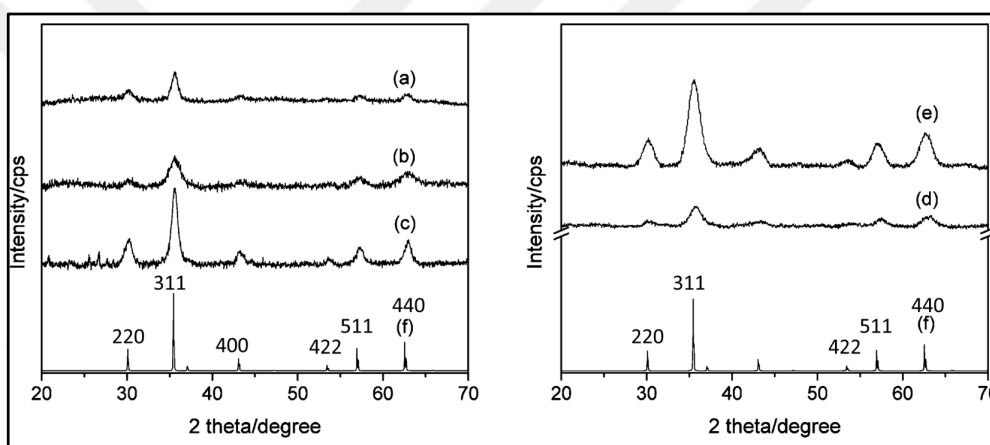
Figure 6.2. X-ray diffraction patterns of (a) FluidMAG-UC/A, (b) FluidMAG-CMX, (c) FluidMAG-Amine, (d) MAG/OA-HEP, (e) MAG/OA-HEX and (f) simulated powder diffraction data for magnetite.

As the XRD patterns of magnetite and its oxidized form maghemite are similar, Raman spectroscopy was also performed to verify the magnetite phase. In order to prevent transformation into hematite [17, 206], a laser power of less than 0.2 mW was utilized. The results are shown in Figure 6.3 and all intensity peaks given in Table 6.1 are compared with those reported for Raman spectroscopy on iron oxide nanoparticles [207, 208]. As can be seen from Figure 6.3 and Table 6.1, all commercial and synthesized samples have a distinguishable intense peak around 670 cm^{-1} which is accepted as the signature peak of bulk magnetite [17, 206-210]. Three other theoretical frequencies of magnetite give peaks around 303-306, 450-510 and 528-538 cm^{-1}.
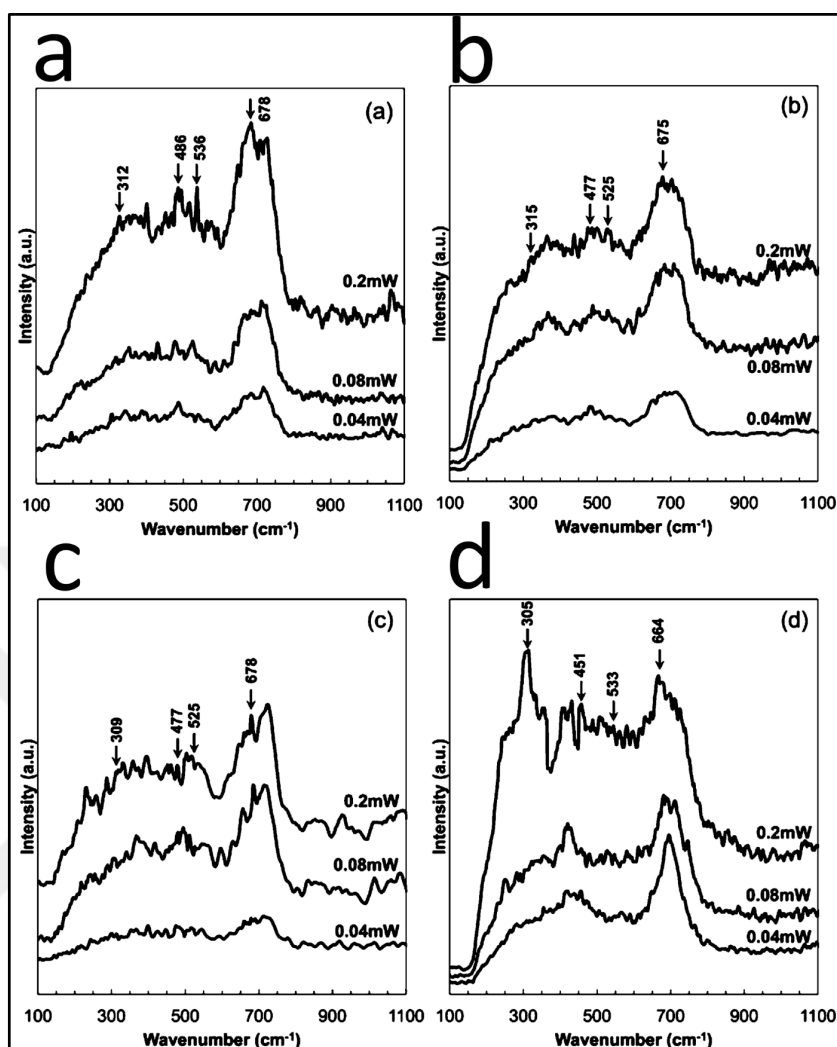
Figure 6.3. Intensity as a function of wavelength from confocal raman measurements of (a) FluidMAG-UC/A, (b) FluidMAG-Amine, (c) FluidMAG-CMX and (d) MAG-OA.

The Raman spectrum of bare particles (FluidMAG-UC/A) showed an intense peak at 678 cm^{-1} and additional signals at 312, 486 and 536 cm^{-1}, which are in good agreement with previous studies [207]. The wide shoulder around 700-720 cm^{-1} is attributed to maghemite, possibly revealing from the oxidation of magnetite during sample preparation [207, 208, 210, 211]. Functionalized commercial samples, FluidMAG-Amine and FluidMAG-CMX both have intensive peaks at 675 cm^{-1} and 678 cm^{-1}, respectively, along with other representative peaks, indicating the existence of magnetite. However, both samples, especially FluidMAG-CMX, represent additional peaks around 710 cm^{-1} indicating the presence of maghemite. Although the existence of maghemite phase is demonstrated by

Raman spectroscopy, it is not possible to quantify the magnetite to maghemite ratio, thus it was assumed that all samples consist of pure magnetite in the calculations. The shoulders visible at 277 cm^{-1} and 326 cm^{-1} for carboxymethyl dextran coated particles provided additional evidence that these samples consisted of magnetite [208]. Oleic acid coated nanoparticles (MAG-OA) also have an intense peak with a shoulder at 664 cm^{-1} and peaks at 305, 451 and 533 cm^{-1}, suggesting that the synthesis method followed in this study produces magnetite nanoparticles and minor amounta of maghemite.

Table 6.1. Summary of the Raman Frequencies (cm^{-1}) of the samples. st:strong.

MAG UC/A	MAG Amine	MAG CMX	MAG OA	Maghemite [208]	Magnetite [207]
678	675	678	664	703 (st)	668 (st)
536	525	525	533	652	538
486	477	477	451	502	450-490
312	315	309	305	330	306

The presence of the surface coatings for commercial samples was validated by X-ray photo-electron spectroscopy (XPS). Wide range scans for FluidMAG-UC/A, FluidMAG-Amine, FluidMAG-CMX and the carbon tape used to mount the samples are shown in Figure 6.4 where the regions scanned with high resolution and used for detailed surface analysis are specifically marked. The insets show Fe $2p_{3/2}$ and $2p_{1/2}$ peaks for commercial samples at 711.0 eV and 724.6 eV binding energies, respectively, which are in good agreement with the literature [155, 212-215]. The low intensity seen for Fe2p peaks of FluidMAG-CMX suggest a thick carboxymethyl dextran coating on the surface of the particles inhibiting the penetration of X-rays to the iron core. The hydroxyl groups present both on the uncoated (FluidMAG-UC/A) and amine coated (FluidMAG-Amine) sample exhibit an O1s peak at 530.2 eV, as shown previously [214]. FluidMAG-Amine contains aminosilane groups that expose their amino groups to the surface of the particle. The presence of this group is confirmed by the presence of peaks at 399.9 eV and 401.0 eV, which represent –NH$_2$ groups [216]. FluidMAG-CMX has an O1s peak at 532.4 eV which is a signature of the carboxymethyl dextran coating [217]. This sample also contains peaks at 287.4 eV and 288.9

eV corresponding to C-O-C bond and carboxyl group (-COOH), respectively [218]. These results support the existence of surface coatings around the particles as reported by the manufacturer.
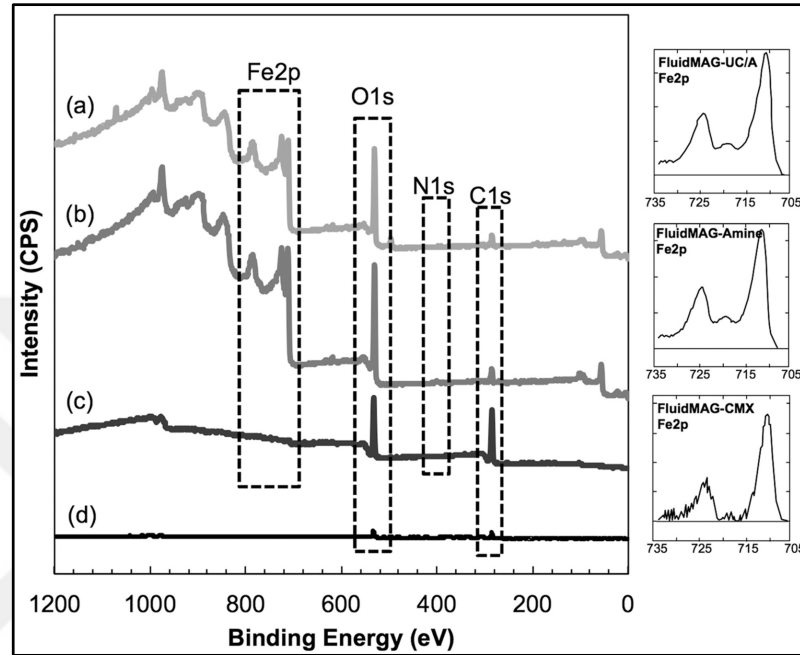
Figure 6.4. XPS spectra in the Fe2p, O1s, N1s and C1s regions of (a) FluidMAG-UC/A, (b) FluidMAG-Amine, (c) FluidMAG-CMX and (d) carbon tape. Insets: Higher resolution of Fe2p regions for the samples.

For the analysis of magnetic phase reduction due to the presence of a surface coating around the magnetic nanoparticles, results of the tiron chelation test were compared with magnetic properties as derived from the magnetization curves (Figure 6.5). For the tiron chelation test, the absorbance of the samples was measured at 480 nm and the corresponding masses of the magnetite phase were calculated, the results of which are given in Table 6.2. The saturation magnetization of the samples obtained from VSM analysis can be used to estimate the volumetric concentration of the magnetic phase, φ,[219] using Equation 6.3:

$$\varphi = \frac{M_s}{M_b} \tag{6.3}$$

where M_s and M_b are the saturation magnetization of the magnetic nanofluid and bulk iron oxide (446 kA/m[19]), respectively. Finally, the mass concentration of the particles in solution can be determined from:

$$C_M = \varphi \cdot \rho_p \qquad (6.4)$$

Where ρ_p is the mass density of magnetite (5.18 g/mL) [220].
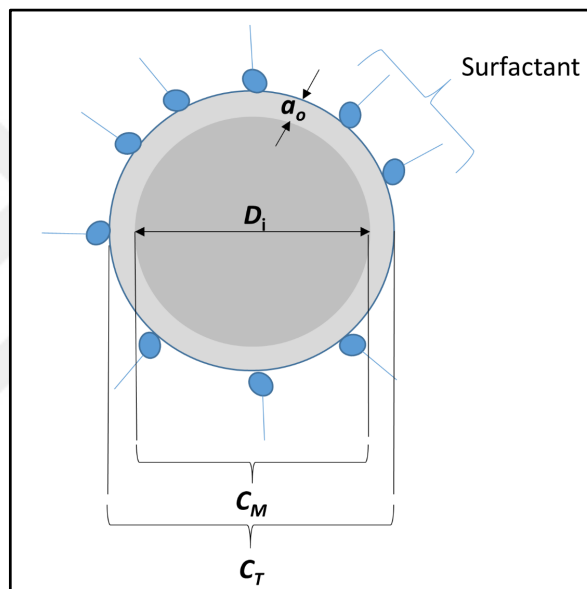
Figure 6.5. Schematic representation of the particle and the non-magnetic layer.

Table 6.2 shows the mass concentrations calculated from the tiron chelation test (C_M) and the magnetization curves (C_T) along with their ratio. This ratio (C_M/C_T) simply represents the proportion of magnetic phase to the entire magnetite mass present in the solution (Figure 6.6). As expected, the magnetization measurements indicate smaller amounts as compared to tiron chelation test due to the reduction in the magnetic phase as a result of the surface modification [197, 221]. Therefore, (C_M/C_T) will be used as a measure of magnetic phase reduction which accounts for the surface disorder that causes the non-magnetic layer within the magnetic core and not the surfactant layer around the particles.

For the analysis of the effective radius of the magnetic core and the thickness of the nonmagnetic layer, the experimental magnetization is fitted by the modified Langevin model [197]. For polydisperse suspensions, the magnetization of the ferrofluid of volume V_o with n_i particles of volume v_i can be calculated by using size distributions from:

$$\frac{M}{M_b} = \sum_{i=1}^{\infty} \left\{ \coth\left(\frac{v_i.M_b H}{4\pi kT}\right) - \frac{4\pi kT}{v_i.M_b H} \right\}.n_i.v_i/V_o \tag{6.5}$$

where k is the Boltzmann constant, T is the absolute temperature, H is the applied field, and M_b is the bulk magnetization of the material. The volume concentration, φ_o of the total mass of magnetite is:

$$\varphi_o = \left(\sum_{i=1}^{\infty} n_i.V_i\right)/V_o \tag{6.6}$$

where $V_i = (\pi/6).D_i^3$ is the total volume of the particle, including the nonmagnetic surface layer. The effective volume of the magnetic core can then be expressed by;

$$V_i = \left(\frac{\pi}{6}\right).(D_i - 2a_o)^3 \tag{6.7}$$

where a_o is the thickness of the nonmagnetic layer formed due to the presence of the surface coating. By substituting Equations 6.6 and 6.7 into 6.5, the final expression for saturation magnetization as a function of material properties is obtained as:

$$\frac{M}{\varphi_o.M_b} = \sum_{i=1}^{\infty} \left\{ \coth\left(\frac{(D_i - 2a_o)^3.M_b H}{24kT}\right) - \frac{24kT}{(D_i - 2a_o)^3.M_b H} \right\}.n_i.(D_i - 2a_o)^3 / \sum_{i=1}^{\infty} n_i.D_i^3 \tag{6.8}$$

Table 6.2. Mass concentration of magnetic phase as calculated from magnetization curves and from Tiron chelation test.

Sample	Tiron test C_T (mg/mL)	Magnetization test C_M (mg/mL)	C_M/C_T	a_o (nm)
FluidMAG-UC/A	23.6	14.2	0.602	1.06 ± 0.34
FluidMAG-Amine	30.9	15.4	0.498	1.51 ± 0.51
FluidMAG-CMX	33.8	21.6	0.639	0.54 ± 0.22
MAG/OA-HEP	28.2	14.9	0.528	0.58 ± 0.07
MAG/OA-HEX	14.9	5.9	0.396	0.97 ± 0.12

Equation 6.8 was fitted against the experimental magnetization as a function of the applied field. The numbers of particles n_i, and the corresponding diameter D_i were obtained from the histograms of the samples (Figure 6.1). The volume concentration of total magnetite phase φ_o was determined from the mass concentration from the tiron chelation test, C_T and the density of the particles. The fits together with experimental magnetization curves are shown in Figure 6.6. By using the size distributions of the samples, three optimal a_o values for each magnetization curves were obtained and their averages along with their standard errors are shown in Table 6.2. For FluidMAG-Amine, and FluidMAG-CMX particles, the end groups of the coatings are attached to the surface of magnetite through hydrolysis reactions and the formation of Si-O and C-O bonds [222]. The maximum reduction of the magnetic phase is observed in the FluidMAG-Amine sample, where the average thickness of the nonmagnetic layer is approximately 1.5 nm. On the other hand, the smallest reduction of the magnetic phase occurs in FluidMAG-CMX, where the nonmagnetic layer is only 0.54 nm. It has been reported that the saturation magnetization of iron oxide nanoparticles decreases with decreasing particle size in the superparamagnetic regime [223]. Most studies attribute this deterioration in saturation magnetization to the existence of surface coatings on the surface of the particles [197-199], which causes the spins of the iron atoms on the surface to be pinned [224]. These coatings also affect the canting angles of magnetic moments of Fe atoms thus producing magnetic disorder [225]. As a consequence, different coatings exhibiting

different interactions with the surface are expected to produce different effects leading to unique nonmagnetic layer thicknesses.
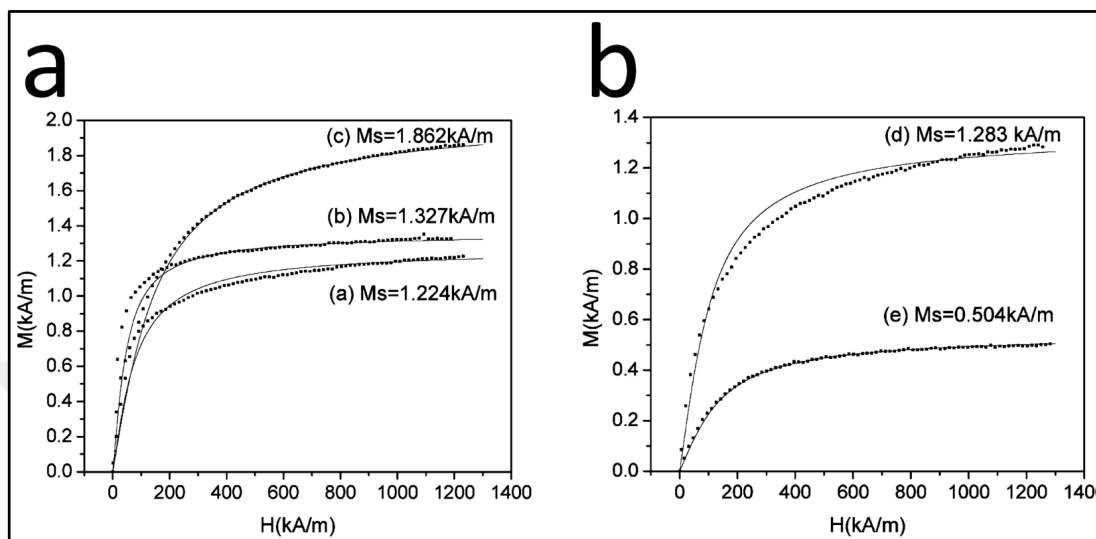
Figure 6.6. Experimental (■) and fitted (-) magnetization as a function of applied field for FluidMAG-UC/A (a), FluidMAG-Amine (b), FluidMAG-CMX (c), MAG/OA-HEP (d) and MAG/OA-HEX (e).

Interestingly, particles in FluidMAG-UC/A, which have no coating, show a reduction in magnetization and an effective nonmagnetic layer of 1.06 ± 0.34 nm. The existence of this nonmagnetic layer can be a result of the positive surface charge which affects the electron states thus causing disorder at the surface [226]. This local magnetic anisotropy which arises due to the surface spin disorder, prevents complete alignment of the magnetic moment of the particle and reduces the effective magnetic dipole. Additionally the possible presence of a maghemite phase, most likely at the surface of the particle will also decrease the total magnetization of the sample as the total magnetization of maghemite is less than that of magnetite and this in turn affects the mass concentration of the particles calculated from the magnetization test. In order to overcome this, it is necessary to know the exact ratio of magnetite to maghemite phase via additional analysis i.e. conventional peak deconvolution technique by using X-ray diffraction [227]. It is then possible to calculate the overall saturation magnetization for the composite consisting of a core with saturation magnetization M_{S1} and a shell with saturation magnetization M_{S2} by;

$$M_s = \frac{M_{s1}.V_1 + M_{s2}.V_2}{V_1 + V_2} \tag{6.9}$$

where V_1 and V_2 are volumes of the core and shell, respectively.[228] By following this, calculations for each sample should be performed independently and Equations 6.5 - 6.8 should be reorganized accordingly.

For synthesized oleic acid coated nanoparticles, COO- group bonding with Fe ions also leads to the formation of a magnetically disordered layer. The reduction of the magnetic phase is expected to depend on the solvent used to suspend the particles [197]. The calculated reductions (C_M/C_T) for heptane and hexane are 0.53 and 0.4, while corresponding thicknesses of the nonmagnetic layers are 0.58 nm and 0.97 nm, respectively. The thinner layer for magnetic particles in heptane may be attributed to higher oleic acid adsorption (2.4 mmol/g) compared to those in hexane (1.6 mmol/g) for oleic acid coated magnetic nanoparticles [229, 230]. Thus, it is possible that heptane as a base fluid hinders the interactions between oleic acid and magnetite more and therefore causes thinner nonmagnetic layer formation.

6.4. CONCLUSION

In this study, the tiron chelation test and magnetization measurements were applied to determine the mass concentrations of the magnetic phase and the total amount of magnetite in ferrofluids. Commercial magnetic nanoparticles with different biocompatible coatings dispersed in water along with synthesized particles coated with oleic acid dispersed in hexane and heptane were studied. It was shown that the reduction of the magnetic phase in nanoparticles changes with different coatings as well as solvents. The magnetic phase reduction observed in commercial samples may be due to the surface spin disorder caused by the absorbance of coatings. For the oleic acid coated samples, the difference observed amongst two that are in different solvents may be attributed to the compatibility of the solvent with the surfactant layer that affects the solvation thus the thickness of the stabilizing layer causing a difference in the non-magnetic layer.

As a consequence, in order to optimize the properties of the magnetic nanoparticles for various applications, it is essential to consider the reduction of magnetic phase in the presence of different coatings and suspension base fluids. These interactions affect not only the effective magnetic phase but also other properties that depend on the size of the magnetic core such as relaxation.

7. DETERIORATION IN EFFECTIVE THERMAL CONDUCTIVITY OF AQUEOUS MAGNETIC NANOFLUIDS

7.1. INTRODUCTION

Thermal conductivity is one of the essential properties of materials that directly affect the rate of heat transfer in applications involving a temperature gradient. It is known that heat transfer fluids, such as mineral oil, ethylene glycol and water, have low thermal conductivities thus there is an increasing need for replacing these fluids or improving their thermal properties for better heat transfer. On the other hand, solids have thermal conductivities superior to many of the above mentioned heat transfer fluids [231]. Although an enhancement in efficient thermal conductivity was obtained with micrometer size solid particles dispersed in a carrier fluid, problems of particle sedimentation and clogging prevented the use of these suspensions in heat transfer applications. In order to overcome these limitations, nanometer size particles with high surface area and better stability have been used and many theoretical and experimental investigations were performed on thermal conductivity enhancement of these particles [232-235]. Brownian motion and aggregation which improves the thermal transport were claimed to be the reasons of enhanced thermal conductivity of nanofluids [236, 237].

Thermal conductivities of magnetic nanofluids composed of iron oxide nanoparticles dispersed in various base fluids have been investigated experimentally and the results showed that the thermal conductivity linearly increases with increasing particle concentration but also depends on the method of preparation and the base fluid used [146, 238]. However, there are contradictory results showing enhancement both with increasing [146] and decreasing particle size [239, 240]. It was also shown that at the same volume fractions, Fe_3O_4 nanofluids have higher thermal conductivity than other metal oxide nanofluids such as CuO, TiO_2 and Al_2O_3 as a result of nanoparticle alignment [241]. Although the thermal conductivity of aqueous nanofluids increases while that of non-aqueous nanofluids decreases with temperature, the ratio of the nanofluid thermal conductivity to base fluid thermal conductivity remains constant [238, 242], implying that the temperature dependence of the thermal conductivity does not change upon addition of

nanoparticles. The enhancements obtained in thermal conductivity of nanofluids were found to be higher [146, 241] than the predictions of effective medium theory as proposed by Maxwell [243], and other theoretical models [244]. On the other hand, Timofeeva et al. showed that Al_2O_3-based nanofluids have enhancements that agree well with effective medium theory [245]. Some empirical models for specific conditions were also presented [246].

Previously Abareshi et al. [247] synthesized magnetite nanoparticles via the chemical precipitation method and used tetramethyl ammonium hydroxide to obtain stability in aqueous medium. They showed an increase in thermal conductivity with increasing volume fraction and obtained an enhancement of up to 11.5 % at 3 vol% of nanoparticles. Similarly, Shima et al. reported an enhancement in thermal conductivity of water-based magnetic nanofluids having the same tetramethyl ammonium hydroxide layer stabilizing the particles [242]. On the other hand, Wang et al. [248] showed an enhancement in thermal conductivity for oleic acid coated magnetite particles dispersed in toluene. The same particles dispersed in water after ligand exchange with poly(acrylic acid) showed a fluctuating trend for the thermal conductivity change as a function of particle concentration, which was attributed to the self-assembled aggregation of particles leading to an increase in interfacial thermal resistance. Their results also indicate a deterioration of thermal conductivity of their aqueous dispersions for both 4 nm and 8 nm particles at different particle loadings. However, the possible mechanism responsible for this deterioration upon addition of magnetic nanoparticles to water was not addressed.

The possibility of manipulating the organization and alignment of the magnetic nanoparticles in a system via a fixed or an alternating magnetic field is another essential property of magnetic fluids and shown to affect the thermal properties both in the presence and absence of an applied external magnetic field [237, 238, 249, 250]. The enhancement or deterioration of thermal conductivity of magnetic nanofluids are expected to affect their applications in systems such as heat exchangers [251].

In this study, superparamagnetic magnetite (Fe_3O_4) nanoparticles synthesized by co-precipitation and thermal decomposition methods were used to investigate the change in effective thermal conductivity of water and ethylene glycol at different temperatures as a

function of particle concentration. In order to improve the stability and investigate the effect of surface coating on the thermal conductivity of nanofluids, the synthesized nanoparticles were coated with organic acids, namely citric acid and capric acid. Regardless of the synthesis method and the type of surface coating, the thermal conductivity of water was found to decrease upon addition of magnetite nanoparticles which contradicts almost all previous reports. Furthermore, this deterioration of thermal conductivity also increased with particle loading.

7.2. EXPERIMENTAL

7.2.1. Materials

For the synthesis of magnetite nanoparticles by chemical coprecipitation, ferrous sulfate heptahydrate (FeSO$_4$.7H$_2$O) and ferric chloride (FeCl$_3$) from Riedel-de Haen with sodium hydroxide (NaOH) from J.T. Baker were used. For the synthesis by thermal decomposition, iron (III) acetylacetonate (Fe(C$_5$H$_7$O$_2$)$_3$, 97%) and oleyl amine (C$_{18}$H$_{37}$N, ≥70%) from Fluka, 1,2 tetradecanediol (C$_{14}$H$_{30}$O$_2$, 90%) from Aldrich and oleic acid (C$_{18}$H$_{34}$O$_2$, 99%) from Riedel-de Haen were used. Capric acid (C$_{10}$H$_{20}$O$_2$, 98%) and citric acid (C$_6$H$_8$O$_7$, 99%) were purchased from Fluka and Aldrich respectively. For the determination of iron content of the prepared magnetic fluids, Tiron (98.5%) and 37% HCl (98.5%) were purchased from Riedel-de Haen. The solvents used are dibenzyl ether, (Merck, synthesis grade), 1,2 dichlorobenzene (Fluka, 98%), 25% NH$_4$OH in water (Riedel-de Häen), diethyl ether (Fluka 99%), N,N-dimethyl formamide (Fluka, 98%). All of the stated chemicals were used without any further purification.

7.2.2. Techniques

The size and shape of nanoparticles were investiaged with an FEI Tecnai™ G2 F30 Transmission Electron Microscopy (TEM) in the National Nanotechnology Research Center (UNAM) at Bilkent University, Turkey. For the phase identification and crystallographic identification of the samples, a Rigaku D/MAX-Ultima X-ray diffractometer (XRD) was

used. Thermal conductivities of nanofluids were measured with a Flucon GmBH Lambda thermal conductivity meter equipped with PSL Systemtechnik LabTemp 30190 (temperature controller) using 40-50 mL sample volume at fixed or variable ranges of temperatures.

7.2.3. Synthesis of magnetite nanoparticles

Superparamagnetic magnetite nanoparticles were synthesized using chemical co-precipitation (aqueous) and thermal decomposition (organic) methods. For the aqueous synthesis, ferrous and ferric salts were mixed at a stoichiometric ratio of 1:2 under an oxygen free environment provided by a flow of nitrogen through the reaction medium at 80 °C. Subsequently, ammonium hydroxide solution was added to the iron salts solution to precipitate magnetite as indicated by the color change from orange to black. Magnetic nanoparticles were collected with a handheld magnet and washed with distilled water for purification followed by drying at 60 °C overnight. Particle synthesis was also carried out in the presence of pre-determined amounts of citric acid and capric acid to obtain stability in aqueous medium. The additives were introduced to the synthesis by dissolving in the base solution. For organic phase synthesis, the high temperature decomposition of a ferric salt in dibenzyl ether was used in a procedure which was adopted from a previous report [14, 252]. Briefly, iron (III) acetylacetonate, 1-2 tetradecanediol, oleic acid and oleylamine were dissolved in dibenzylether at an oxygen free environment in a round bottom flask. Subsequently, the reaction medium was heated up to 300 °C at a rate of 2.5 °C/min during which the solution was kept at 100 °C for 15 minutes and at 200 °C for 2 hours. When the final temperature was reached, the resulting solution was aged for 2 hours. The reaction medium was then allowed to cool down to room temperature and the hydrophobic particles were collected after mixing with methanol and centrifugation. For the dispersion of the particles in aqueous medium, ligand exchange from oleic acid to citric acid was performed for which hydrophobic magnetite nanoparticles were dispersed in a 1:1 mixture of 1,2 dichlorobenzene and N,N dimethylformamide in the presence of citric acid. The final solution was heated up to 100 °C and aged for 24 hours. Hydrophilic, citric acid coated particles were then collected via centrifugation after mixing with diethylether for phase separation. The tiron chelation test was applied for the magnetic fluids in order to obtain the

iron/magnetite content for which the measurement and calculation details are given in the chapter 6 of this thesis [117, 253].

7.3. RESULTS AND DISCUSSION

The size and morphology of the synthesized magnetic iron oxide nanoparticles were analyzed by Transmission Electron Microscopy (TEM). As shown in Figure 7.1, for the particles synthesized via thermal decomposition (a) and chemical co-precipitation (b) methods, average diameters of about 6 nm and 10 nm were found, respectively, while particles obtained through thermal decomposition had narrower size distribution. While organic phase synthesis yielded spherical particles, aqueous synthesis produced particles with various morphologies, as previously reported [48].
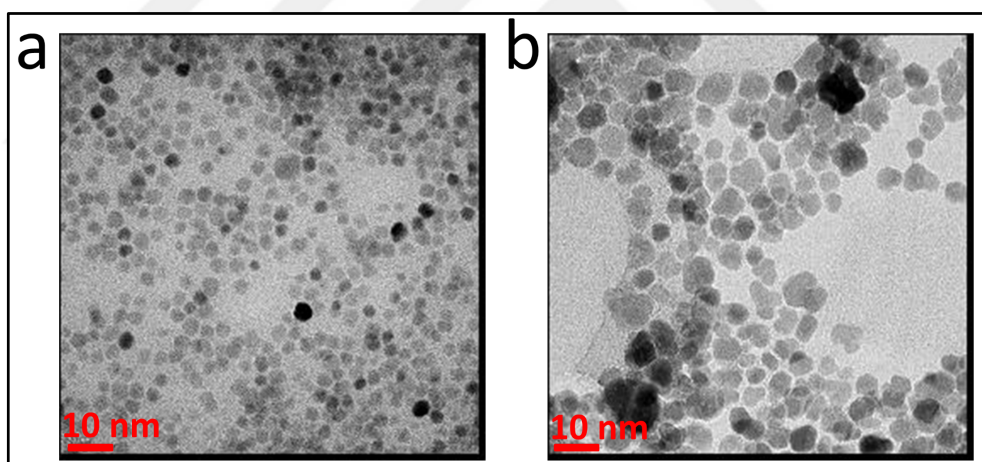
Figure 7.1. TEM images of magnetite nanoparticles synthesized by (a) thermal decomposition (organic) show roughly spherical morphology and an average size of 6 nm (b) co-precipitation (aqueous) methods show various morphologies and an average size of 10 nm.

Phase identification was achieved by X-ray diffraction (XRD) analysis on dried nanoparticles. For the thermal decomposition method, the product was identified as pure magnetite (Figure 7.2). The particles synthesized by the co-precipitation method both in the presence and absence of additives were also assumed to be composed of pure magnetite, as

it was reported in detail previously [53, 254]. As the particles were prepared by dissimilar methods they had different surface modifications in order to improve stability in the base fluid. Oleic acid coated particles resulting from the thermal decomposition method, which underwent ligand exchange with hydrophilic citric acid, showed good dispersibility in water as did the one-step citric acid and capric acid coated particles from the co-precipitation method. All obtained magnetic nanofluids were stable for the duration of the experiment. Further details about the corresponding characterization of the particles prepared by these methods can be found in previous reports [146, 249].
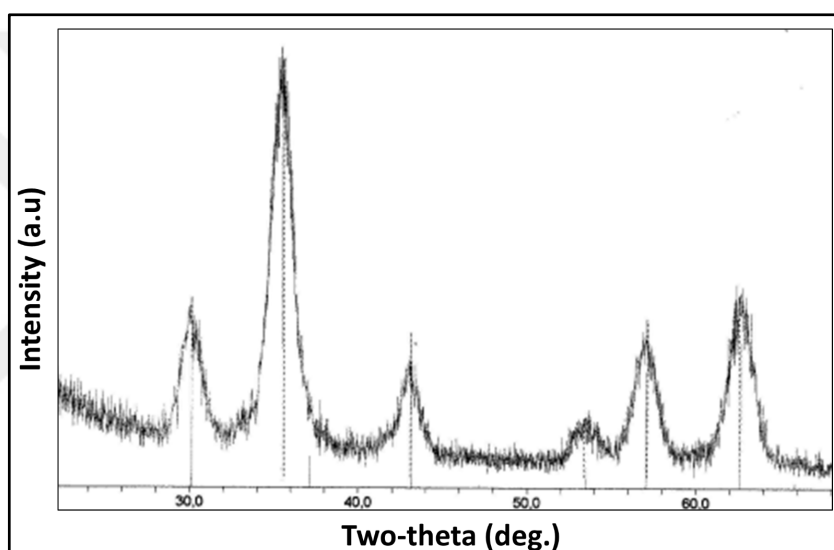
Figure 7.2. XRD pattern for particles synthesized by thermal decomposition method. Relative intensities and peak positions match well with standard magnetite peaks.

Thermal conductivity of magnetic nanofluids were measured with Flucon GmBH Lambda instrument equipped with a PSL Systemtechnik LabTemp 30190 temperature controller. Magnetic nanoparticles capped by hydrophilic surface agents synthesized via both thermal decomposition and chemical coprecipitation methods were dispersed in ethylene glycol and water for the measurements. Figure 7.3 and Figure 7.4 show the effective thermal conductivity of nanofluids functionalized by citric acid and capric acid. Although all previous reports showed enhancement in the thermal conductivity of any type of carrier fluid upon addition of magnetic nanoparticles, the present results illustrate deterioration of thermal conductivity, regardless of particle loading or surfactant type. The thermal

conductivity of citric acid coated magnetic nanoparticles as well as capric acid coated ones (which were stable in water directly after the synthesis) showed a decrease in thermal conductivity up to 60% at 20 °C. Furthermore, this deterioration was found to increase with increasing temperature and particle concentration. This abnormal behavior was first attributed to the presence of excess citric acid or capric acid in the medium, inhibiting the
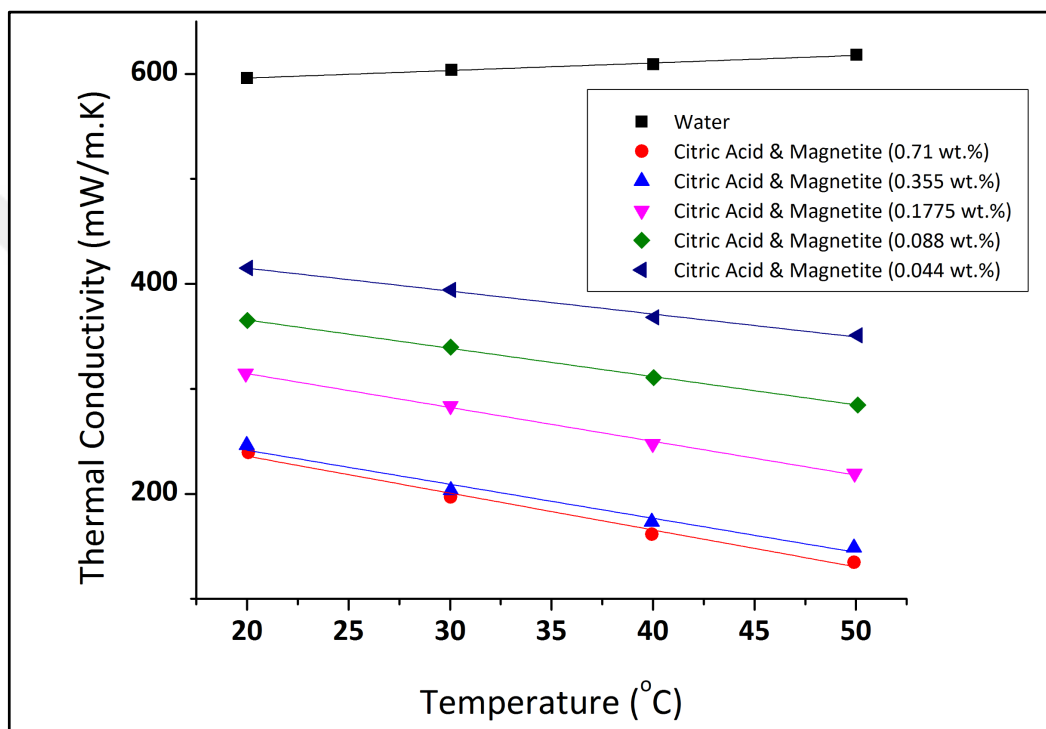
Figure 7.3. Thermal conductivity of citric acid stabilized magnetite nanoparticles dispersed in water at different concentrations as a function of temperature show increasing deterioration in thermal conductivity by increasing magnetite concentration.

thermal transport between the particles, which may affect the thermal conductivity. However, when the citric acid coated particles were washed with methanol several times and dried in vacuum for the removal of excess citric acid, again a significant decrease in thermal conductivity (29%) was obtained. This shows that although the excess additive in the medium decreases the thermal conductivity of water, it is not responsible for the overall deterioration as the thermal conductivity of nanofluid itself is lower in both cases than the corresponding additive solutions that were used as controls (Figure 7.4 and Figure 7.5).
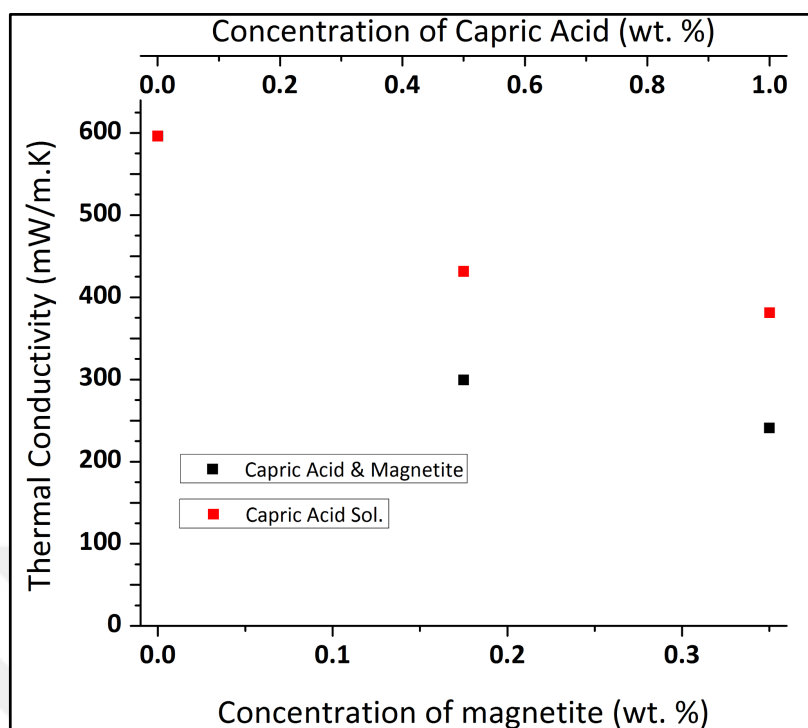
Figure 7.4. Thermal conductivity of capric acid stabilized magnetite nanoparticles synthesized via chemical precipitation, dispersed in water at different concentrations and at 20 °C. Corresponding capric acid concentrations are given for comparison.

As a result of the synthesis method, the surface of the particles is charged at the pH used, due to the presence of ionic stabilizers. In order to have further insight on the effect of electrostatic repulsion of the particles on the thermal conductivity decrease of water, a non-ionic polymer, poly(vinylpyrrolidone) (PVP), was used to stabilize magnetite. Initial results showed that PVP-coated magnetite nanoparticles indeed decreased the thermal conductivity of water demonstrating that the electrostatic repulsion or surface charge is not solely responsible for the deteriorations obtained. It was previously reported that the type of synthesis method and hence the formation mechanism also affects the thermal conductivity of the carrier fluids [146]. In order to compare the deterioration of thermal conductivity for particles synthesized by the aqueous co-precipitation method, magnetite particles were also prepared by the thermal decomposition method. Oleic acid and oleylamine capped particles synthesized via this method underwent a ligand exchange with citric acid and then were dispersed in water and ethylene glycol. Figure 7.6 shows again that the addition of citric acid coated magnetite nanoparticles to water caused a decrease in thermal conductivity at all

temperatures. Remarkably, the decrease in thermal conductivity of water is remarkably lower upon addition of the particles synthesized via thermal decomposition than for those prepared by co-precipitation at comparable particle concentrations. As the average particle sizes obtained from co-precipitation and thermal decomposition methods were comparable, this unexpected loss of thermal properties cannot be explained, neither by the size effect nor by the surface coating around the particles.
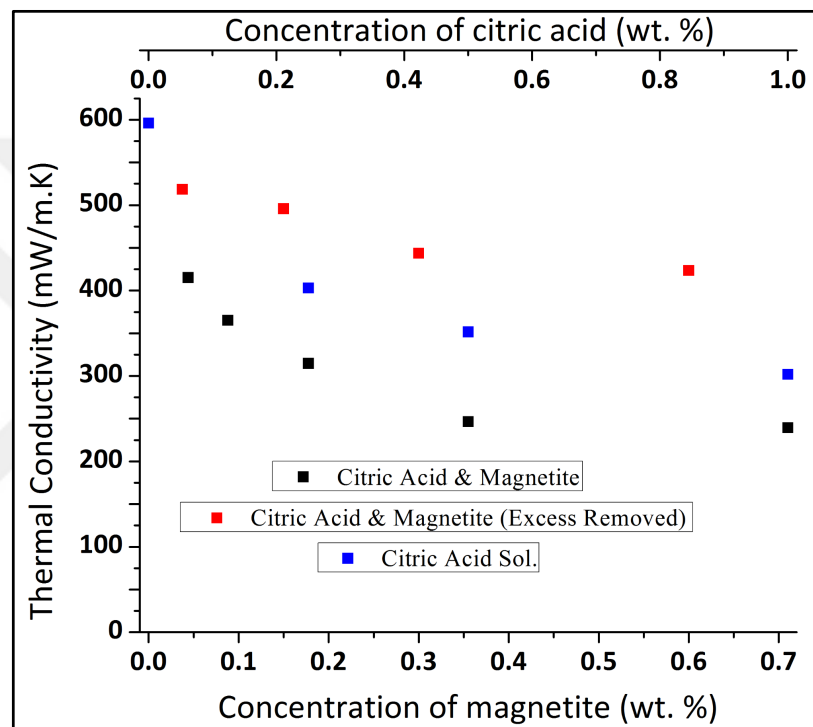
Figure 7.5. Thermal conductivity of citric acid stabilized magnetite nanoparticles synthesized via chemical precipitation, dispersed in water at different concentrations and at 20 °C. Corresponding citric acid concentrations are given for comparison. Citric acid concentration is unknown for the retreated sample (Excess Removed).

To further investigate the effect of the base fluid on the thermal conductivity of polar magnetic nanofluids, particles synthesized by thermal decomposition and functionalized by citric acid were dispersed in ethylene glycol. It was demonstrated that ethylene glycol, which is commonly used as heat transfer fluid shows considerable increase in thermal conductivity upon addition of nanoparticles [255]. However our experiments showed that the addition of

nanoparticles did not lead to a significant decrease in thermal conductivity as in the case of aqueous nanofluids (Figure 7.6); however, no enhancement was observed either.
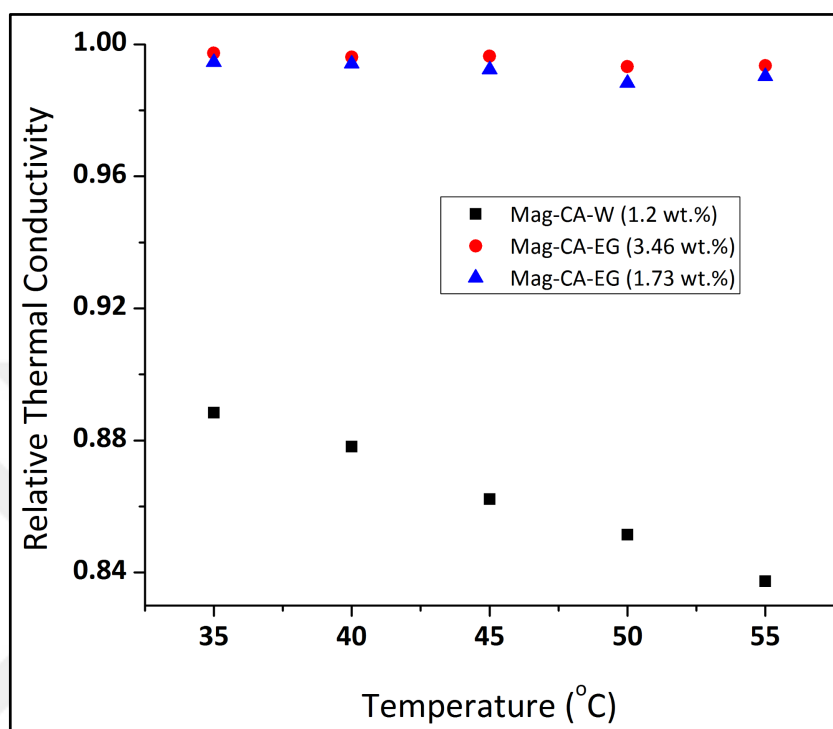
Figure 7.6. Relative thermal conductivity of magnetite nanoparticles synthesized via thermal decomposition method as a function of temperature. (Mag-CA-W: Citric acid stabilized particles in water, Mag-CA-EG: Citric acid stabilized particles in ethylene glycol).

The above results show that the deterioration of thermal conductivity of a nanofluid is higher where the thermal conductivity of the base fluid itself is higher. This variable effect in different carrier fluids can be due to the compatibility of the synthesized particles with the base fluid via the stabilizing layer [146]. It has been reported by many groups that the thermal conductivity of nanofluid systems are higher than that of the base fluid [232, 233, 251]. Also it was pointed out that the dependency of nanofluid thermal conductivity on temperature is similar to that of the base fluid. If the particles are suspended in an organic solvent then the thermal conductivity values are expected to decrease with increasing temperature, while for water reverse is true as water itself has different thermal properties. However, in the present

study, all the measurement were performed on polar nanofluids and interestingly the corresponding thermal conductivity values all were found to decrease with increasing temperature, as in the case of organic carrier fluids. In order to verify the measurements, a sample of citric acid coated magnetite nanoparticles synthesized by chemical co-precipitation method was sent to Flucon GmBH for testing with their most recent thermal conductivity device. The analysis of 1 wt. % citric acid coated magnetic particles in water showed the same decrease in thermal conductivity (Data not shown).

Nanofluid systems contain nanoparticles, in some cases appropriate surfactants and base fluids, either pure or as mixtures. As a whole, these materials form a composite system thus effective medium theory is expected to explain the behavior of the total system. Effective medium theory (EMT) uses the individual properties and relative fractions of the constituents to model the overall system. For the prediction of thermal conductivity of a binary system, Hamilton and Crosser proposed an EMT based model which is a modification of the well-known Maxwell theory [256, 257]. However, these early models under-predict the thermal conductivity changes in nanofluids as a result of accounting only for the volume fraction of the particles and thermal conductivities of both particles and the base fluid. Generally effective medium theory predicts the thermal conductivity enhancement in nanofluid as 3f, where f is defined as the volume fraction of the particles. This prediction fits well if the nanoparticle thermal conductivity is much higher than that of the base fluid (>20 times) [258]. However, in our case, this ratio is ~8, thus EMT is not applicable without further modifications. The under-prediction of EMT based models was attributed to the presence of interfacial thermal resistance (R) between nanoparticles and the surrounding fluid molecules which can limit the interaction of the particles and thereby decrease the thermal transport. The relative importance of this interfacial resistance is described by the equivalent thickness (h) which is defined as the ratio of fluid conductivity (k_f) to the interfacial conductance (G) as in Equation 7.1 [258],

$$h = \frac{k_f}{G} \tag{7.1}$$

Thermal conductance of nanoparticle-fluid systems is known only for a limited number of cases and no data exist for metal oxide nanoparticles and water systems. However, it has

been suggested to estimate the thermal conductance of nanoparticle-water system as 200 MW/m^{2}K [259]. Putnam et al. implemented interfacial thermal resistance in EMT and proposed a new model for the prediction of thermal conductivity of a composite containing low volume fraction of spherical nanoparticles that have bulk thermal conductivity ~10 times higher than the corresponding base fluid, which is given in Equation 7.2 [258].

$$\frac{k_{eff}}{k_f} - 1 = 3f \frac{(\gamma-1)}{(\gamma+2)} \tag{7.2}$$

where k_{eff} is the effective thermal conductivity and γ is the ratio of nanoparticle radius (r_p) to equivalent thickness;

$$\gamma = \frac{r_p}{h} \tag{7.3}$$

As can be seen from Equation 7.2, it is possible to obtain a deterioration in thermal conductivity of a nanofluid if and only if $\gamma < 1$. In order to satisfy this inequality, the equivalent thickness should be larger than the radius of the nanoparticle. For the case of magnetite nanoparticles and water, where all the assumptions for Putnam model are satisfied, the equivalent thickness, h, is ~3 nm. In order to be more accurate, thermal conductivity of the ammonium hydroxide and water mixture was calculated using the Flippov equation given in Equation 7.4 [260].

$$k = \omega_1 k_1 + \omega_2 k_2 - 0.72 \omega_1 \omega_2 (k_2 - k_1) \tag{7.4}$$

where ω and k are the weight fractions and pure component thermal conductivities, respectively. By using the mixtures thermal conductivity, the equivalent thickness was calculated to be 2.84 nm. As the average radius of the particles synthesized via thermal decomposition and coprecipitation are 3 and 5 nm, respectively, interfacial thermal resistance may be the reason behind the thermal conductivity deterioration for organic phase synthesis. However, although the interfacial resistance is relatively high, it is not sufficient to explain the decrease in thermal conductivity obtained for the nanofluids prepared by using

the particles synthesized via coprecipitation. On the other hand, it should be noted that the thermal conductance value used in the calculation of equivalent thickness may not be the appropriate value for the magnetite nanoparticles – water system. Further experimental studies are needed to obtain the specific thermal conductance for magnetite based nanofluids in order to have better approximations of interfacial thermal resistance.

Table 7.1. Properties used for the calculation of equivalent thickness

Thermal Conductance, G	200 MW/m^{2}K
Thermal conductivity of water, k_w	~ 0.6 W/m^{2}K
Thermal conductivity of ammonia, k_{NH4OH}	~ 0.5 W/m^{2}K
Thermal conductivity of mixture, k_f	~ 0.5685 W/m^{2}K
Weight fraction of water, ω_w	0.8
Weight fraction of ammonia, ω_{NH4OH}	0.2
Equivalent thickness, h	2.84 nm

As a consequence, the overall deterioration of thermal conductivity for aqueous magnetic nanofluids cannot be solely explained, neither by the presence of surfactant molecules nor by the interfacial thermal resistance between particles and the base fluid. It is also well known that enhanced thermal properties e.g. thermal conductivity highly depends on the structure of the material. However, although the nanoparticles used in this study were synthesized via co-precipitation, which yields particles with comparably poor crystallinity, the deteriorations obtained for aqueous nanofluids cannot be individually attributed to this effect as the same particles were previously shown to enhance the thermal conductivity of various organic base fluds [146]. It is possible that the combined effect of all these individual factors contribute to the overall deterioration obtained for aqueous magnetic nanofluids. In the past decade there has been a growing interest on the heat transfer applications of nanofluid systems. As a result, the effect of nanoparticles on the thermal conductivities of base fluids has been studied by several groups [233]. Regardless of the synthesis method, concentration or particles size, various nanoparticles from metals [255, 261, 262], metal oxides [263-265] to nanotubes [266, 267] have been shown to enhance the thermal conductivity of corresponding base fluids that are generally used for heat transfer

applications such as water [263, 265], ethylene glycol [255, 263] and derivatives of alkanes [264, 268]. On the other hand, studies concentrating on magnetite nanoparticles are quite limited in the literature [146, 237, 246-250]. However, those studies also indicated enhancements in the thermal conductivity of the carrier fluid. Furthermore, our group previously showed that oleic acid coated magnetite nanoparticles increased the thermal conductivity of both hexane and heptane in the presence and absence of an external magnetic field [146, 249]. As all these studies involve different composition of particles, base fluids, particle concentrations and even synthesis methods, it is difficult to build a common understanding. Indeed where all the mentioned studies demonstrated an enhancement upon addition of nanoparticles to base fluids, the deteriorations obtained with magnetite nanoparticles in this study still remain a challenge to explain.

7.4. CONCLUSION

Following the previous studies that focus on the thermal conductivity enhancement of magnetic nanoparticles in the presence and absence of an external magnetic field for organic solvents, we further investigated the effect of particles having both ionic and non-ionic surface agents on the thermal conductivity of water. The measurements on the thermal conductivity of aqueous magnetic nanofluids were contradictory with previous studies on both magnetite and other nanoparticle systems. The thermal conductivity of both water as well as ethylene glycol was found to decrease upon addition of magnetic nanoparticles. This decrease was found to increase with particle loading and excess of stabilizing agents. It was further pointed out that the preparation method also changes the thermal properties of the particles, even though the particle sizes are comparable. We believe further studies on magnetic nanoparticles in polar base fluids are needed to fully understand the mechanism of this deterioration in thermal properties.

8. CONCLUSION AND RECOMMENDATIONS

Iron oxides are encountered frequently in our daily life and exist in different forms in Nature. Magnetite is one of the most important iron oxides that is used in various applications owing to its biocompatibility and superior magnetic properties. As the magnetic properties of magnetite mainly depend on its size and shape, it is important to control the formation of magnetite through synthetic routes. Although magnetite was the subject of countless studies for decades, the synthesis pathways at ambient conditions mimicking the perfection of nature still remain as a challenge.

The objective of the research presented in this thesis was to study extensively the formation, properties and applications of magnetite nanoparticles. For this purpose, initially the control over magnetite formation via different synthetic routes was investigated. Chapter 3 presented the study that focused on the control over magnetite formation via co-precipitation and partial oxidation methods at ambient conditions in the presence of random poly(amino acids) which inspired by the mineralization process in Nature specifically that of magnetotactic bacteria. The synthesis of magnetite nanoparticles by aqueous partial oxidation of ferrous hydroxide precursor in alkaline medium which was conducted at room temperature without additives produced big aggregates of cubic and octahedral ferrimagnetic magnetite nanoparticles having an average size of roughly 35 nm. When the synthesis was performed in the presence of pAsp, the average size, morphology, organization and stability in aqueous medium was found to be affected due to the polymer attachment onto the surface of magnetite crystals. Results showed a decrease of average particle size from 35 nm to 25 nm while the morphology of the particles changed from edged to spherical. It was also shown by liquid STEM and cryo-TEM analyses that the particles formed micro sized chains composed of several individual magnetite crystals and the existence of pAsp also enhanced the stability of the particles due to negative surface charge which gives the opportunity to use the synthesized particles in different applications. As the same additive had no influence on the final product in the co-precipitation method, the importance of the reaction kinetics on the controlled formation of magnetite nanoparticles was pointed out. The slower reaction kinetics of the partial oxidation method were attributed to the formation of ferrous hydroxide precursor at the early stages of magnetite formation which prevented extreme solution

supersaturations and allow the additives to have impact on the formation. Although the early stages of magnetite formation was investigated with cryo-TEM and LDED, the same approach in the presence of pAsp or other functional additives may give further information about their corresponding impact on the formation of magnetite nanoparticles at initial stages.

As the effective use of magnetite in desired applications depends on the stability and the magnetic properties of the particles, various polymers and surfactants were introduced to the most common synthetic methods to enhance the colloidal stability in aqueous medium. In chapters 4 and 5, the polymers used for the colloidal stability of both superparamagnetic and ferrimagnetic magnetite nanoparticles are demonstrated. For this purpose, magnetite was synthesized by co-precipitaton and partial oxidation methods in the presence of biocompatible polymers and their effect on morphology and stability were examined. By using co-precipitation, the function of the synthetic thermoresponsive PEI-*graft*-POEGMA was demonstrated as a stabilizer in the preparation of superparamagnetic magnetite nanoparticles which retained all the characteristics of the bare nanoparticles. However, further analyses are needed for the thermo-responsiveness (aggregation-precipitation behavior) of the magnetite-PEI-*graft*-POEGMA complex, as it is a potential candidate for biomedical applications. On the other hand, ferrimagnetic magnetite nanoparticles were synthesized by partial oxidation of ferrous hydroxide in the presence of poly(acrylic acid) (450 kDa) and dispersible particles were obtained which showed excellent colloidal stability in water for several days. To our knowledge, this is the first study that is capable of producing ferrimagnetic magnetite nanoparticles with high saturation magnetization via partial oxidation of ferrous hydroxide which can be stabilized in aqueous medium using a hydrophilic biocompatible polymer at neutral pH. These stable ferromagnetic magnetite nanoparticles can be a potential candidate for biomedical applications such as hyperthermia in cancer treatment as those possess hysteresis and high saturation magnetization which may lead to high heating capacity that possibly can be validated by corresponding specific absorption rate (SAR).

Furthermore, the effect of suitable surface agents on the magnetic properties of the particles was studied. Chapter 6 presents the reduction of magnetic properties due to presence of a magnetically disordered layer at the outmost shell of magnetite nanoparticles upon

application of surface agents that are mainly used to stabilize magnetite. For this purpose, the Tiron chelation test and magnetization measurements were applied to determine the mass concentrations of magnetic phase and the total amount of magnetite in ferrofluids. Reduction of this magnetic phase was investigated for (amine and carboxyl functionalized magnetic nanoparticles dispersed in water along with synthesized particles coated with oleic acid dispersed in hexane and heptane. It was shown that the reduction of the magnetic phase in nanoparticles depend on the type of coating as well as the solvent. The magnetic phase reduction observed in commercial samples is attributed to the surface spin disorder caused by the absorption of coatings. For the oleic acid coated samples, the difference observed is attributed to the compatibility of the solvent with the surfactant layer that affects the solvation thus the thickness of the stabilizing layer, causing a difference in the non-magnetic layer. These results pointed out the necessity to consider the reduction of magnetic phase in order to optimize the properties of the magnetic nanoparticles for various applications.

Finally, the possible applications of magnetite nanoparticles in heat transfer systems were analyzed by investigating the impact of the presence of magnetite nanoparticles on the thermal conductivity of different base fluids. Magnetite nanoparticles were prepared by different synthetic routes in the presence of additives (citric acid and capric acid). The changes in thermal conductivity of water and ethylene glycol, which are common heat transfer fluids were studied as a function of temperature and particle concentration. The measurements on the thermal conductivity of aqueous magnetic nanofluids were contradictory with previous studies focused on both magnetite and other nanoparticle – base fluid systems. The thermal conductivity of both water as well as ethylene glycol was found to decrease upon addition of magnetic nanoparticles. This decrease was found to increase with particle loading and excess amount of stabilizing agents. It was further pointed out that the preparation method also changed the thermal properties of the particles, even though the particle sizes were comparable. It was concluded that further studies on magnetic nanoparticles in polar base fluids are needed, e.g. the effect of particle aggregation or the use of ferrimagnetic particles, to fully understand the mechanism of this deterioration in thermal properties.

REFERENCES

1. R.M. Cornell and U. Schwertmann, *Introduction to the Iron Oxides*, in *The Iron Oxides*. 2004, Wiley-VCH Verlag GmbH & Co. KGaA. p. 1-7.

2. E. Matijević and P. Scheiner. Ferric hydrous oxide sols: III. Preparation of uniform particles by hydrolysis of Fe(III)-chloride, -nitrate, and -perchlorate solutions. *Journal of Colloid and Interface Science*. 63: 509-524, 1978.

3. J.K. Bailey, C.J. Brinker, and M.L. Mecartney. Growth Mechanisms of Iron Oxide Particles of Differing Morphologies from the Forced Hydrolysis of Ferric Chloride Solutions. *Journal of Colloid and Interface Science*. 157: 1-13, 1993.

4. Y. Cudennec and A. Lecerf. The transformation of ferrihydrite into goethite or hematite, revisited. *Journal of Solid State Chemistry*. 179: 716-722, 2006.

5. U. Schwertmann, H. Stanjek, and H.-H. Becher. Long-term in vitro transformation of 2-line ferrihydrite to goethite/hematite at 4, 10, 15 and 25°C. *Clay Minerals*. 39: 433-438, 2004.

6. U. Schwertmann and E. Murad. Effect of pH on the formation of goethite and hematite from ferrihydrite. *Clays and Clay Minerals*. 31: 277-284, 1983.

7. F. Vereda, J. de Vicente, M.d.P. Morales, F. Rull, and R. Hidalgo-Álvarez. Synthesis and characterization of single-domain monocrystalline magnetite particles by oxidative aging of Fe (OH) 2. *The Journal of Physical Chemistry C*. 112: 5843-5849, 2008.

8. T. Sugimoto and E. Matijević. Formation of uniform spherical magnetite particles by crystallization from ferrous hydroxide gels. *Journal of Colloid and Interface Science*. 74: 227-243, 1980.

9. K. Nishio, M. Ikeda, N. Gokon, S. Tsubouchi, H. Narimatsu, Y. Mochizuki, S. Sakamoto, A. Sandhu, M. Abe, and H. Handa. Preparation of size-controlled (30–100nm) magnetite nanoparticles for biomedical applications. *Journal of Magnetism and Magnetic Materials*. 310: 2408-2410, 2007.

10. M. Siles-Dotor, A. Morales, M. Benaissa, and A. Cabral-Prieto. Synthesis of nanostructured goethite and magnetite particles from the oxidation of $Fe(OH)_2$ in a high-oxygen-flow-rate medium. *Nanostructured materials*. 8: 657-673, 1997.

11. L. Carlson and U. Schwertmann. Natural occurrence of feroxyhite (6'-FeOOH). *Clays Clay Miner*. 28: 272-280, 1980.

12. O. Muller, R. Wilson, and W. Krakow. δ-FeO(OH) and its solid solutions. *Journal of Materials Science*. 14: 2929-2936, 1979.

13. Z. Li, M. Kawashita, N. Araki, M. Mitsumori, M. Hiraoka, and M. Doi. Preparation of Magnetic Iron Oxide Nanoparticles for Hyperthermia of Cancer in a $FeCl_2$-$NaNO_3$-NaOH Aqueous System. *Journal of Biomaterials Applications*. 25: 643-661, 2011.

14. S. Sun and H. Zeng. Size-Controlled Synthesis of Magnetite Nanoparticles. *Journal of the American Chemical Society*. 124: 8204-8205, 2002.

15. Z. Li, Q. Sun, and M. Gao. Preparation of water-soluble magnetite nanocrystals from hydrated ferric salts in 2-pyrrolidone: mechanism leading to Fe_3O_4. *Angewandte Chemie International Edition*. 44: 123-126, 2005.

16. A.H. Munsell, *A Color Notation*. 1905: G. H. Ellis Company.

17. L. Slavov, M. Abrashev, T. Merodiiska, C. Gelev, R. Vandenberghe, I. Markova-Deneva, and I. Nedkov. Raman spectroscopy investigation of magnetite nanoparticles in ferrofluids. *Journal of Magnetism and Magnetic Materials*. 322: 1904-1911, 2010.

18. C.L. Altan and S. Bucak. The effect of Fe3O4 nanoparticles on the thermal conductivities of various base fluids. *Nanotechnology*. 22: 285713, 2011.

19. M. Pastoriza-Gallego, L. Lugo, J. Legido, and M. Piñeiro. Enhancement of thermal conductivity and volumetric behavior of FexOy nanofluids. *Journal of Applied Physics*. 110: 014309, 2011.

20. R. Azizian, E. Doroodchi, T. McKrell, J. Buongiorno, L.W. Hu, and B. Moghtaderi. Effect of magnetic field on laminar convective heat transfer of magnetite nanofluids. *International Journal of Heat and Mass Transfer*. 68: 94-109, 2014.

21. H. Sun, L. Cao, and L. Lu. Magnetite/reduced graphene oxide nanocomposites: One step solvothermal synthesis and use as a novel platform for removal of dye pollutants. *Nano Research*. 4: 550-562, 2011.

22. J.T. Mayo, C. Yavuz, S. Yean, L. Cong, H. Shipley, W. Yu, J. Falkner, A. Kan, M. Tomson, and V.L. Colvin. The effect of nanocrystalline magnetite size on arsenic removal. *Science and Technology of Advanced Materials*. 8: 71, 2007.

23. V. Chandra, J. Park, Y. Chun, J.W. Lee, I.-C. Hwang, and K.S. Kim. Water-Dispersible Magnetite-Reduced Graphene Oxide Composites for Arsenic Removal. *ACS Nano*. 4: 3979-3986, 2010.

24. S.H. Gee, Y.K. Hong, D.W. Erickson, M.H. Park, and J.C. Sur. Synthesis and aging effect of spherical magnetite (Fe_3O_4) nanoparticles for biosensor applications. *Journal of Applied Physics*. 93: 7560-7562, 2003.

25. G.F. Cheng, J. Zhao, Y.H. Tu, P.A. He, and Y.H. Fang. A sensitive DNA electrochemical biosensor based on magnetite with a glassy carbon electrode modified by muti-walled carbon nanotubes in polypyrrole. *Analytica Chimica Acta*. 533: 11-16, 2005.

26. S. Bucak, S. Sharpe, S. Kuhn, and T.A. Hatton. Cell Clarification and Size Separation Using Continuous Countercurrent Magnetophoresis. *Biotechnology Progress*. 27: 744-750, 2011.

27. H. Honda, A. Kawabe, M. Shinkai, and T. Kobayashi. Development of chitosan-conjugated magnetite for magnetic cell separation. *Journal of Fermentation and Bioengineering*. 86: 191-196, 1998.

28. T.K. Jain, J. Richey, M. Strand, D.L. Leslie-Pelecky, C.A. Flask, and V. Labhasetwar. Magnetic nanoparticles with dual functional properties: drug delivery and magnetic resonance imaging. *Biomaterials*. 29: 4012-4021, 2008.

29. S.J. Guo, D. Li, L.M. Zhang, J. Li, and E.K. Wang. Monodisperse mesoporous superparamagnetic single-crystal magnetite nanoparticles for drug delivery. *Biomaterials*. 30: 1881-1889, 2009.

30. S. Chen, Y. Li, C. Guo, J. Wang, J.H. Ma, X.F. Liang, L.R. Yang, and H.Z. Liu. Temperature-responsive magnetite/PEO-PPO-PEO block copolymer nanoparticles for controlled drug targeting delivery. *Langmuir*. 23: 12669-12676, 2007.

31. S. Laurent, S. Dutz, U.O. Häfeli, and M. Mahmoudi. Magnetic fluid hyperthermia: focus on superparamagnetic iron oxide nanoparticles. *Advances in Colloid and Interface Science*. 166: 8-23, 2011.

32. A. Jordan, R. Scholz, P. Wust, H. Schirra, T. Schiestel, H. Schmidt, and R. Felix. Endocytosis of dextran and silan-coated magnetite nanoparticles and the effect of intracellular hyperthermia on human mammary carcinoma cells in vitro. *Journal of Magnetism and Magnetic Materials*. 194: 185-196, 1999.

33. Y.-X.J. Wang, S.M. Hussain, and G.P. Krestin. Superparamagnetic iron oxide contrast agents: physicochemical characteristics and applications in MR imaging. *European radiology*. 11: 2319-2331, 2001.

34. J. Kim, H.S. Kim, N. Lee, T. Kim, H. Kim, T. Yu, I.C. Song, W.K. Moon, and T. Hyeon. Multifunctional Uniform Nanoparticles Composed of a Magnetite Nanocrystal Core and a Mesoporous Silica Shell for Magnetic Resonance and Fluorescence Imaging and for Drug Delivery. *Angewandte Chemie International Edition*. 47: 8438-8441, 2008.

35. S. Nishikawa. *Structure of some crystals of the spinel group*. in *Proceedings of the Physico-Mathematical Socety Tokyo*. 1915.

36. R. Hergt, W. Andra, C.G. d'Ambly, I. Hilger, W.A. Kaiser, U. Richter, and H.-G. Schmidt. Physical limits of hyperthermia using magnetite fine particles. *Magnetics, IEEE Transactions on*. 34: 3745-3754, 1998.

37. B.A. Maher. Magnetic properties of some synthetic sub-micron magnetites. *Geophysical Journal International*. 94: 83-96, 1988.

38. D. Dunlop. Superparamagnetic and single-domain threshold sizes in magnetite. *Journal of Geophysical Research*. 78: 1780-1793, 1973.

39. A. Ito, K. Tanaka, H. Honda, S. Abe, H. Yamaguchi, and T. Kobayashi. Complete regression of mouse mammary carcinoma with a size greater than 15 mm by frequent repeated hyperthermia using magnetite nanoparticles. *Journal of Bioscience and Bioengineering*. 96: 364-369, 2003.

40. O. Baudisch and L.W. Bass. Eisen als licht-chemischer Katalysator, I.: Über die Zersetzung von Ferrocyankalium im Tageslicht. *Berichte der deutschen chemischen Gesellschaft (A and B Series)*. 55: 2698-2706, 1922.

41. W.Y. William, J.C. Falkner, C.T. Yavuz, and V.L. Colvin. Synthesis of monodisperse iron oxide nanocrystals by thermal decomposition of iron carboxylate salts. *Chemical Communications*, 2306-2307, 2004.

42. A. Roca, M. Morales, K. O'Grady, and C. Serna. Structural and magnetic properties of uniform magnetite nanoparticles prepared by high temperature decomposition of organic precursors. *Nanotechnology*. 17: 2783, 2006.

43. P.A. Dresco, V.S. Zaitsev, R.J. Gambino, and B. Chu. Preparation and properties of magnetite and polymer magnetite nanoparticles. *Langmuir*. 15: 1945-1951, 1999.

44. Y. Lee, J. Lee, C.J. Bae, J.G. Park, H.J. Noh, J.H. Park, and T. Hyeon. Large-scale synthesis of uniform and crystalline magnetite nanoparticles using reverse micelles as nanoreactors under reflux conditions. *Advanced Functional Materials*. 15: 503-509, 2005.

45. T. Daou, G. Pourroy, S. Begin-Colin, J. Greneche, C. Ulhaq-Bouillet, P. Legaré, P. Bernhardt, C. Leuvrey, and G. Rogez. Hydrothermal synthesis of monodisperse magnetite nanoparticles. *Chemistry of Materials*. 18: 4399-4404, 2006.

46. R. Fan, X. Chen, Z. Gui, L. Liu, and Z. Chen. A new simple hydrothermal preparation of nanocrystalline magnetite Fe_3O_4. *Materials Research Bulletin*. 36: 497-502, 2001.

47. T. Indira and P. Lakshmi. Magnetic nanoparticles—A review. *International Journal of Pharmaceutical Sciences and Nanotechnology*. 3: 1035-1042, 2010.

48. A.H. Lu, E.e.L. Salabas, and F. Schüth. Magnetic nanoparticles: synthesis, protection, functionalization, and application. *Angewandte Chemie International Edition*. 46: 1222-1244, 2007.

49. A.K. Gupta and M. Gupta. Synthesis and surface engineering of iron oxide nanoparticles for biomedical applications. *Biomaterials*. 26: 3995-4021, 2005.

50. W. Wu, Q. He, and C. Jiang. Magnetic iron oxide nanoparticles: synthesis and surface functionalization strategies. *Nanoscale Research Letters*. 3: 397-415, 2008.

51. R. Lavinsky, *Magnetite*, Magnetite-278427.jpg, mindat.org.

52. B.-L. Lin, X.-D. Shen, and S. Cui. Application of nanosized Fe3O4 in anticancer drug carriers with target-orientation and sustained-release properties. *Biomedical Materials*. 2: 132, 2007.

53. R.A. Frimpong, J. Dou, M. Pechan, and J.Z. Hilt. Enhancing remote controlled heating characteristics in hydrophilic magnetite nanoparticles via facile co-precipitation. *Journal of Magnetism and Magnetic Materials*. 322: 326-331, 2010.

54. R. Kumar, B.S. Inbaraj, and B. Chen. Surface modification of superparamagnetic iron nanoparticles with calcium salt of poly (γ-glutamic acid) as coating material. *Materials Research Bulletin*. 45: 1603-1607, 2010.

55. I. Martínez-Mera, M. Espinosa-Pesqueira, R. Pérez-Hernández, and J. Arenas-Alatorre. Synthesis of magnetite (Fe$_3$O$_4$) nanoparticles without surfactants at room temperature. *Materials Letters*. 61: 4447-4451, 2007.

56. T. Iwasaki, N. Mizutani, S. Watano, T. Yanagida, and T. Kawai. Size control of magnetite nanoparticles by organic solvent-free chemical coprecipitation at room temperature. *Journal of Experimental Nanoscience*. 5: 251-262, 2010.

57. Y.S. Kang, S. Risbud, J.F. Rabolt, and P. Stroeve. Synthesis and characterization of nanometer-size Fe3O4 and γ-Fe2O3 particles. *Chemistry of Materials*. 8: 2209-2211, 1996.

58. J. Baumgartner, A. Dey, P.H. Bomans, C. Le Coadou, P. Fratzl, N.A. Sommerdijk, and D. Faivre. Nucleation and growth of magnetite from solution. *Nature materials*. 12: 310-314, 2013.

59. J. Baumgartner, L. Bertinetti, M. Widdrat, A.M. Hirt, and D. Faivre. Formation of Magnetite Nanoparticles at Low Temperature: From Superparamagnetic to Stable Single Domain Particles. *Plos One*. 8, 2013.

60. J. Zhang and R. Misra. Magnetic drug-targeting carrier encapsulated with thermosensitive smart polymer: core–shell nanoparticle carrier and drug release response. *Acta Biomaterialia*. 3: 838-850, 2007.

61. C.Y. Wang, J.M. Hong, G. Chen, Y. Zhang, and N. Gu. Facile method to synthesize oleic acid-capped magnetite nanoparticles. *Chinese Chemical Letters*. 21: 179-182, 2010.

62. M. Pileni. Reverse micelles as microreactors. *The Journal of Physical Chemistry*. 97: 6961-6973, 1993.

63. Y.-h. Zheng, Y. Cheng, F. Bao, and Y.-s. Wang. Synthesis and magnetic properties of Fe_3O_4 nanoparticles. *Materials Research Bulletin*. 41: 525-529, 2006.

64. J. Wang, J. Sun, Q. Sun, and Q. Chen. One-step hydrothermal process to prepare highly crystalline Fe_3O_4 nanoparticles with improved magnetic properties. *Materials Research Bulletin*. 38: 1113-1118, 2003.

65. B.S. Inbaraj, T.H. Kao, T.Y. Tsai, C.P. Chiu, R. Kumar, and B.H. Chen. The synthesis and characterization of poly(γ-glutamic acid)-coated magnetite nanoparticles and their effects on antibacterial activity and cytotoxicity. *Nanotechnology*. 22: 075101, 2011.

66. F. Vereda, J. de Vicente, and R. Hidalgo-Alvarez. Oxidation of ferrous hydroxides with nitrate: A versatile method for the preparation of magnetic colloidal particles. *Journal of Colloid and Interface Science*. 392: 50-56, 2013.

67. M.A. Vergés, R. Costo, A. Roca, J. Marco, G. Goya, C. Serna, and M. Morales. Uniform and water stable magnetite nanoparticles with diameters around the monodomain–multidomain limit. *Journal of Physics D: Applied Physics*. 41: 134003, 2008.

68. F. Vereda, J. de Vicente, M.D.P. Morales, F. Rull, and R. Hidalgo-Alvarez. Synthesis and characterization of single-domain monocrystalline magnetite particles by oxidative aging of $Fe(OH)_2$. *Journal of Physical Chemistry C*. 112: 5843-5849, 2008.

69. T. Matsunaga, T. Suzuki, M. Tanaka, and A. Arakaki. Molecular analysis of magnetotactic bacteria and development of functional bacterial magnetic particles for nano-biotechnology. *Trends in Biotechnology*. 25: 182-188, 2007.

70. D.A. Bazylinski and R.B. Frankel. Magnetosome formation in prokaryotes. *Nature Reviews Microbiology*. 2: 217-230, 2004.

71. R.F. Butler and S.K. Banerjee. Theoretical single-domain grain size range in magnetite and titanomagnetite. *Journal of Geophysical Research*. 80: 4049-4058, 1975.

72. Z. Oestreicher, S.K. Lower, W. Lin, and B.H. Lower. Collection, Isolation and Enrichment of Naturally Occurring Magnetotactic Bacteria from the Environment. *Journal of Visualized Experiments*. 69: e50123, 2012.

73. B. Devouard, M. Posfai, X. Hua, D.A. Bazylinski, R.B. Frankel, and P.R. Buseck. Magnetite from magnetotactic bacteria: Size distributions and twinning. *American Mineralogist*. 83: 1387-1398, 1998.

74. R.B. Frankel. Magnetic guidance of organisms. *Annual Review of Biophysics and Bioengineering*. 13: 85-103, 1984.

75. S. Mann, N.H.C. Sparks, R.B. Frankel, D.A. Bazylinski, and H.W. Jannasch. Biomineralization of ferrimagnetic greigite (Fe_3S_4) and iron pyrite (FeS_2) in a magnetotactic bacterium. *Nature*. 343: 258-261, 1990.

76. R. Blakemore. Magnetotactic bacteria. *Science*. 190: 377-379, 1975.

77. A. Arakaki, J. Webb, and T. Matsunaga. A novel protein tightly bound to bacterial magnetic particles in Magnetospirillum magneticum strain AMB-1. *Journal of Biological Chemistry*. 278: 8745-8750, 2003.

78. T. Prozorov, S.K. Mallapragada, B. Narasimhan, L. Wang, P. Palo, M. Nilsen-Hamilton, T.J. Williams, D.A. Bazylinski, R. Prozorov, and P.C. Canfield. Protein-mediated synthesis of uniform superparamagnetic magnetite nanocrystals. *Advanced Functional Materials*. 17: 951-957, 2007.

79. Y. Amemiya, A. Arakaki, S.S. Staniland, T. Tanaka, and T. Matsunaga. Controlled formation of magnetite crystal by partial oxidation of ferrous hydroxide in the presence of recombinant magnetotactic bacterial protein Mms6. *Biomaterials*. 28: 5381-5389, 2007.

80. J.M. Galloway, J.P. Bramble, A.E. Rawlings, G. Burnell, S.D. Evans, and S.S. Staniland. Nanomagnetic arrays formed with the biomineralization protein Mms6. *Journal of Nano Research*. 17: 127-146, 2012.

81. A. Arakaki, F. Masuda, Y. Amemiya, T. Tanaka, and T. Matsunaga. Control of the morphology and size of magnetite particles with peptides mimicking the Mms6 protein from magnetotactic bacteria. *Journal of Colloid and Interface Science*. 343: 65-70, 2010.

82. J. Aizenberg, J.C. Weaver, M.S. Thanawala, V.C. Sundar, D.E. Morse, and P. Fratzl. Skeleton of Euplectella sp.: Structural hierarchy from the nanoscale to the macroscale. *Science*. 309: 275-278, 2005.

83. J.C. Weaver, G.W. Milliron, A. Miserez, K. Evans-Lutterodt, S. Herrera, I. Gallana, W.J. Mershon, B. Swanson, P. Zavattieri, E. DiMasi, and D. Kisailus. The Stomatopod Dactyl Club: A Formidable Damage-Tolerant Biological Hammer. *Science*. 336: 1275-1280, 2012.

84. J. Aizenberg, A. Tkachenko, S. Weiner, L. Addadi, and G. Hendler. Calcitic microlenses as part of the photoreceptor system in brittlestars. *Nature*. 412: 819-822, 2001.

85. V.C. Sundar, A.D. Yablon, J.L. Grazul, M. Ilan, and J. Aizenberg. Fibre-optical features of a glass sponge - Some superior technological secrets have come to light from a deep-sea organism. *Nature*. 424: 899-900, 2003.

86. S.H.K. Eder, H. Cadiou, A. Muhamad, P.A. McNaughton, J.L. Kirschvink, and M. Winklhofer. Magnetic characterization of isolated candidate vertebrate magnetoreceptor cells. *Proceedings of the National Academy of Sciences of the United States of America*. 109: 12022-12027, 2012.

87. S. Staniland, B. Ward, A. Harrison, G. van der Laan, and N. Telling. Rapid magnetosome formation shown by real-time x-ray magnetic circular dichroism. *Proceedings of the National Academy of Sciences of the United States of America*. 104: 19524-19528, 2007.

88. J.W.C. Dunlop and P. Fratzl. Biological Composites. *Annual Review of Materials Research, Vol 40*. 40: 1-24, 2010.

89. F.C. Meldrum and H. Colfen. Controlling Mineral Morphologies and Structures in Biological and Synthetic Systems. *Chemical Reviews*. 108: 4332-4432, 2008.

90. S. Weiner. Biomineralization: A structural perspective. *Journal of Structural Biology*. 163: 229-234, 2008.

91. C. Sun, J.S. Lee, and M. Zhang. Magnetic nanoparticles in MR imaging and drug delivery. *Advanced Drug Delivery Reviews*. 60: 1252-1265, 2008.

92. F.-Y. Cheng, C.-H. Su, Y.-S. Yang, C.-S. Yeh, C.-Y. Tsai, C.-L. Wu, M.-T. Wu, and D.-B. Shieh. Characterization of aqueous dispersions of Fe_3O_4 nanoparticles and their biomedical applications. *Biomaterials*. 26: 729-738, 2005.

93. F. Nudelman and N.A.J.M. Sommerdijk. Biomineralization as an Inspiration for Materials Chemistry. *Angewandte Chemie-International Edition*. 51: 6582-6596, 2012.

94. T. Prozorov, D.A. Bazylinski, S.K. Mallapragada, and R. Prozorov. Novel magnetic nanomaterials inspired by magnetotactic bacteria: Topical review. *Materials Science and Engineering: R: Reports*. 74: 133-172, 2013.

95. S. Weiner and L. Addadi. Crystallization pathways in biomineralization. *Annual Review of Materials Research*. 41: 21-40, 2011.

96. J. Baumgartner, G. Morin, N. Menguy, T.P. Gonzalez, M. Widdrat, J. Cosmidis, and D. Faivre. Magnetotactic bacteria form magnetite from a phosphate-rich ferric hydroxide via nanometric ferric (oxyhydr) oxide intermediates. *Proceedings of the National Academy of Sciences*. 110: 14883-14888, 2013.

97. R. Massart and V. Cabuil. Effect of Some Parameters on the Formation of Colloidal Magnetite in Alkaline-Medium - Yield and Particle-Size Control. *Journal De Chimie Physique Et De Physico-Chimie Biologique*. 84: 967-973, 1987.

98. R.M. Cornell and U. Schwertmann, *The iron oxides: structure, properties, reactions, occurrences and uses*. Wiley. 2003

99. A.H. Lu, E.L. Salabas, and F. Schuth. Magnetic nanoparticles: Synthesis, protection, functionalization, and application. *Angewandte Chemie-International Edition*. 46: 1222-1244, 2007.

100. W. Wu, Q.G. He, and C.Z. Jiang. Magnetic Iron Oxide Nanoparticles: Synthesis and Surface Functionalization Strategies. *Nanoscale research letters*. 3: 397-415, 2008.

101. T. Prozorov, S.K. Mallapragada, B. Narasimhan, L.J. Wang, P. Palo, M. Nilsen-Hamilton, T.J. Williams, D.A. Bazylinski, R. Prozorov, and P.C. Canfield. Protein-mediated synthesis of uniform superparamagnetic magnetite nanocrystals. *Advanced Functional Materials*. 17: 951-957, 2007.

102. L.J. Wang, T. Prozorov, P.E. Palo, X.P. Liu, D. Vaknin, R. Prozorov, S. Mallapragada, and M. Nilsen-Hamilton. Self-Assembly and Biphasic Iron-Binding Characteristics of Mms6, A Bacterial Protein That Promotes the Formation of Superparamagnetic Magnetite Nanoparticles of Uniform Size and Shape. *Biomacromolecules*. 13: 98-105, 2012.

103. J. Baumgartner, M. Antonietta Carillo, K.M. Eckes, P. Werner, and D. Faivre. Biomimetic Magnetite Formation: From Biocombinatorial Approaches to Mineralization Effects. *Langmuir*. 30: 2129-2136, 2014.

104. J. Baumgartner, A. Dey, P.H.H. Bomans, C. Le Coadou, P. Fratzl, N.A.J.M. Sommerdijk, and D. Faivre. Nucleation and growth of magnetite from solution. *Nature Materials*. 12: 310-314, 2013.

105. O. Baudisch and L.W. Bass. Eisen als licht-chemischer Katalysator, I.: Über die Zersetzung von Ferrocyankalium im Tageslicht. *Berichte der deutschen chemischen Gesellschaft (A and B Series)*. 55: 2698-2706, 1922.

106. Z.X. Li, M. Kawashita, N. Araki, M. Mitsumori, M. Hiraoka, and M. Doi. Preparation of Magnetic Iron Oxide Nanoparticles for Hyperthermia of Cancer in a $FeCl_2$-$NaNO_3$-NaOH Aqueous System. *Journal of Biomaterials Applications*. 25: 643-661, 2011.

107. K. Nishio, M. Ikeda, N. Gokon, S. Tsubouchi, H. Narimatsu, Y. Mochizuki, S. Sakamoto, A. Sandhu, M. Abe, and H. Handa. Preparation of size-controlled (30-100 nm) magnetite nanoparticles for biomedical applications. *Journal of Magnetism and Magnetic Materials*. 310: 2408-2410, 2007.

108. T. Sugimoto and E. Matijevic. Formation of Uniform Spherical Magnetite Particles by Crystallization from Ferrous Hydroxide Gels. *Journal of Colloid and Interface Science*. 74: 227-243, 1980.

109. M.A. Verges, R. Costo, A.G. Roca, J.F. Marco, G.F. Goya, C.J. Serna, and M.P. Morales. Uniform and water stable magnetite nanoparticles with diameters around the monodomain-multidomain limit. *Journal of Physics D-Applied Physics*. 41, 2008.

110. H. Iida, K. Takayanagi, T. Nakanishi, and T. Osaka. Synthesis of Fe_3O_4 nanoparticles with various sizes and magnetic properties by controlled hydrolysis. *Journal of Colloid and Interface Science*. 314: 274-280, 2007.

111. M.R. Vos, P.H.H. Bomans, P.M. Frederik, and N.A.J.M. Sommerdijk. The development of a glove-box/Vitrobot combination: Air-water interface events visualized by cryo-TEM. *Ultramicroscopy*. 108: 1478-1483, 2008.

112. J.R. Kremer, D.N. Mastronarde, and J.R. McIntosh. Computer visualization of three-dimensional image data using IMOD. *Journal of Structural Biology*. 116: 71-76, 1996.

113. L. Slavov, M.V. Abrashev, T. Merodiiska, C. Gelev, R.E. Vandenberghe, I. Markova-Deneva, and I. Nedkov. Raman spectroscopy investigation of magnetite nanoparticles in ferrofluids. *Journal of Magnetism and Magnetic Materials*. 322: 1904-1911, 2010.

114. P. Yang, W. Chen, and C. Wang. Preparation and in vitro cytotoxicity study of poly (aspartic acid) stabilized magnetic nanoparticles. *Frontiers of Chemistry in China*. 6: 9-14, 2011.

115. M. Sousa, J. Rubim, P. Sobrinho, and F. Tourinho. Biocompatible magnetic fluid precursors based on aspartic and glutamic acid modified maghemite nanostructures. *Journal of Magnetism and Magnetic Materials*. 225: 67-72, 2001.

116. N. de Jonge and F.M. Ross. Electron microscopy of specimens in liquid. *Nature Nanotechnology*. 6: 695-704, 2011.

117. Y. Yuan, D. Rende, C.L. Altan, S. Bucak, R. Ozisik, and D.-A. Borca-Tasciuc. Effect of surface modification on magnetization of iron oxide nanoparticle colloids. *Langmuir*. 28: 13051-13059, 2012.

118. S.E. Ziemniak, M.E. Jones, and K.E.S. Combs. Magnetite Solubility and Phase-Stability in Alkaline Media at Elevated-Temperatures. *Journal of Solution Chemistry*. 24: 837-877, 1995.

119. M. Chanana, Z.W. Mao, and D.Y. Wang. Using Polymers to Make Up Magnetic Nanoparticles for Biomedicine. *Journal of Biomedical Nanotechnology*. 5: 652-668, 2009.

120. Z.R. Stephen, F.M. Kievit, and M.Q. Zhang. Magnetite nanoparticles for medical MR imaging. *Materials Today*. 14: 330-338, 2011.

121. C. Alexiou, R.J. Schmid, R. Jurgons, M. Kremer, G. Wanner, C. Bergemann, E. Huenges, T. Nawroth, W. Arnold, and F.G. Parak. Targeting cancer cells: magnetic nanoparticles as drug carriers. *European Biophysics Journal with Biophysics Letters*. 35: 446-450, 2006.

122. F.Y. Cheng, C.H. Su, Y.S. Yang, C.S. Yeh, C.Y. Tsai, C.L. Wu, M.T. Wu, and D.B. Shieh. Characterization of aqueous dispersions of Fe3O4 nanoparticles and their biomedical applications. *Biomaterials*. 26: 729-738, 2005.

123. S. Purushotham, P.E.J. Chang, H. Rumpel, I.H.C. Kee, R.T.H. Ng, P.K.H. Chow, C.K. Tan, and R.V. Ramanujan. Thermoresponsive core-shell magnetic nanoparticles for combined modalities of cancer therapy. *Nanotechnology*. 20, 2009.

124. Q.A. Pankhurst, J. Connolly, S.K. Jones, and J. Dobson. Applications of magnetic nanoparticles in biomedicine. *Journal of Physics D-Applied Physics*. 36: R167-R181, 2003.

125. A.F. Thunemann, D. Schutt, L. Kaufner, U. Pison, and H. Mohwald. Maghemite nanoparticles protectively coated with poly(ethylene imine) and poly(ethylene oxide)-block-poly(glutamic acid). *Langmuir*. 22: 2351-2357, 2006.

126. X.Q. Liu, Y.P. Guan, Z.Y. Ma, and H.Z. Liu. Surface modification and characterization of magnetic polymer nanospheres prepared by miniemulsion polymerization. *Langmuir*. 20: 10278-10282, 2004.

127. L.A. Harris, J.D. Goff, A.Y. Carmichael, J.S. Riffle, J.J. Harburn, T.G. St Pierre, and M. Saunders. Magnetite nanoparticle dispersions stabilized with triblock copolymers. *Chemistry of Materials*. 15: 1367-1377, 2003.

128. M. Mikhaylova, D.K. Kim, N. Bobrysheva, M. Osmolowsky, V. Semenov, T. Tsakalakos, and M. Muhammed. Superparamagnetism of magnetite nanoparticles: Dependence on surface modification. *Langmuir*. 20: 2472-2477, 2004.

129. H.K. Nguyen, P. Lemieux, S.V. Vinogradov, C.L. Gebhart, N. Guerin, G. Paradis, T.K. Bronich, V.Y. Alakhov, and A.V. Kabanov. Evaluation of polyether-polyethyleneimine graft copolymers as gene transfer agents. *Gene Therapy*. 7: 126-138, 2000.

130. O. Boussif, F. Lezoualch, M.A. Zanta, M.D. Mergny, D. Scherman, B. Demeneix, and J.P. Behr. A Versatile Vector for Gene and Oligonucleotide Transfer into Cells in Culture and in-Vivo - Polyethylenimine. *Proceedings of the National Academy of Sciences of the United States of America*. 92: 7297-7301, 1995.

131. M. Turk, S. Dincer, I.S. Yulug, and E. Piskin. In vitro transfection of HeLa cells with temperature sensitive polycationic copolymers. *Journal of Controlled Release*. 96: 325-340, 2004.

132. C.Y. Quan, H. Wei, Y.X. Sun, S.X. Cheng, K. Shen, Z.W. Gu, X.Z. Zhang, and R.X. Zhuo. Polyethyleneimine modified biocompatible poly(N-isopropylacrylamide)-based nanogels for drug delivery. *Journal of Nanoscience and Nanotechnology*. 8: 2377-2384, 2008.

133. H. Cheng, J.L. Zhu, Y.X. Sun, S.X. Cheng, X.Z. Zhang, and R.X. Zhuo. Novel thermoresponsive nonviral gene vector: P(NIPAAm-co-NDAPM)-b-PEI with adjustable gene transfection efficiency. *Bioconjugate Chemistry*. 19: 1368-1374, 2008.

134. T. Gillich, C. Acikgöz, L. Isa, A.D. Schlüter, N.D. Spencer, and M. Textor. PEG-Stabilized Core–Shell Nanoparticles: Impact of Linear versus Dendritic Polymer Shell Architecture on Colloidal Properties and the Reversibility of Temperature-Induced Aggregation. *ACS Nano*. 7: 316-329, 2012.

135. D.C. Popescu, R. Lems, N.A.A. Rossi, C.T. Yeoh, J. Loos, S.J. Holder, C.V.C. Bouten, and N.A.J.M. Sommerdijk. The patterning and alignment of muscle cells using the selective adhesion of poly(oligoethylene glycol methyl ether methacrylate)-based ABA block copolymers. *Advanced Materials*. 17: 2324-+, 2005.

136. J.F. Lutz. Thermo-Switchable Materials Prepared Using the OEGMA-Platform. *Advanced Materials*. 23: 2237-2243, 2011.

137. C. Flesch, Y. Unterfinger, E. Bourgeat-Lami, E. Duguet, C. Delaite, and P. Dumas. Poly(ethylene glycol) surface coated magnetic particles. *Macromolecular Rapid Communications*. 26: 1494-1498, 2005.

138. A. Kleine, C.L. Altan, U.E. Yarar, N.A.J.M. Sommerdijk, S. Bucak, and S.J. Holder. The polymerisation of oligo(ethylene glycol methyl ether) methacrylate from a multifunctional poly(ethylene imine) derived amide: a stabiliser for the synthesis and dispersion of magnetite nanoparticles. *Polymer Chemistry*. 5: 524-534, 2014.

139. R. Sondjaja, T.A. Hatton, and M.K.C. Tam. Clustering of magnetic nanoparticles using a double hydrophilic block copolymer, poly(ethylene oxide)-b-poly(acrylic acid). *Journal of Magnetism and Magnetic Materials*. 321: 2393-2397, 2009.

140. A. Ditsch, P.E. Laibinis, D.I.C. Wang, and T.A. Hatton. Controlled clustering and enhanced stability of polymer-coated magnetic nanoparticles. *Langmuir*. 21: 6006-6018, 2005.

141. J.F. Berret, N. Schonbeck, F. Gazeau, D. El Kharrat, O. Sandre, A. Vacher, and M. Airiau. Controlled clustering of superparamagnetic nanoparticles using block copolymers: Design of new contrast agents for magnetic resonance imaging. *Journal of the American Chemical Society*. 128: 1755-1761, 2006.

142. J.H. Park, G. von Maltzahn, L.L. Zhang, M.P. Schwartz, E. Ruoslahti, S.N. Bhatia, and M.J. Sailor. Magnetic iron oxide nanoworms for tumor targeting and imaging. *Advanced Materials*. 20: 1630, 2008.

143. S.A. Corr, S.J. Byrne, R. Tekoriute, C.J. Meledandri, D.F. Brougham, M. Lynch, C. Kerskens, L. O'Dwyer, and Y.K. Gun'ko. Linear assemblies of magnetic nanoparticles as MRI contrast agents. *Journal of the American Chemical Society*. 130: 4214-+, 2008.

144. K. Ogrady and A. Bradbury. Particle-Size Analysis in Ferrofluids. *Journal of Magnetism and Magnetic Materials*. 39: 91-94, 1983.

145. Y. Yuan, D. Rende, C.L. Altan, S. Bucak, R. Ozisik, and D.A. Borca-Tasciuc. Effect of Surface Modification on Magnetization of Iron Oxide Nanoparticle Colloids. *Langmuir*. 28: 13051-13059, 2012.

146. C.L. Altan and S. Bucak. The effect of Fe3O4 nanoparticles on the thermal conductivities of various base fluids. *Nanotechnology*. 22, 2011.

147. M.J. Pastoriza-Gallego, L. Lugo, J.L. Legido, and M.M. Pineiro. Enhancement of thermal conductivity and volumetric behavior of FexOy nanofluids. *Journal of Applied Physics*. 110, 2011.

148. S. Laurent, S. Dutz, U.O. Hafeli, and M. Mahmoudi. Magnetic fluid hyperthermia: Focus on superparamagnetic iron oxide nanoparticles. *Advances in Colloid and Interface Science*. 166: 8-23, 2011.

149. Y.X.J. Wang, S.M. Hussain, and G.P. Krestin. Superparamagnetic iron oxide contrast agents: physicochemical characteristics and applications in MR imaging. *European Radiology*. 11: 2319-2331, 2001.

150. R.F. Butler and S.K. Banerjee. Theoretical single-domain grain size range in magnetite and titanomagnetite. *Journal of Geophysical Research*. 80: 4049-4058, 1975.

151. S.H. Sun and H. Zeng. Size-controlled synthesis of magnetite nanoparticles. *Journal of the American Chemical Society*. 124: 8204-8205, 2002.

152. W.W. Yu, J.C. Falkner, C.T. Yavuz, and V.L. Colvin. Synthesis of monodisperse iron oxide nanocrystals by thermal decomposition of iron carboxylate salts. *Chemical Communications*,2306-2307, 2004.

153. A.G. Roca, M.P. Morales, K. O'Grady, and C.J. Serna. Structural and magnetic properties of uniform magnetite nanoparticles prepared by high temperature decomposition of organic precursors. *Nanotechnology*. 17: 2783-2788, 2006.

154. Y. Lee, J. Lee, C.J. Bae, J.G. Park, H.J. Noh, J.H. Park, and T. Hyeon. Large-scale synthesis of uniform and crystalline magnetite nanoparticles using reverse micelles as nanoreactors under reflux conditions. *Advanced Functional Materials*. 15: 503-509, 2005.

155. T.J. Daou, G. Pourroy, S. Begin-Colin, J.M. Greneche, C. Ulhaq-Bouillet, P. Legare, P. Bernhardt, C. Leuvrey, and G. Rogez. Hydrothermal synthesis of monodisperse magnetite nanoparticles. *Chemistry of Materials*. 18: 4399-4404, 2006.

156. Y. Qian, Y. Xie, C. He, J. Li, and Z. Chen. Hydrothermal Preparation and Characterization of Ultrafine Magnetite Powders. *Materials Research Bulletin*. 29: 953-957, 1994.

157. R. Massart. Preparation of Aqueous Magnetic Liquids in Alkaline and Acidic Media. *Ieee Transactions on Magnetics*. 17: 1247-1248, 1981.

158. J. Popplewell and L. Sakhnini. The Dependence of the Physical and Magnetic-Properties of Magnetic Fluids on Particle-Size. *Journal of Magnetism and Magnetic Materials*. 149: 72-78, 1995.

159. M. Tada, S. Hatanaka, H. Sanbonsugi, N. Matsushita, and M. Abe. Method for synthesizing ferrite nanoparticles similar to 30 nm in diameter on neutral pH condition for biomedical applications. *Journal of Applied Physics*. 93: 7566-7568, 2003.

160. M. Ma, Y. Wu, H. Zhou, Y.K. Sun, Y. Zhang, and N. Gu. Size dependence of specific power absorption of Fe_3O_4 particles in AC magnetic field. *Journal of Magnetism and Magnetic Materials*. 268: 33-39, 2004.

161. R. Hergt, W. Andra, C.G. d'Ambly, I. Hilger, W.A. Kaiser, U. Richter, and H.G. Schmidt. Physical limits of hyperthermia using magnetite fine particles. *Ieee Transactions on Magnetics*. 34: 3745-3754, 1998.

162. B. Gleich and R. Weizenecker. Tomographic imaging using the nonlinear response of magnetic particles. *Nature*. 435: 1214-1217, 2005.

163. M. Shinkai. Functional magnetic particles for medical application. *Journal of Bioscience and Bioengineering*. 94: 606-613, 2002.

164. S. Lu, R.J. Pugh, and E. Forssberg, *Interfacial Separation of Particles*. 2005: Elsevier Science.

165. A.C. Foss, T. Goto, M. Morishita, and N.A. Peppas. Development of acrylic-based copolymers for oral insulin delivery. *European Journal of Pharmaceutics and Biopharmaceutics*. 57: 163-169, 2004.

166. Y. Tian, L. Bromberg, S.N. Lin, T.A. Hatton, and K.C. Tam. Complexation and release of doxorubicin from its complexes with pluronic P85-b-poly(acrylic acid) block copolymers. *Journal of Controlled Release*. 121: 137-145, 2007.

167. S. Kim, J.Y. Kim, K.M. Huh, G. Acharya, and K. Park. Hydrotropic polymer micelles containing acrylic acid moieties for oral delivery of paclitaxel. *Journal of Controlled Release*. 132: 222-229, 2008.

168. L. Serra, J. Domenech, and N.A. Peppas. Drug transport mechanisms and release kinetics from molecularly designed poly(acrylic acid-g-ethylene glycol) hydrogels. *Biomaterials*. 27: 5440-5451, 2006.

169. J. Ge, Y. Hu, M. Biasini, C. Dong, J. Guo, W.P. Beyermann, and Y. Yin. One-Step Synthesis of Highly Water-Soluble Magnetite Colloidal Nanocrystals. *Chemistry – A European Journal*. 13: 7153-7161, 2007.

170. J.P. Ge, Y.X. Hu, M. Biasini, W.P. Beyermann, and Y.D. Yin. Superparamagnetic magnetite colloidal nanocrystal clusters. *Angewandte Chemie-International Edition*. 46: 4342-4345, 2007.

171. C.L. Lin, C.F. Lee, and W.Y. Chiu. Preparation and properties of poly(acrylic acid) oligomer stabilized superparamagnetic ferrofluid. *Journal of Colloid and Interface Science*. 291: 411-420, 2005.

172. R.M. Cornell and U. Schwertmann, *The Iron Oxides: Structure, Properties, Reactions, Occurrences and Uses*. Wiley. 2006

173. J.P. Ge, Y.X. Hu, M. Biasini, C.L. Dong, J.H. Guo, W.P. Beyermann, and Y.D. Yin. One-step synthesis of highly water-soluble magnetite colloidal nanocrystals. *Chemistry-a European Journal*. 13: 7153-7161, 2007.

174. Z.Y. Wang, G. Liu, J. Sun, B.Y. Wu, Q.Y. Gong, B. Song, H. Ai, and Z.W. Gu. Self-Assembly of Magnetite Nanocrystals with Amphiphilic Polyethylenimine: Structures and Applications in Magnetic Resonance Imaging. *Journal of Nanoscience and Nanotechnology*. 9: 378-385, 2009.

175. I.Y. Goon, C.C. Zhang, M. Lim, J.J. Gooding, and R. Amal. Controlled Fabrication of Polyethylenimine-Functionalized Magnetic Nanoparticles for the Sequestration and Quantification of Free Cu^{2+}. *Langmuir*. 26: 12247-12252, 2010.

176. M.D. Butterworth, L. Illum, and S.S. Davis. Preparation of ultrafine silica- and PEG-coated magnetite particles. *Colloids and Surfaces a-Physicochemical and Engineering Aspects*. 179: 93-102, 2001.

177. Y. Zhang, N. Kohler, and M.Q. Zhang. Surface modification of superparamagnetic magnetite nanoparticles and their intracellular uptake. *Biomaterials*. 23: 1553-1561, 2002.

178. C.M. Cheng, Y.H. Wen, X.F. Xu, and H.C. Gu. Tunable synthesis of carboxyl-functionalized magnetite nanocrystal clusters with uniform size. *Journal of Materials Chemistry*. 19: 8782-8788, 2009.

179. J. Liu, Z.K. Sun, Y.H. Deng, Y. Zou, C.Y. Li, X.H. Guo, L.Q. Xiong, Y. Gao, F.Y. Li, and D.Y. Zhao. Highly Water-Dispersible Biocompatible Magnetite Particles with Low Cytotoxicity Stabilized by Citrate Groups. *Angewandte Chemie-International Edition*. 48: 5875-5879, 2009.

180. J.Y. Jing, Y. Zhang, J.Y. Liang, Q.B. Zhang, E. Bryant, C. Avendano, V.L. Colvin, Y.D. Wang, W.Y. Li, and W.W. Yu. One-step reverse precipitation synthesis of water-dispersible superparamagnetic magnetite nanoparticles. *Journal of Nanoparticle Research*. 14, 2012.

181. M. Chanda, *Introduction to Polymer Science and Chemistry: A Problem-Solving Approach*. 2013: CRC Press.

182. M. Talelli, C.J.F. Rijcken, T. Lammers, P.R. Seevinck, G. Storm, C.F. van Nostrum, and W.E. Hennink. Superparamagnetic Iron Oxide Nanoparticles Encapsulated in Biodegradable Thermosensitive Polymeric Micelles: Toward a Targeted Nanomedicine Suitable for Image-Guided Drug Delivery. *Langmuir*. 25: 2060-2067, 2009.

183. M. Mahmoudi, A. Simchi, M. Imani, and U.O. Hafeli. Superparamagnetic Iron Oxide Nanoparticles with Rigid Cross-linked Polyethylene Glycol Fumarate Coating for Application in Imaging and Drug Delivery. *Journal of Physical Chemistry C*. 113: 8124-8131, 2009.

184. Q.M. Quan, J. Xie, H.K. Gao, M. Yang, F. Zhang, G. Liu, X. Lin, A. Wang, H.S. Eden, S. Lee, G.X. Zhang, and X.Y. Chen. HSA Coated Iron Oxide Nanoparticles as Drug Delivery Vehicles for Cancer Therapy. *Molecular Pharmaceutics*. 8: 1669-1676, 2011.

185. S. Santra, C. Kaittanis, J. Grimm, and J.M. Perez. Drug/Dye-Loaded, Multifunctional Iron Oxide Nanoparticles for Combined Targeted Cancer Therapy and Dual Optical/Magnetic Resonance Imaging. *Small*. 5: 1862-1868, 2009.

186. X.Q. Yang, H. Hong, J.J. Grailer, I.J. Rowland, A. Javadi, S.A. Hurley, Y.L. Xiao, Y.A. Yang, Y. Zhang, R. Nickles, W.B. Cai, D.A. Steeber, and S.Q. Gong. cRGD-functionalized, DOX-conjugated, and Cu-64-labeled superparamagnetic iron oxide nanoparticles for targeted anticancer drug delivery and PET/MR imaging. *Biomaterials*. 32: 4151-4160, 2011.

187. H.E. Daldrup-Link, D. Golovko, B. Ruffell, D.G. DeNardo, R. Castaneda, C. Ansari, J.H. Rao, G.A. Tikhomirov, M.F. Wendland, C. Corot, and L.M. Coussens. MRI of Tumor-Associated Macrophages with Clinically Applicable Iron Oxide Nanoparticles. *Clinical Cancer Research*. 17: 5695-5704, 2011.

188. K. Andreas, R. Georgieva, M. Ladwig, S. Mueller, M. Notter, M. Sittinger, and J. Ringe. Highly efficient magnetic stem cell labeling with citrate-coated superparamagnetic iron oxide nanoparticles for MRI tracking. *Biomaterials*. 33: 4515-4525, 2012.

189. J.S. Basuki, A. Jacquemin, L. Esser, Y. Li, C. Boyer, and T.P. Davis. A block copolymer-stabilized co-precipitation approach to magnetic iron oxide nanoparticles for potential use as MRI contrast agents. *Polymer Chemistry*, 2014.

190. C.H. Hou, S.M. Hou, Y.S. Hsueh, J. Lin, H.C. Wu, and F.H. Lin. The in vivo performance of biomagnetic hydroxyapatite nanoparticles in cancer hyperthermia therapy. *Biomaterials*. 30: 3956-3960, 2009.

191. F.M. Kievit and M.Q. Zhang. Surface Engineering of Iron Oxide Nanoparticies for Targeted Cancer Therapy. *Accounts of Chemical Research*. 44: 853-862, 2011.

192. E.S. Day, J.G. Morton, and J.L. West. Nanoparticles for Thermal Cancer Therapy. *Journal of Biomechanical Engineering-Transactions of the Asme*. 131, 2009.

193. C. Grüttner, K. Müller, J. Teller, and F. Westphal. Synthesis and functionalisation of magnetic nanoparticles for hyperthermia applications. *International Journal of Hyperthermia*. 29: 777-789, 2013.

194. V.V. Mody, A. Singh, and B. Wesley. Basics of magnetic nanoparticles for their application in the field of magnetic fluid hyperthermia. *European Journal of Nanomedicine*. 5: 11-21, 2013.

195. C. Grüttner, K. Müller, J. Teller, F. Westphal, A. Foreman, and R. Ivkov. Synthesis and antibody conjugation of magnetic nanoparticles with improved specific power absorption rates for alternating magnetic field cancer therapy. *Journal of Magnetism and Magnetic Materials*. 311: 181-186, 2007.

196. K.M. Krishnan. Biomedical Nanomagnetics: A Spin Through Possibilities in Imaging, Diagnostics, and Therapy. *IEEE Transactions on Magnetics*. 46: 2523-2558, 2010.

197. R. Kaiser and G. Miskolczy. Magnetic Properties of Stable Dispersions of Subdomain Magnetite Particles. *Journal of Applied Physics*. 41: 1064-1072, 1970.

198. C.R. Vestal and Z.J. Zhang. Effects of surface coordination chemistry on the magnetic properties of $MnFe_2O_4$ spinel ferrite nanoparticles. *Journal of the American Chemical Society*. 125: 9828-9833, 2003.

199. R.W. Chantrell, J. Popplewell, and S. Charles. Measurements of particle size distribution parameters in ferrofluids. *Magnetics, IEEE Transactions on*. 14: 975-977, 1978.

200. N. Kohler, G.E. Fryxell, and M.Q. Zhang. A bifunctional poly(ethylene glycol) silane immobilized on metallic oxide-based nanoparticles for conjugation with cell targeting agents. *Journal of the American Chemical Society*. 126: 7206-7211, 2004.

201. J.R. McCarthy and R. Weissleder. Multifunctional magnetic nanoparticles for targeted imaging and therapy. *Advanced Drug Delivery Reviews*. 60: 1241-1251, 2008.

202. S. Sun, H. Zeng, D.B. Robinson, S. Raoux, P.M. Rice, S.X. Wang, and G. Li. Monodisperse MFe_2O_4 (M= Fe, Co, Mn) nanoparticles. *Journal of the American Chemical Society*. 126: 273-279, 2004.

203. G. Kataby, M. Cojocaru, R. Prozorov, and A. Gedanken. Coating carboxylic acids on amorphous iron nanoparticles. *Langmuir*. 15: 1703-1708, 1999.

204. J.H. Yoe and A.L. Jones. Colorimetric determination of iron with disodium-1, 2-dihydroxybenzene-3, 5-disulfonate. *Industrial & Engineering Chemistry Analytical Edition*. 16: 111-115, 1944.

205. W. McBryde. A spectrophotometric reexamination of the spectra and stabilities of the iron (III)-tiron complexes. *Canadian Journal of Chemistry*. 42: 1917-1927, 1964.

206. M. Hanesch. Raman spectroscopy of iron oxides and (oxy) hydroxides at low laser power and possible applications in environmental magnetic studies. *Geophysical Journal International*. 177: 941-948, 2009.

207. O.N. Shebanova and P. Lazor. Raman spectroscopic study of magnetite ($FeFe_2O_4$): a new assignment for the vibrational spectrum. *Journal of Solid State Chemistry*. 174: 424-430, 2003.

208. I. Chourpa, L. Douziech-Eyrolles, L. Ngaboni-Okassa, J.-F. Fouquenet, S. Cohen-Jonathan, M. Soucé, H. Marchais, and P. Dubois. Molecular composition of iron oxide nanoparticles, precursors for magnetic drug targeting, as characterized by confocal Raman microspectroscopy. *Analyst*. 130: 1395-1403, 2005.

209. N. Pinna, S. Grancharov, P. Beato, P. Bonville, M. Antonietti, and M. Niederberger. Magnetite nanocrystals: Nonaqueous synthesis, characterization, and solubility. *Chemistry of Materials*. 17: 3044-3049, 2005.

210. M. Legodi and D. De Waal. The preparation of magnetite, goethite, hematite and maghemite of pigment quality from mill scale iron waste. *Dyes and Pigments*. 74: 161-168, 2007.

211. M. Soler, G. Alcantara, F. Soares, W. Viali, P. Sartoratto, J. Fernandez, S. Da Silva, V. Garg, A. Oliveira, and P. Morais. Study of molecular surface coating on the stability of maghemite nanoparticles. *Surface Science*. 601: 3921-3925, 2007.

212. S.H. Xuan, L.Y. Hao, W.Q. Jiang, X.L. Gong, Y.A. Hu, and Z.Y. Chen. Preparation of water-soluble magnetite nanocrystals through hydrothermal approach. *Journal of Magnetism and Magnetic Materials*. 308: 210-213, 2007.

213. M. Aronniemi, J. Lahtinen, and P. Hautojarvi. Characterization of iron oxide thin films. *Surface and Interface Analysis*. 36: 1004-1006, 2004.

214. J. Moulder, W. Stickle, P. Sobol, and K. Bomben. Handbook of X-ray photoelectron spectroscopy, 1995, Physical Electronics. *Inc., Eden Prairie, MN*,

215. M. Monti, B. Santos, A. Mascaraque, O.R. de la Fuente, M.A. Nino, T.O. Mentes, A. Locatelli, K.F. McCarty, J.F. Marco, and J. de la Figuera. Magnetism in nanometer-thick magnetite. *Physical Review B*. 85, 2012.

216. H. Sugimura, A. Hozumi, T. Kameyama, and O. Takai. Organosilane self-assembled monolayers formed at the vapour/solid interface. *Surface and Interface Analysis*. 34: 550-554, 2002.

217. S.L. Iconaru, E. Andronescu, C.S. Ciobanu, A.M. Prodan, P. Le Coustumer, and D. Predoi. Biocompatible Magnetic Iron Oxide Nanoparticles Doped Dextran Thin Films Produced by Spin Coating Deposition Solution. *Digest Journal of Nanomaterials and Biostructures*. 7: 399-409, 2012.

218. A. Bratt and A.R. Barron. *XPS of Carbon Nanomaterials*. 2011; Available from: http://cnx.org/content/m34549/1.2/.

219. Y. Yuan and D.-A.B. Tasciuc. Comparison between experimental and predicted specific absorption rate of functionalized iron oxide nanoparticle suspensions. *Journal of Magnetism and Magnetic Materials*. 323: 2463-2469, 2011.

220. R.E. Rosensweig. Heating magnetic fluid with alternating magnetic field. *Journal of Magnetism and Magnetic Materials*. 252: 370-374, 2002.

221. A. Kihal, G. Fillion, B. Bouzabata, and B. Barbara. High field surface magnetic study of Fe_3O_4 nanoparticles. *physica status solidi (b)*. 249: 604-614, 2012.

222. A.P. Herrera, C. Barrera, and C. Rinaldi. Synthesis and functionalization of magnetite nanoparticles with aminopropylsilane and carboxymethyldextran. *Journal of Materials Chemistry*. 18: 3650-3654, 2008.

223. M. Morales, S. Veintemillas-Verdaguer, M. Montero, C. Serna, A. Roig, L. Casas, B. Martinez, and F. Sandiumenge. Surface and internal spin canting in γ-Fe_2O_3 nanoparticles. *Chemistry of Materials*. 11: 3058-3064, 1999.

224. M. Blanco-Mantecon and K. O'Grady. Interaction and size effects in magnetic nanoparticles. *Journal of Magnetism and Magnetic Materials*. 296: 124-133, 2006.

225. A. Roca, D. Niznansky, J. Poltierova-Vejpravova, B. Bittova, M. Gonzalez-Fernandez, C. Serna, and M. Morales. Magnetite nanoparticles with no surface spin canting. *Journal of Applied Physics*. 105: 114309, 2009.

226. R.L. Rebodos and P.J. Vikesland. Effects of Oxidation on the Magnetization of Nanoparticulate Magnetite. *Langmuir*. 26: 16745-16753, 2010.

227. W. Kim, C.-Y. Suh, S.-W. Cho, K.-M. Roh, H. Kwon, K. Song, and I.-J. Shon. A new method for the identification and quantification of magnetite–maghemite mixture using conventional X-ray diffraction technique. *Talanta*. 94: 348-352, 2012.

228. J. Mürbe, A. Rechtenbach, and J. Töpfer. Synthesis and physical characterization of magnetite nanoparticles for biomedical applications. *Materials Chemistry and Physics*. 110: 426-433, 2008.

229. V. Korolev, A. Ramazanova, V. Yashkova, O. Balmasova, and A. Blinov. Adsorption of fatty acids from solutions in organic solvents on the surface of finely dispersed magnetite: 1. Isotherms of adsorption of oleic, linoleic, and linolenic acid from carbon tetrachloride and hexane. *Colloid Journal*. 66: 700-704, 2004.

230. V. Korolev, O. Balmasova, and A. Ramazanova. The sorption isotherms of oleic, linoleic, and linolenic acids from solutions in cyclohexane and heptane on magnetite. *Russian Journal of Physical Chemistry A*. 83: 1018-1021, 2009.

231. J. Molgaard and W.W. Smeltzer. Thermal conductivity of magnetite and hematite. *Journal of Applied Physics*. 42: 3644-&, 1971.

232. X.Q. Wang and A.S. Mujumdar. Heat transfer characteristics of nanofluids: a review. *International Journal of Thermal Sciences*. 46: 1-19, 2007.

233. W.H. Yu, D.M. France, J.L. Routbort, and S.U.S. Choi. Review and comparison of nanofluid thermal conductivity and heat transfer enhancements. *Heat Transfer Engineering*. 29: 432-460, 2008.

234. H.A. Mintsa, G. Roy, C.T. Nguyen, and D. Doucet. New temperature dependent thermal conductivity data for water-based nanofluids. *International Journal of Thermal Sciences*. 48: 363-371, 2009.

235. X. Wang, X. Xu, and S.U. S. Choi. Thermal Conductivity of Nanoparticle - Fluid Mixture. *Journal of Thermophysics and Heat Transfer*. 13: 474-480, 1999.

236. P. Keblinski, R. Prasher, and J. Eapen. Thermal conductance of nanofluids: is the controversy over? *Journal of Nanoparticle Research*. 10: 1089-1097, 2008.

237. J. Philip, P.D. Shima, and B. Raj. Enhancement of thermal conductivity in magnetite based nanofluid due to chainlike structures. *Applied Physics Letters*. 91, 2007.

238. K. Parekh and H.S. Lee. Magnetic field induced enhancement in thermal conductivity of magnetite nanofluid. *Journal of Applied Physics*. 107, 2010.

239. B.D. Wang, B.G. Wang, P.F. Wei, X.B. Wang, and W.J. Lou. Controlled synthesis and size-dependent thermal conductivity of Fe_3O_4 magnetic nanofluids. *Dalton Transactions*. 41: 896-899, 2012.

240. P.D. Shima, J. Philip, and B. Raj. Role of microconvection induced by Brownian motion of nanoparticles in the enhanced thermal conductivity of stable nanofluids. *Applied Physics Letters*. 94, 2009.

241. H.T. Zhu, C.Y. Zhang, S.Q. Liu, Y.M. Tang, and Y.S. Yin. Effects of nanoparticle clustering and alignment on thermal conductivities of Fe_3O_4 aqueous nanofluids. *Applied Physics Letters*. 89, 2006.

242. P.D. Shima, J. Philip, and B. Raj. Synthesis of Aqueous and Nonaqueous Iron Oxide Nanofluids and Study of Temperature Dependence on Thermal Conductivity and Viscosity. *Journal of Physical Chemistry C*. 114: 18825-18833, 2010.

243. J.C. Maxwell and J.J. Thomson, *Treatise on Electricity and Magnetism*. 1904: At the Clarendon Press.

244. E.J. Wasp, J.P. Kenny, and R.L. Gandhi, *Solid-liquid flow slurry pipeline transportation*. 1977: Trans Tech Publications.

245. E.V. Timofeeva, A.N. Gavrilov, J.M. McCloskey, Y.V. Tolmachev, S. Sprunt, L.M. Lopatina, and J.V. Selinger. Thermal conductivity and particle agglomeration in alumina nanofluids: Experiment and theory. *Physical Review E*. 76, 2007.

246. V.E. Fertman, L.E. Golovicher, and N.P. Matusevich. Thermal-conductivity of magnetite magnetic fluids. *Journal of Magnetism and Magnetic Materials*. 65: 211-214, 1987.

247. M. Abareshi, E.K. Goharshadi, S.M. Zebarjad, H.K. Fadafan, and A. Youssefi. Fabrication, characterization and measurement of thermal conductivity of Fe_3O_4 nanofluids. *Journal of Magnetism and Magnetic Materials*. 322: 3895-3901, 2010.

248. W. Jiang and L.Q. Wang. Monodisperse magnetite nanofluids: Synthesis, aggregation, and thermal conductivity. *Journal of Applied Physics*. 108, 2010.

249. C.L. Altan, A. Elkatmis, M. Yuksel, N. Aslan, and S. Bucak. Enhancement of thermal conductivity upon application of magnetic field to Fe3O4 nanofluids. *Journal of Applied Physics*. 110, 2011.

250. I. Nkurikiyimfura, Y.M. Wang, and Z.D. Pan. Effect of chain-like magnetite nanoparticle aggregates on thermal conductivity of magnetic nanofluid in magnetic field. *Experimental Thermal and Fluid Science*. 44: 607-612, 2013.

251. I. Nkurikiyimfura, Y.M. Wang, and Z.D. Pan. Heat transfer enhancement by magnetic nanofluids-A review. *Renewable & Sustainable Energy Reviews*. 21: 548-561, 2013.

252. S. Sun, H. Zeng, D.B. Robinson, S. Raoux, P.M. Rice, S.X. Wang, and G. Li. Monodisperse MFe_2O_4 (M = Fe, Co, Mn) Nanoparticles. *Journal of the American Chemical Society*. 126: 273-279, 2003.

253. J.H. Yoe and A.L. Jones. Colorimetric Determination of Iron with Disodium-1,2-dihydroxybenzene-3,5-disulfonate. *Industrial & Engineering Chemistry Analytical Edition*. 16: 111-115, 1944.

254. E. Cheraghipour, S. Javadpour, and A.R. Mehdizadeh. Citrate capped superparamagnetic iron oxide nanoparticles used for hyperthermia therapy. *Journal of Biomedical Science & Engineering*. 5, 2012.

255. J. Eastman, S. Choi, S. Li, W. Yu, and L. Thompson. Anomalously increased effective thermal conductivities of ethylene glycol-based nanofluids containing copper nanoparticles. *Applied Physics Letters*. 78: 718-720, 2001.

256. J.C. Maxwell, *A Treatise on Electricity and Magnetism*. Vol. 1. 1881: Clarendon press.

257. R. Hamilton and O. Crosser. Thermal conductivity of heterogeneous two-component systems. *Industrial & Engineering Chemistry Fundamentals*. 1: 187-191, 1962.

258. S.A. Putnam, D.G. Cahill, B.J. Ash, and L.S. Schadler. High-precision thermal conductivity measurements as a probe of polymer/nanoparticle interfaces. *Journal of Applied Physics*. 94: 6785-6788, 2003.

259. P. Keblinski, J.A. Eastman, and D.G. Cahill. Nanofluids for thermal transport. *Materials Today*. 8: 36-44, 2005.

260. L. Filippov and N. Novoselova. *The thermal conductivity of solutions of normal liquid Vesten Mosk Univ Ser Fiz Mat Estestv Nauk (1955)(3) 10~ 2) 37-40*. in *Chemical Abstracts*. 1955.

261. T.K. Hong, H.S. Yang, and C.J. Choi. Study of the enhanced thermal conductivity of Fe nanofluids. *Journal of Applied Physics*. 97, 2005.

262. M.S. Liu, M.C.C. Lin, C.Y. Tsai, and C.C. Wang. Enhancement of thermal conductivity with Cu for nanofluids using chemical reduction method. *International Journal of Heat and Mass Transfer*. 49: 3028-3033, 2006.

263. S. Lee, S.U.S. Choi, S. Li, and J.A. Eastman. Measuring thermal conductivity of fluids containing oxide nanoparticles. *Journal of Heat Transfer-Transactions of the ASME*. 121: 280-289, 1999.

264. X.W. Wang, X.F. Xu, and S.U.S. Choi. Thermal conductivity of nanoparticle-fluid mixture. *Journal of Thermophysics and Heat Transfer*. 13: 474-480, 1999.

265. H. Masuda, A. Ebata, K. Teramae, and N. Hishinuma. Alteration of thermal conductivity and viscosity of liquid by dispersing ultra-fine particles. *Netsu Bussei*. 7: 227-233, 1993.

266. M.S. Liu, M.C.C. Lin, I.T. Huang, and C.C. Wang. Enhancement of thermal conductivity with carbon nanotube for nanofluids. *International Communications in Heat and Mass Transfer*. 32: 1202-1210, 2005.

267. F.D.S. Marquis and L.P.F. Chibante. Improving the heat transfer of nanofluids and nanolubricants with carbon nanotubes. *The Journal of the Minerals, Metals & Materials Society*. 57: 32-43, 2005.

268. B. Yang and Z.H. Han. Temperature-dependent thermal conductivity of nanorod-based nanofluids. *Applied Physics Letters*. 89, 2006.